universität wien

MASTERARBEIT / MASTER'S THESIS

Titel der Masterarbeit / Title of the Master's Thesis

Mechanism of action of hyperthermic intraperitoneal chemotherapy (HIPEC) in different types of high grade serous ovarian cancer cell lines

verfasst von / submitted by

Elisabeth Steindl, BSc

angestrebter akademischer Grad / in partial fulfilment of the requirements for the degree of

Master of Science (MSc)

Wien, 2018 / Vienna 2018

Studienkennzahl lt. Studienblatt / degree programme code as it appears on the student record sheet:	A 066 834
Studienrichtung lt. Studienblatt / degree programme as it appears on the student record sheet:	Masterstudium Molekulare Biologie
Betreut von / Supervisor:	Priv.-Doz. Mag. Dr. Dietmar Pils, MSc, MA

Acknowledgements

I want to say special thanks to my supervisor Dietmar Pils. He supported me during my thesis by sharing his great knowledge. I acquired extensive research experience by working independently and planning my experiments. He didn't hesitate to answer all my questions and giving explanations. I gained a lot of new knowledge and enjoyed my work in the laboratory. Additionally I want to thank Thomas Grunt for supporting me during my cell culture experiments.

At least, special thanks to my parents for their big support, motivation and understanding.

Table of Contents

Acknowledgements ii

Summary 1

Zusammenfassung 3

Introduction 5

Ovarian cancer 5

Origin of ovarian cancer 7

Metastasic spread in ovarian cancer 7

Treatment of HGSC patients - hyperthermic intraperitoneal chemotherapy (HIPEC) 9

Peritoneal tumor spread types: miliary and non-miliary 10

DNA methylation in cancer 13

DNA methylation in ovarian cancer 15

Cell death pathways: Apoptosis and Necroptosis 16

Apoptosis 16

Necroptosis 19

Heat shock proteins 23

Transfer-RNA halves and fragments 23

Hypothesis and outline of the project. 25

Methods 27

Cell Culture 27

In vitro ”HIPEC“ treatment of tumor cell lines 28

Immunefluorescence (IF) staining of FFPE sections 29

Data analysis – CellProfiler 2.2.0 30

RNA Preparation 32

RNA libraries and sequencing 32

DNA Preparation and Sequencing 33

Coverslip experiments 33
ICC Staining 34
Immunogenicity of necroptosis 35
Treatment of ES-2 and OVCAR-3 cells 35
Isolation of peripheral blood mononuclear cells (PBMC) with Ficoll 36
Isolation of $CD14^+$ cells 36
Blood monocyte activation through DAMPS 37
Results 38
Evidence for Necroptosis 38
Quantified analysis of necroptosis upon in vitro HIPEC treatment 38
Co-localization of pMLKL, RIPK3, and Hsp90 upon HIPEC treatment 42
Further evidence for necroptosis 45
Cell death by apoptosis 51
Cell line expression of RIPK1, RIPK3 and caspase 8 52
Immunogenic cell death through DAMP release 53
Hsp90 is an essential key player promoting necroptosis 54
Levels of tiRNA are lower in tumor cells of non miliary spread type. 55
Comparison of 5'tiRNA fragments abundance and angiogenin and angiogenin inhibitor expression in miliary and non-miliary tumors of HGSC patients 58
Early epigenetic changes after chemotherapy treatment 61
Discussion 67
References 74

List of tables and figures

Figure 1. Summary of miliary and non miliary tumor spread types. 12

Figure 2. Apoptosis 18

Figure 3. Mechanisms of necroptosis 20

Figure 4. Different ways of complex formation to induce apoptosis or necroptosis. 21

Figure 5. Generation of tRFs and tiRNA. 24

Figure 6. Schematic overview of the hypothesis for this work 25

Figure 7. Scheme of the *in vitro* HIPEC treatment. 28

Figure 8. Used CellProfiler Pipeline. 31

Figure 9. Scatter plot of pMLKL, RIPK3, and Hsp90 staining in tumor cells of both spread types after 20 h post-HIPEC cultivation 39

Figure 10. Comparison of the relative change of $pMLKL^{+}/RIPK3^{+}$ cells compared to untreated cells in both tumor spread types of non-miliary and miliary and their putative non-malignant precursor cells 41

Figure 11. Confocal microscopy images of miliary (tubal) and non-miliary (ovarian) cell lines treated with HIPEC or normothermic chemotherapy conditions and controls 44

Figure 12. ES-2 (left) and OVCAR-3 (right) cells treated with or without chemotherapy (CHT) and Necrostatin-1 (Nec-1) at 37°C and 42°C. 46

Figure 13. pMLKL,RIPK3, and Hsp90 staining of ES-2 cells after HIPEC treatment. 47

Figure 14. pMLKL, RIPK3, and Hsp90 staining of ES-2 cells after 42°C treatment and after Nec-1 inhibiton and HIPEC treatment. 48

Figure 15. pMLKL, RIPK3, and Hsp90 staining of ES-2 cells at 37°C. 48

Figure 16. OVCAR-3 cells stained for pMLKL, RIPK3, and Hsp90. 49

Figure 17. OVCAR-3 cells stained for pMLKL, RIPK3, and Hsp90. 49

Figure 18. pMLKL/RIPK3/Hsp90 staining of OVCAR-3 50

Figure 19. Confocal microscopy images of apoptosis in ES-2 and OVCAR-3 cells. 51

Figure 20. RIPK3, RIPK1, and caspase 8 expression data. 52

Figure 21. relative IL6 measurements in ES-2 cells. 53

Figure 22. Levels of Hsp90-alpha and Hsp90-beta in cell free ascites of both tumor spread types. 54

Figure 23. Levels of 5´halves at 37°C and 2 hours in miliary and non-miliary cells. 56

Figure 24. Abundance of 5´tiRNA in IOSE80 (left) and IOSE364 (right) at 37°C treated with chemotherapy (black line) and 42°C treated with chemotherapy (red line) after 2 hours and 20 hours. 56

Figure 25. Abundance of 5´tiRNA in ES-2 (left) and Tyk-nu (right) at 37°C treated with chemotherapy (black line) and 42°C treated with chemotherapy (red line) after 2 hours and 20 hours. 57

Figure 26. Abundance of 5´tiRNA in FT194 (left), CAOV-3 (middle) and OVCAR-3 (right) at 37°C treated with chemotherapy (black line) and 42°C treated with chemotherapy (red line) after 2 hours and 20 hours. 57

Figure 27. Percent change from 37°C to 42°C of 5´halves after 2 hours and 20 hours after chemotherapy treatment. 58

FIGURE 28. A) ABUNDANCE OF TRNA FRAGMENTS IN TUMOR CELLS AND TUMOR TISSUE OF HGSC PATIENTS B) EXPRESSION OF ANGIOGENIN IN TUMOR CELLS AND TISSUES C) EXPRESSION OF ANGIOGENIN INHIBITOR RNH1 IN TUMOR CELLS AND TISSUE. 59
FIGURE 29. SHOTGUN PROTEOMICS OF CELL FREE ASCITES OF PATIENTS WITH MILIARY (MI) AND NON-MILIARY (NMI) TUMOR SPREAD. 60
FIGURE 30. SCHEME OF ANGIOGENIN MEDIATED TRNA CLEAVAGE IN MILIARY ASCITES TUMOR CELLS. 60
FIGURE 31. METHYLATION CHANGES IN *LINE1* AND EXPRESSION OF *LINE1*. 62
FIGURE 32. HYPOMETHYLATION OF RGPD3 AFTER CHEMOTHERAPY TREATMENT. 63
FIGURE 33. DIFFERENTIALLY METHYLATED CLUSTER C1_154 BETWEEN MILIARY AND NON-MILIARY CELL LINES. 65
FIGURE 34. EXPRESSION DIFFERENCES IN MILIARY AND NON-MILIARY CELL LINES (ESTIMATED FROM RNA-SEQUENCING). 66
FIGURE 35. BOXPLOTS OF BETA VALUES OF ALL CALLED CPGS IN ALL CELL LINES AND ALL EXAMINED CONDITIONS. 66
FIGURE 36. 5´TIRNA LEVELS IN CELLS OF MILIARY TUMOR SPREAD TYPE. 71
FIGURE 37. 5´TIRNA LEVELS IN CELLS OF NON-MILIARY TUMOR SPREAD TYPE. 71

"Ich habe mich bemüht, sämtliche Inhaber der Bildrechte ausfindig zu machen und ihre Zustimmung zur Verwendung der Bilder in dieser Arbeit eingeholt. Sollte dennoch eine Urheberrechtsverletzung bekannt werden, ersuche ich um Meldung bei mir."

Summary

High grade serous ovarian cancer (HGSC) is one of the most deadly malignancies among women. Most of ovarian cancer patients are diagnosed at advanced stage of the disease because at early stage patients are without specific symptoms [2]. The most challenging issues in HGSC is the development of peritoneal carcinomatosis and chemotherapy resistance. Patients often relapse and die on recurrences with only 30% five-year survival for HGSC patients [3]. To improve outcome, many therapies are discussed involving hyperthermic intraperitoneal chemotherapy (HIPEC). Some advantages of HIPEC is hyperthermia that support penetration of chemotherapeutics into tissue, and the local administration of chemotherapeutics are tolerated at higher concentrations. High grade serous ovarian cancer is a very heterogeneous disease. Our group described recently two peritoneal tumor spread types called miliary and non-miliary [4]. Miliary is presumed to be of tubal origin whereas non-miliary probably of ovarian origin. Miliary has a more epithelial cell characteristic and appear with many millet sized lesions covering the whole peritoneum. Non-miliary have a more mesenchymal characteristic and presents with only a few bulky implants in their peritoneum. They show a more adaptive immune response in contrast to milary spread type with a more systemic inflammatory reaction. In general, non-miliary have a better overall survival [4-6].

Until now the molecular mechanisms of HIPEC are unknown. Therefore we developed a hypothesis: Heat induced stress combined with chemotherapeutics could cause a shift from apoptosis to immunogenic necroptosis. Several studies reported tRNA fragments to inhibit apoptosis which could support the shift towards necroptosis [7]. In the course of cell death by necroptosis, “damage associated molecular patterns” (DAMPS) are released which could promote a tumor directed immune response and therefore increase patients´ survival [8].

To examine this hypothesis, we choose HGSC cell lines from miliary and non-miliary tumor spread type as described by Auer *et al.* [4, 5]. These cell lines were treated with a chemotherapy solution consisting of Carboplatin and Paclitaxel at 42°C or 37°C. Controls were performed without chemotherapeutic treatment for each temperature. After treatment cells were fixed, embedded in agarose and paraffin and slides thereof stained immunofluorescently for necroptosis marker with anti-pMLKL, anti-RIPK3 and anti-Hsp90 antibodies, and for apoptosis marker with anti-Caspase 3, M30 and anti-cleaved PARP

antibodies. The slides were scanned with TissueFAX® and quantified with CellProfiler™ software.

Additionally, these staining were repeated with cultured cells on coverslips and stained for necroptosis and apoptosis. The coverslips were analyzed by confocal microscopy to analyze co-localization of the necroptosis markers. The necroptosis inhibitor Necrostatin-1 was used as specific inhibitor of necroptosis. Supernatants were collected after treatment and incubated with blood monocytes of healthy women to investigate immune response via IL6 measurement. To estimate tRNA fragment expression, RNA was isolated after 30 minutes incubation with fresh cell culture medium after chemotherapy treatment at normothermic or hyperthermic conditions and libraries were prepared for small RNA sequencing.

Co-localization of necroptosis marker pMLKL, RIPK3, and interestingly Hsp90 was found at cell boarders indicating successful necrosome formation and necroptosis, but only in non-miliary cell lines. There was a significant difference in miliary and non-miliary cells. Triple staining at substantial frequencies was only found in non-miliary cell lines (ES-2, Tyk-nu, IOSE364, IOSE80) whereas miliary (OVCAR-3, CAOV-3, FT194, FT33) seems not to respond. Necrosome formation was inhibited by Nec-1. Markers for apoptosis were found only at a few cells of both tumor spread types interpreted as basic apoptosis in cell culture. Blood monocytes reacted with increased IL6 production upon incubation with the supernatant of necroptotic non-miliary ES-2 cells. IL6 increase was only seen in the non-miliary cell line ES-2 treated at HIPEC conditions. At normothermic conditions (37°C) and in the miliary cell line OVCAR-3 no IL6 increase was seen. Furthermore, IL6 increase was inhibited by Necrostatin-1. In contrast to this matching findings, tRNA fragments act the other way round. Increased levels of tRNA fragments were found in miliary and decreased levels in non-miliary.

One additional project was to look for early epigenetic events. We collected DNA from each condition after 20 h incubation in fresh culture medium after treatment, i.e. at 37°C and 42°C chemotherapy treatment and an untreated sample. Surprisingly we found first epigenetic events already after 20 hours after chemotherapy treatment. Global DNA methylation was reduced upon chemotherapy treatment at both temperatures.

To conclude, non-miliary cell lines reacted upon HIPEC treatment with immunogenic necroptosis. tRNA fragment levels are higher at 42°C and differ between the tumor spread types. Furthermore we found first epigenetic modifications already after 20 hours after chemotherapy treatment with a global decrease in DNA methylation.

Zusammenfassung

Das Ovarialkarzinom ist unter den gynäkologischen Karzinomen das tödlichste. Aufgrund von fehlenden Symptomen in den frühen Stadien der Erkrankung werden die meisten Patienten im späten Stadium mit undifferenziertem serösen Ovarialkarzinom (Grad 2-3) diagnostiziert. Eine der Therapieformen ist hypertherme intraperitoneale Chemotherapie (HIPEC). Dabei wird das Peritoneum mit 42°C erwärmter Chemotherapie Lösung gespült. Der Vorteil dieser Methode ist die Toleranz erhöhter Konzentration der Chemotherapie durch lokale Applikation und besseres Eindringen ins Gewebe verursacht durch Hyperthermie [9, 10]. Patienten mit Ovarialkarzinom entwickeln oft Rezidive und Resistenzen nach der Chemotherapie. Das Ovarialkarzinom ist eine sehr heterogene Erkrankung. Auer *et al.* hat kürzlich zwei Metastasierungsmuster „miliary“ und „non-miliary“ beschrieben [4]. Der „miliary“ Phänotyp hat einen epithelialen Charakter und entwickelt sich von der Tube ausgehend. Patienten mit miliary Metastasierungsmuster haben eine schlechtere Prognose als Patienten mit non-miliary Metastasierung. Die Ursache der schlechten Prognose resultiert von den „millet sized“ Läsionen im Peritoneum. Non-miliary Patienten haben weniger Metastasen im Peritoneum die zudem knotenförmig erscheinen. Der non-miliary Phänotyp hat mesenchymale Eigenschaften und entwickelt sich aus dem Ovar. Beide Phänotypen unterscheiden sich auch in der Immunantwort, worin miliary eine eher inflammatorische Immunantwort hervorruft und non-miliary eine adaptive Immunantwort [4-6, 11]. Um die Auswirkungen der HIPEC auf Patienten mit serösen Ovarialkarzinom zu studieren formulierten wir eine Hypothese: Durch Hyperthermie in Kombination mit Chemotherapie könnte es zu einer Verschiebung von nicht immunogener Apoptose zu immunogener Necroptose kommen. Durch Zelltod durch Necroptose kommt es zu einer Ausschüttung von DAMPS, die das Immunsystem aktivieren [8]. Dadurch wirkt der Zelltod durch Necroptose immunogen im Vergleich zu Apoptose. Zusätzlich berichten Studien über tRNA Fragmente die Apoptose inhibieren, wodurch Necroptose bevorzugt eintreten könnte [7].

Wir behandelten Zelllinien von beiden Metastasierungsmustern mit Chemotherapie bei 42°C und 37°C und ohne Chemotherapie als Kontrolle. Die Zellen wurden in Paraffin eingebettet, geschnitten und mit typischen Necroptose (pMLKL, RIPK3, Hsp90) und Apoptose (Caspase 3, M30, fragmentiertem PARP) Markern gefärbt und mittel TissueFAX® eingescannt. Die quantitative Auswertung erfolgte mittels CellProfiler™ Software. Zusätzlich wurde das

Experiment mit auf Deckgläsern gezüchteten Zellen wiederholt. Diese wurden auch mit und ohne Chemotherapie bei 37°C oder 42°C behandelt und mit Necroptose und Apoptose Marker gefärbt. Um Necroptose nachzuweisen wurde die Co-lokalisation der drei Necroptosemarker an der Plasmamembran mittels Konfokalmikroskop untersucht. Zusätzlich wurden die Überstände mit Blutmonozyten inkubiert um eine Immunreaktion (IL6) nachzuweisen. Als negativ Kontrolle wurde Necrostatin-1, ein spezifischer Inhibitor für Necroptose, eingesetzt. Zusätzlich wurde nach 30 Minuten Inkubation in frischen Zellkulturmedium nach der Chemotherapiebehandlung RNA isoliert und sequenziert um Expressionsunterschiede der tRNA Fragmente zu untersuchen.

Zellen mit non-miliary Phänotyp zeigten Co-lokalisation von pMLKL, RIPK3 und Hsp90 an der Plasmamembran nur in 42°C Chemotherapie behandelten Zellen. Zellen mit miliary Phänotyp zeigten keinen Nachweis von Necroptose. Zusätzlich konnte Necroptose mit Necrostatin-1 inhibiert werden. Blutmonozyten reagierten mit erhöhter IL6 Produktion nach Inkubation mit Zellkulturmedium von necroptotisch sterbenden non-miliary Zellen. In Necrostatin-1 oder 37°C Chemotherapie behandelten Zellen konnte man keine Erhöhung von IL6 feststellen.

Im Gegensatz dazu verhalten sich tRNA Fragmente anders. In miliary sind tRNA Fragmente erhöht und in non-miliary erniedrigt.

Ein weiteres Projekt war den epigenetischen Effekt auf Chemotherapie anzusehen. Bereits nach 20 Stunden nach Chemotherapie Behandlung findet eine Demethylierung der DNA statt.

Introduction

Ovarian cancer

Ovarian cancer is one of the most frequent causes of cancer deaths in females in the western countries. The poor prognosis of this patients results from late diagnosis at advanced stages. For high grade serous ovarian cancer, they only have a five year survival of 15%-37% [12]. Ovarian tumors can develop from epithelial cells, germ cells (ovar) or sex cord stomal cells. A minor fraction with about 40% are of non-epithelial origin and often benign, so called teratoma, and only a few of them develop to teratocarcinoma. The predominant form of cancer are of epithelial origin (EOC). There are four major histological subtypes: serous, endometrioid, mucinous, and clear cell [2]. The new WHO classification system 2014 added Brenner tumors (former called transitional cell tumors) and a new subtype called seromucinous tumors [13]. Each subtype is then further divided into benign, borderline (low malignant potential) and malignant. The clinical outcome depend among other things on the malignancy and histology of tumors. 60% of malignant tumors are of serous subtype with high grade serous as the most aggressive form of ovarian cancer. Further, the clinical outcome depend on chemotherapy response. High grade and low grade serous respond (initially) well to chemotherapy in contrast to clear cell tumors [2].

Another classification system is the one according types. Epithelial ovarian cancer can be divided in two types. Type I are low grade tumors of any histology, which are well differentiated and Type II are high grade (mainly serous) tumors which are poorly differentiated. Type I tumor patients carry mutations in *KRAS, PTEN, BRAF,* and type II tumors have nearly always *TP53* and often *BRCA1/2* mutations, which are mostly absent in type I [14]. The International Federation of Gynecology and Obstetrics (FIGO) classified four staging types according tumor spread and extent, latest version of 2014 is shown in Table 1 [14].

Stage I	Tumor is confined to ovaries or fallopian tubes
IA	Tumor limited to 1 ovary with intact capsule intact or fallopian tube; no tumor on the surface; no tumor cells in ascites.
IB	Tumor limited to both ovaries or fallopian tubes; no tumor on ovarian or fallopian tube surface; no malignant cells in the ascites or peritoneal washings
IC	Tumor limited to 1 or both ovaries or fallopian tube(s)
Stage II	Tumor involves 1 or both ovaries or fallopian tubes with pelvic extension (below pelvic brim) or primary peritoneal cancer
IIA	Extension and/or implants on uterus and/or fallopian tubes and/ or fallopian tubes and/or ovaries
IIB	Extension to other pelvic intra- peritoneal tissues
Stage III	Tumor involves 1 or both ovaries or fallopian tubes, or primary peritoneal cancer, with cytologically or histologically confirmed spread to the peritoneum outside the pelvis and/or metastasis to the retroperitoneal lymph nodes
IIIA1	Positive retroperitoneal lymph nodes only (cytologically or histologically proven)
IIIA1 (i)	Metastasis up to 10 mm in greatest dimension
IIIA1 (ii)	Metastasis more than 10 mm in greatest dimension
IIIA2	Microscopic extra-pelvic (above the pelvic brim) peritoneal involvement with or without positive retroperitoneal lymph nodes
IIIB	Macroscopic peritoneal metastasis beyond the pelvis up to 2 cm in greatest dimension, with or without metastasis to the retro- peritoneal lymph nodes (includes extension of tumor to capsule of liver and spleen without parenchymal involvement of either organ)
IIIC	Macroscopic peritoneal metastasis beyond the pelvis more than 2 cm in greatest dimension, with or without metastasis to the retro-peritoneal lymph nodes (includes extension of tumor to capsule of liver and spleen without parenchymal involvement of either organ)
Stage IV	Distant metastasis excluding peritoneal metastases
IVA	Pleural effusion with positive cytology
IVB	Parenchymal metastases and metastases to extra-abdominal organs (including inguinal lymph nodes and lymph nodes outside of the abdominal cavity)

Table 1. FIGO staging 2014 from [14, 15]

Origin of ovarian cancer

The origin of ovarian cancer is still in discussion. One presumed origin is the ovarian surface epithelium (OSE). The ovarian surface consists of flat layer of mesothelial cells which are damaged during each ovulation. Therefore this cells have a high plasticity to repair these damages and show a high ability for epithelial to mesenchymal transition (EMT). DNA of OSE cells can be damaged by reactive oxygen or chemokines during ovulation. At advanced womens´ age, invaginations of the ovarian surface epithelium into the cortical stroma can occur which then form "*cortical inclusion cysts*". This *inclusion cysts* are then able to differentiate to a Müllerian like epithelium. The other way round Müllerian derived epithelia can also incorporate into inclusion cysts from ovarian surface epithelium. In the cortical stroma of the ovary are high levels of hormones which can promote growth and proliferation. The damaged epithelial cells in the stroma of the ovary are then boosted for proliferation, which can promote cancer development. The model of "*cortical inclusion cysts"* may be one explanation for the origin of ovarian cancer [2].

Later the fallopian tube epithelium (FTE) was presumed as origin of ovarian cancer. Women with *BRCA* mutations, who have an about 40% risk of developing ovarian cancer, underwent risk-reducing salpingo-oophorectomy. In these patients precursor lesions were found in the fallopian tube. The FTE is composed of ciliated and secretory cells. Several studies reported the fimbria, which is located at the distal end of the fallopian tube, as site of serous carcinoma development. Several other studies agreed with a high incidence for "*serous tubal intraepithelial carcinomas*" (STIC) originating from FTE and primary at the fimbria. The fimbria of the fallopian tube is close to the ovarian surface and thereby it can be assumed that cancerogenic FTE cells spread to the ovarian surface and develop to ovarian cancer and/or the peritoneum and cause primary peritoneal carcinoma. This idea supports the origin of high grade serous ovarian cancer [2]. But Eckert *et al.* reported that STICs could also resemble metastases adhering secondary to the fallopian tube rather than constituting the origin of HGSC [16].

Metastasic spread in ovarian cancer

Ovarian cancer is often associated with peritoneal carcinomatosis. Peritoneal tumor spread is one of the major problems associated with the accumulation of malignant peritoneal fluid (ascites) [3]. On the site of primary tumor, ovarian cancer cells detach and disseminate

through the peritoneal fluid to the omentum of the peritoneum [17]. Ascites may constitute a favorable microenvironment for tumor cells. These tumor cells have to evade anoikis, a form of programmed cell death of epithelial cells that follows detachment from the surrounding extracellular matrix, by cell aggregation and epithelial to mesenchymal transition (EMT). In general, EMT is a crucial event in cancer progression [4].

In comparison to other tumors entities, ovarian cancer spread locally, to organs into the peritoneum and the peritoneal wall which is presumably not associated with spread via circulatory systems. Also, clinical experience showes that ovarian cancer metastasize predominatly in the peritoneum but more seldom to distant organs, compared to other cancer types. During the metastasis process, cells often undergo epithelial to mesenchymal transition (EMT). During the EMT process E-Cadherin, which mediates cell adhesion through α- and β-catenin, is downregulated in floating tumor cells. Matrix metalloproteases, other key proteins in EMT, cleave E-Cadherin and allow cell detachment. When cancer cells detached they are carried by the peritoneal fluid to the target site and attach via integrin receptors. After attachment, cells undergo mesenchymal to epithelial transition (MET) and start again growing as solid tumors. Ovarian carcinomas can further secrete vascular endothelial growth factor (VEGF) which induce ascites production. VEGF inhibitors are in clinical use to prevent ascites formation. High expression of VEGF is associate with poor outcome of patients. One explanation for this was that VEGF is possibly responsible for anoikis evasion. In general, ascites formation seems to be an important factor for metastasizing. Variable numbers of floating tumor cells and tumor cell aggregates, called spheroids, are present in ascites. To date it is not clear whether spheroids or single tumor cells attach on the target site and are therefore responsible for local metastasizing. For the attachment several molecules are known to facilitate cell adhesion like integrins, VCAM-1, and cell surface receptor CD44. Other proteins affecting the metastatic process are metalloprotease 2 and transglutaminase promoting adhesion and EMT. The biggest difference to other tumor entities is that ovarian cancer disseminate predominaltly through the peritoneal cavity and not through circulatory systems like blood and lymph vessels [17].

Treatment of HGSC patients - hyperthermic intraperitoneal chemotherapy (HIPEC)

HGSC patients are treated with primary cytoreductive surgery (CRS) or interval cytoreductive surgery and adjuvant (and neodajuvant) chemotherapy. At advanced stage patients often receive three cycles of Carboplatin and Taxol based neoadjuvant chemotherapy to reduce tumor for a better debulking outcome. After neoadjuvant chemotherapy patients undergo interval cytoreductive surgery. After surgery they get another three to eight cycles of adjuvant chemotherapy depending on patients condition and response. Additionally, some patients receive angiogenesis inhibiting drugs like bevacizumab® [4]. Bevacizumab® is an inhibitor that binds VEGF [18]. Other therapeutic strategies are PARP inhibitors. PARP proteins are implemented in base excision repair (BER) pathway. In normal cells, PARP proteins detect the sites of single strand DNA damage, synthesizes poly ADP ribose and recruit proteins for DNA damage repair. HGSC patients often carry *BRCA1/2* mutations, where homologous recombination (HR) is deficient. PARP inhibitors preferentially kill *BRCA2* deficient cells compared to normal cells and are also reported to increase cytotoxity in combination with chemotherapeutics [19].

Hyperthermic intraperitoneal chemotherapy (HIPEC) is another current therapy strategy in HGSC which combines cytoreductive surgery and intraperitoneal chemotherapy at hyperthemic conditions [20]. There are several options when HIPEC can be performed. Normally, HIPEC takes place during primary or interval cytoreductive surgery. It can be performed as open or closed procedure through catheters with pre-warmed Cis/Carboplatin (seldom together with Paclitaxel) solution heated up to 42°C [9].

HIPEC has several advantages. The local administration of chemotherpeutics in the peritoneal cavity allows a higher concentration which improve its cytotoxic effect. Furthermore, systemic side effects are minimized through intraperitoneal (IP) administration of chemotherapeutics [9]. Hyperthermia itself has several cytotoxic effects. One is to increase drug penetration and affect DNA repair and the other is to induce apoptosis together with Platinum derived drugs which induce DNA damage. Furthermore, it activates heat shock proteins which can activate the immune system and inhibit angiogenesis [9].

A major problem in therapy of ovarian cancer patients is that the majority (about 70%) of patients relapse and develop platinum resistance after several cycles of chemotherapy treatment [2, 21].

Peritoneal tumor spread types: miliary and non-miliary

High grade serous ovarian cancer was shown to be a very heterogeneous disease, *e.g.* can present with very different peritoneal tumor spread types. Auer *et al.* (2015) described recently two tumor spread types in HGSC, named miliary and non-miliary. The classification of miliary and non-miliary was developed following clinical observations and established by molecular analyses like flow cytometry, transcriptomics, and survival analyses [4].

During surgery, patients with the miliary spread type present with many *millet sized lesions* covering large parts of the peritoneal wall and patients with non-milary spread type with only "*few big exophytically implants"* or no peritoneal involvement at all. Flow cytometry analysis revealed that non-miliary patients have higher levels of CD44 positive tumor cells which is a stemness marker which is accompanied by a more systemic inflamed status [4]. CD44 is a receptor for hyaluronic acid and plays an important role in EMT in cancer cells [22]. There was also a higher expression of NF-κB, IL7, IL8, and RIPK2, which contribute to a more inflamed status in non-miliary tumor cells. Furthermore, they found higher levels of EpCAM in miliary tumor cells, a cell adhesion molecule in epithelial cells, that fits to a more epithelial transcriptional gene expression signature in miliary [4].

Transcriptome analyses revealed expression differences in tumor cells of miliary and non-miliary spread type. They compared single ascites cells (A), Spheroids (S), solid tumor from ovary (P) and metastatic implants from the peritoneum (M). Gene expression differences were higher in floating tumor cells (A and S) compared with solid tumor masses (P and M) between non-miliary and in miliary. Miliary tumor cells showed downregulated genes for glucose metabolism, whereas the TNF and RAS pathways were upregulated. In miliary tumor cells the Erb, estrogen and chemokine signaling pathways as well as cytokine-cytokine interactions are inhibited. Furthermore, there were several deregulated pathways involved in cell metabolism and cell cycle comparing miliary and non-miliary. Miliary tumor cells have a reduced cell metabolism and a deregulated competing endogenous RNA network with microRNAs miR-221, miR-181, and miR-30 downregulated. Furthermore, miliary tumor cells showed a global reduction in transcriptional activity. Miliary tumor cells seems more adapted

to the microenvironment in the tumor due to remodeling of energy pathways and allowing them to survive in anoxic conditions. Furthermore, they are more capable for peritoneal tumor spread. Matrix metalloproteases (MMP) are downregulated in miliary tumor cells [4]. MMPs are endopeptidases which play a role in tumor metastasis through degradation of the extracellular matrix [4, 23]. The epithelial cell adhesion protein keratin-4 is upregulated in miliary tumor cells [4].

To sum up, non-miliary tumor cells show less peritoneal tumor spread and seem more bulky. They have a lower tumor spread factor (TSF), derived from gene expression differences between these two spread types, which is correlated with a better overall survival. Non-miliary cells have more CD44, MMP9, and MMP12 expression. They have reduced epithelial characteristics indicating a more mesenchymal cell behavior, and seem to origin form ovaries. In contrast, miliary tumor cells are from tubal origin with more epithelial characteristic. They are associated with an unfavorable overall survival [4].

There is also a difference in the immune response of patients with miliary and non-miliary tumor spread type. The non-miliary tumor spread type showed more signs of an adaptive immune response whereas the miliary spread type showed more signs of an innate immune response and a higher systemic inflammation. Immunofluorescence staining of immune cells of non-miliary spread revealed elevated levels of macrophages and monocytes in ascites. Furthermore, $CD8^+$ cytotoxic T-cells and GM-CSF were enriched in non-miliary indicating an anti-tumor immune response. In miliary tumor cells B-cells, IL10, and regulatory T cells (T_{reg}) were increased. Recently, studies reported an inhibitory effect of B-cells to anti-tumor immune response. Auer *et al.* (2016), discussed the possibility of *"a shift of the immune system from tumor surveillance to pro-tumorigenic actions*" in miliary tumor cells. Furthermore, in non-miliary tumor cells the immune checkpoint inhibitor PD1 is increased [6]. PD1 is reported to inactivate T cells and therefore promote immune suppression [11].

To conclude, miliary tumor cells have a more epithelial characteristic and more signs of an innate immune response and systemic inflammation and less PD1 expression and a less adaptive immune response [4, 6]. Additionally they have an unfavorable clinical outcome [4, 5]. Transcriptome analysis revealed that miliary are more fallopian tube like and non-miliary are more OSE like [5].

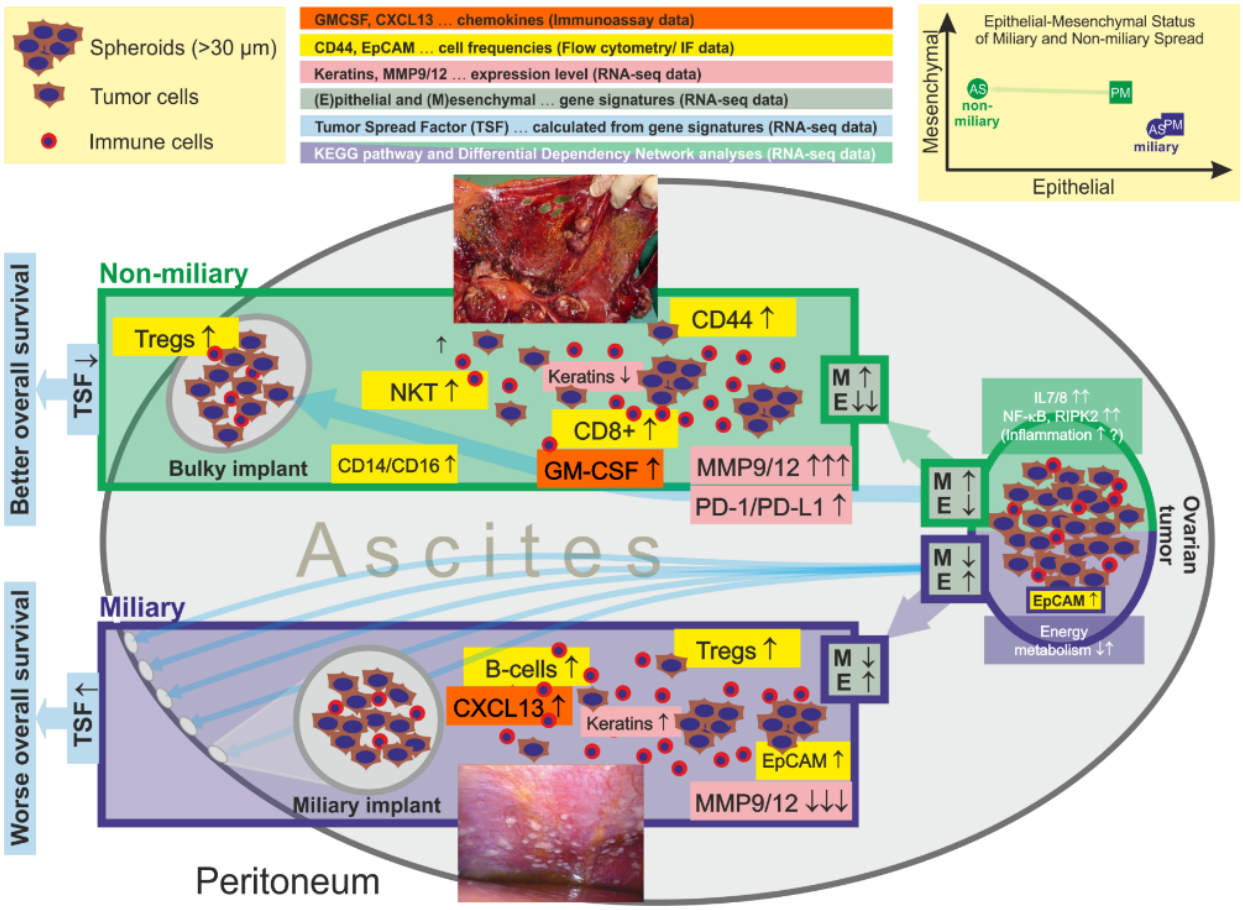

Figure 1. Summary of miliary and non miliary tumor spread types.

This figure was adapted from [4-6]. Non-miliary tumor cells from HGSC patients show upregulation of CD44, NKT, CD14/CD16 positive cells, T_{regs} and metalloproteinases MMP9/12. Furthermore, they show lower expression levels of keratins. Non miliary tumor cells show an increased mesenchymal makeup, especially in ascites cells and spheroids in comparison to solid tumor masses (Primum and Metastasis). They have a better overall survival indicated by a lower tumor spread factor. Levels of immune checkpoint inhibitors PD-1 and PD-1 ligand (PD-L1) were higher in non-miliary. Miliary tumor cells are more epithelial in solid tumor tissues (Primum and Metastasis) and floating tumor cells in ascites. They show elevated levels of B-cells and T-regulatory cells. Miliary tumor spread is correlated with a worse outcome (A: single ascites cells, S: Spheroids, P: Primum, M: Metastasis; yellow are flow cytometry and immunofluorescence data, orange are Luminex cytokine and chemokine data, purple, blue, and green are RNA sequencing data as described in the table shown in the upper part of the Figure; TSF: tumor spread factor) [3-6, 11].

DNA methylation in cancer

Epigenetic mechanisms including DNA methylation are important in the control of gene expression. DNA methylation affect a broadly range of biological mechanisms including development and differentiation. Alterations in DNA methylation are associated with different diseases, including cancer [24, 25].

Knudson postulated a "*two hit hypothesis"* which stated that it is necessary for tumorigenesis to inactivate putative tumor suppressor genes on both chromosomes because (nearly) every gene has two copies due to the diploid genome. Frequently, it was found that large chromosomal aberrations (deletions) can affect one allele (this would lead to loss of heterozygosity) and the second allele is often mutated (probably already in germline) or inactivated during cancerogensis by hypermethylation of the corresponding CpG islands of the promoter and therefore both genes are inactivated [26, 27]. Loss of heterozygosity can lead to the complete removal of one gene if a single mutation is present in the remaining allel or the allele is hypermethylated and thus transcriptional silenced. [27]. The importance for epigenetic events in tumor progression was shown for *e.g. BRCA1* [27]. Increased methylation could lead to loss of function of tumor suppressor genes such as *BRCA1* in breast and ovarian cancer [28, 29]. *BRCA1* is maintaining genomic stability and responsible for DNA repair [25]. Most inherited forms of breast cancer have a mutation in *BRCA1* or *BRCA2* and not-inherited forms show often a hypermethylation affecting *BRCA1* which would lead to inactivation of this gene. Gene expression analysis revealed that hypermethylation of the *BRCA1* gene in spontaneous cancers are identical with inherited *BRCA1* mutations carriers [27].

Alterations in methylation can promote tumor formation due to activation of oncogenes or inactivation of tumor suppressors [25]. Hypermethylation of CpG islands affect promoter regions of tumor suppressor genes leading to their inactivation and cancer progression [27, 29].

Therefore, methylation inhibitors such as Azacitidin (Vidaza®) are in use for cancer treatment. They could restore the function of tumor suppressor genes leading to reduced cancer growth [29]. The inhibitor Azacitidin is a nucleoside analoga with a nitrogen on the 5´-position. It is incorporated into DNA and therefore prevents DNA methyltransferases (DNMT) from methylation on the 5´-position [27]. One arising question could be whether this drug cause genomic instability through demethylation of normally highly methylated promoters as

in the inactivated X-chromosome in women. The question about genomic instability through transposable elements is under further investigation, but in case of X-inactivation already investigated. Inactivation of the X-chromosome is not affected by the drug [27].

Methylation occurs at the 5´-position of cytosines catalysed by DNA methyltransferases (DMNT) resulting in 5´-methyl cytosine. In humans, methylation occurs only on cytosines before guanosines (CpGs, the shortest possible palindrome) which are often enriched in so-called CpG-island next to promoter regions. Usually, CpG-islands are unmethylated in or next to promoter regions to maintain gene transcription, with exceptions of imprinted genes and the second X-chromosome in women [28]. Different aberrant methylation-patterns are typical in cancer. CpG-islands in promoter regions (of tumor suppressor genes) are hypermethylated, which prevent transcription initiation and lead to loss of gene function (*e.g.* as second hit following Knudsens two-hit-hypothesis), and some regions such as pericentromeric heterochromatin, which are normally highly methylated, are hypomethylated [27, 28]. Loss of methylation in pericentromeric regions of chromosomes could result in altered replication and decreased chromosomal stability. Additionally, hypomethylation can cause genetic instability through higher activity of transposable elements [28]. When DNA is hypermethylated at CpG-islands of promoter regions, chromatin is tightly packed and transcription cannot be initiated [30] [27, 28].

The histone code seems to be connected to DNA methylation. Methylations sites in histone H3 have a significant role in determining transcriptional active and repressive sites. For example methylation of lysine 9 is transcriptional repressive, whereas methylation of lysine 4 is transcriptional active [27].

Not only methylation as a gene sequence based DNA-modification affecting gene expression but also histone acetylation is important in transcription regulation. Enzymes called histone deacetylases (HDAC) are responsible for deacetylation resulting in a transcriptionally inactive state. Histon acetylation would lead to a more open conformation of the chromatin and therefore allow the access for transcription initiation [28, 29]. In cancer therapy, HDAC inhibitors are used which result in increased gene expression of putatively silenced tumor suppressor genes which could lead to apoptosis, cell cycle and growth arrest [29, 31, 32]. Nevertheless, DNA methylation is dominant in comparison to histone acetylation, therefore HDAC inhibitors are often used together with methylation inhibitors [29, 32].

DNA methylation in ovarian cancer

Epithelial ovarian cancer occurs in 90% of cases sporadic and about 10% are inherited. Most of inherited ovarian cancer patients carry *BRCA1* or *BRCA2* mutations. Several epigenetic phenomena could be observed in ovarian cancer. Heterochromatin is globally hypomethylated and CpG-islands in promoter regions of tumor suppressors (e.g. *BRCA1*) are hypermethylated leading to decreased expression. This leads to uncontrolled cell proliferation, metastasis and tumor progression. Hypermethylation of *BRCA1* has been found in 15% of sporadic ovarian carcinomas and is reported to be more frequently in high grade serous ovarian carcinomas. Several other tumor suppressor genes seems to be affected from hypermethylation including DNA mismatch repair (MMR) genes. Other genes are p15 and p16, which are involved in cell cycle control, E-Cadherin, H-Cadherin and Hox genes are responsible for differentiation and development. As mentioned above, hypomethylation results in genomic instability through increased expression of transposable elements. Hypomethylation in centromeric regions can lead to chromosomal translocations. Additionally, oncogenes are overexpressed in ovarian cancer due to decreased methylation. Genes involved in drug transport such as *ABCG2*, a transporter responsible for taxane resistance, and *TUBB* are affected from deregulated methylation leading to drug resistance [25].

Methylation changes are associated with histological types and stages of ovarian cancer. Hypomethylation is common in advanced stage disease (FIGO III and IV) and indicate poor outcome. Serous ovarian cancer patients show more often and more pronounced hypomethylation in comparison to other subtypes, whereas hypermethylation seems not so important in high grade serous ovarian cancer development. In contrast, clear cell carcinomas show CpG-island hypermethylation more frequently. Early FIGO stages (I and II) have more methylation in tumor suppressor genes than later FIGO stages. In low grade endometrioid ovarian cancer CpG-islands are less hypermethylated than in high grade stages. High grade serous stages can be distinguished from low grade stages. In general, high grade serous stages show less hypermethylation than low grade stages, therefore it seems that they are more similar to normal tissue regarding methylation patterns, which exemplifies again the type classification, *i.e.* type I versus type II, see above, surpassing the histological classification [33]. Regarding chemotherapy resistance, several effects on methylation patterns have been reported. It has been stated that methylation changes may occur in resistance development

[33]. Cell line experiments with chemotherapy resistant cells treated with Cisplatin and DNA methylation inhibitor Deciatabine show recurring sensitizing to Cisplatin [33, 34].

Cell death pathways: Apoptosis and Necroptosis

HIPEC is probably associated with different types of cell death, including apoptosis and the recently described and increasingly investigated necroptosis. Besides apoptosis and necroptosis there are several other cell death types including necrosis which is an uncontrolled lytic event. Cell death is a crucial event in enabling tissue homeostasis. In multicellular organisms there must be a balance between cell death, proliferation and differentiation. Different forms of cell death are implicated in human immunological pathologies and other diseases including neurodegeneration and cancer [1].

Apoptosis

Apoptosis is a non–lytic programmed cell death and thought to be immunologically silent because apoptotic cells don´t release their cytoplasmic contents. Morphologically apoptotic cells show cell shrinkage and rounding, pyknosis (chromatin condensation), membrane blebbing and release of apoptotic bodies [35].

There are two main pathways of apoptosis called the extrinsic and the intrinsic (mitochondrial) pathway and additionally the perforin/granzyme pathway mediated by cytotoxic T cells (CTLs) and natural killer cells (NK). Granzymes were delivered in granules from CTLs and NK cells through a pore forming protein called perforin to the target cell. Granzyme B activate pro-caspase 10 and further activate caspase 3 or directly activate caspase 3 which leads then to the apoptosis execution pathway. Granzyme A activates apoptotic DNA cleavage [35].

The extrinsic pathway is driven by extracellular stress signals that bind to death receptors from the TNF superfamily. Other ligands that stimulate apoptosis are FasL, TNFα, Apo3L, Apo2L and TNF- related apoptosis inducing ligand (TRAIL). Upon ligand binding adapter proteins like FADD or TRADD are recruited which binds to caspase 8 and leads subsequentially to caspase 8 activation through the death induced signaling complex (DISC). Caspase 8 activation lead to activation of executioner caspases caspase 3, 6, and 7. This results in degradation of nuclear proteins and cytoskeletal proteins, cytokeratin, PARP and others.

Caspase 3 activation leads to activation of endonuclease CAD which degrades chromosomal DNA and causes pyknosis. The activation of these executioner caspases are responsible for the morphological changes [35].

The intrinsic pathway is initiated by internal stimuli like DNA damage, growth and hormone factor withdrawal, radiation, toxins, hypoxia, viral infections and free radicals. These stimuli result in mitochondrial outer membrane permeabilisation (MOMP) and following cytochrome c release which binds and activates apoptotic protease activating factor 1 (Apaf-1) which then oligomerizes and thereby promotes apoptosome formation and caspase 9 activation. Upon caspase 9 activation executioner caspases (caspase 3 and caspase 7) are activated [1, 35].

Other proteins like Smac that are released by MOMP block inhibitors of apoptosis like caspase inhibitor "X linked inhibitor of apoptosis protein" (XIAP). Pro-apoptotic proteins like AIF, endonuclease G and CAD are released from mitochondria and cause DNA fragmentation and nuclear chromatin condensation. This happens at late stage of apoptosis when the cell has been committed to death [1, 35].

The apoptotic mitochondrial pathway is regulated by Bcl-2 family proteins. They can be pro and anti-apoptotic and finally determine if the cell undergo apoptosis or not. Anti-apoptotic proteins like BCL-2, pro-apoptotic BH3 only proteins like PUMA, BID, BIM and pro-apoptotic effector proteins like BAX, BAK and BOK are the three subfamilies of Bcl2 proteins regulating apoptosis. BH3 only proteins can activate BAX and BAK and therefore promote MOMP [1].

Once a cell underwent apoptosis and released apoptotic bodies they have to be cleared by the immune system. This is done by efferocytosis where apoptotic bodies release "*find me and eat me signals"* to be phagocytosed. Efferocytosis is immunologically silent. If the clearance of apoptotic bodies fails it will lead to secondary necrosis which causes DAMP release and is therefore not immunologically silent anymore [1, 35].

There is also a cross talk between the extrinsic and intrinsic pathways through caspase 8. It can cleave BID into tBID and activate BAX and BAK and therefore initiate MOMP which leads to activation of caspase 9. Caspase 8 is an important regulatory protein together with RIPK1 and RIPK3. If caspase 8 is activated, RIPK1 and RIPK3 are cleaved. If caspase 8 is inhibited, signaling via RIPK1 extends and activates RIPK3 which then induce necroptosis [1].

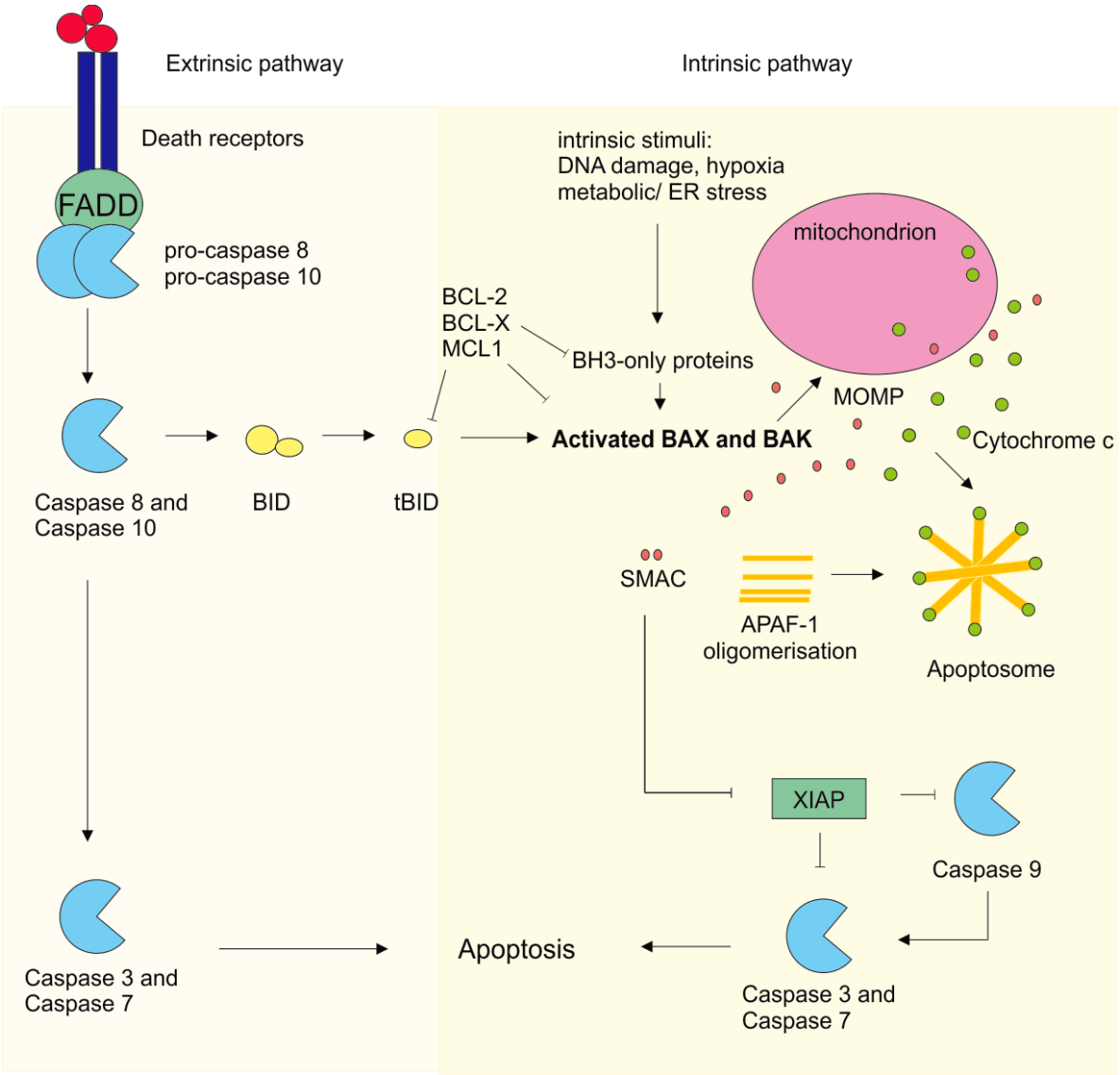

Figure 2. Apoptosis.

There are two major types of apoptotic signaling pathways – the intrinsic and extrinsic signaling pathway. The extrinsic signaling pathway is induced by external death signal that bind to death receptors such as those for TRAIL and FAS. Upon induction, FADD and procaspase 8 bind and activate caspase 8 which sub sequentially activate caspase 3 and caspase 7 which lead to apoptosis. The intrinsic pathway is induced by internal stimuli like DNA damage and endoplasmatic reticulum (ER) stress which result in MOMP and cytochrome c release and apoptosome formation. Caspase 9 is then activated and further caspase 3 and caspase 7. Upon MOMP other proteins like SMAC are released which inhibit XIAP and promote apoptosis. Image adapted from [1].

Necroptosis

Necroptosis is an alternative cell death pathway which is regarded to be immunological active. It is a regulated mechanism in response to stress and active mostly upon blocked apoptosis. It can be induced by several cytokines like TNF alpha and chemotherapeutic drugs. Due to the fact that necroptosis is regarded to be immunological active – in contrast to apoptosis – it is an attractive strategy for cancer treatment.

Necroptosis is morphologically similar to necrosis. Necroptotic cells have no intact plasma membrane and they show cytoplasm swelling and swollen mitochondria, whereas apoptotic cells have an intact plasma membrane and no vacuolization or swollen mitochondria. In contrast, apoptotic cells have condensed and fragmented nuclei. Necroptosis is a less energy consuming process than apoptosis, therefore a necroptotic cell needs less ATP. One of the most important facts is that necroptosis is immunologically active. Through their plasma membrane disruption they release so called damage-associated molecular patterns (DAMPs) which trigger an immune response. Despite the differences, necroptosis is tightly connected to apoptosis. In necroptosis the key regulator proteins RIPK1, RIPK3, and MLKL are involved. Stimuli are members of the TNF family like TNFα, TRAIL, FAS ligand, LPS, dsRNA, CD3, CD28, and INFγ. Upon extrinsic stimulation with TNFα, the receptors get activated and interact with RIPK1. RIPK1 then recruits cIAPs to activate pro-survival NF-κB and MAPKs. RIPK1 itself gets polyubiquitinated and degraded. If cIAPs are inhibited by SMAC, CYLD removes the polyubiquitin chain from RIPK1 and prevents from degradation. Then RIPK1 dissociates from the plasma membrane and form a complex with FADD and caspase 8 to induce apoptosis. If caspase 8 activity is inhibited, RIPK1 bind to RIPK3 through their RIP homotypic interaction motif (RHIM) domain which leads to autophosphorylation of RIPK3 and recruitment of MLKL. MLKL gets phosphorylated and oligomerizes and inserts into the plasma membrane leading to plasma membrane rupture and necroptotic death [8, 36]. It depends on the stimulus which complex is formed and if the cell is committed to death or if the cell survives. Upon TNF stimulation, complex I is formed which is composed of TRADD, TRAF2, IAP, LUBAC, and RIPK1. TRADD recruits TRAF, cIAP and LUBAC and ubiquitinylates RIPK1. This induces a pro-inflammatory signal and cell survival through MAPK and NF-κB activation. If complex I is destabilized another complex (TRADD, FADD, caspase 8) is formed which lead to caspase 8 dependent apoptosis. Complex IIb (RIPK1, RIPK3, FADD, caspase 8, $FLIP_L$) is formed if IAPs are

inhibited or depleted or upon NEMO, TAK1, Pelino knockdown which leads to apoptosis in a RIPK1 dependent way. If caspase 8 is inhibited, RIPK1 and RIPK3 bind to each other though their RHIM domains and form the necrosome. Upon Fas ligand stimulation, DISC is formed that activates caspase 8 to induce apoptosis. When caspase 8 is blocked it triggers necroptosis. Other stimuli like cellular stress, bacterial or viral infections can activate toll like receptors (TLR) that form a complex including TRIF which contains a RHIM domain and can directly bind to RIPK1 and RIPK3. TRIF can also directly activate RIPK3 in absence of RIPK1. Upon viral DNA stimulation, DNA-dependent activator of IFN regulatory factors (DAI) bind to RIPK3 through its RHIM domain and activate RIPK3 directly. Another example for RIPK3 activation without RIPK1 is through LPS stimulation and therefore activation of TRIF which binds through their RHIM domain directly to RIPK3 [36].

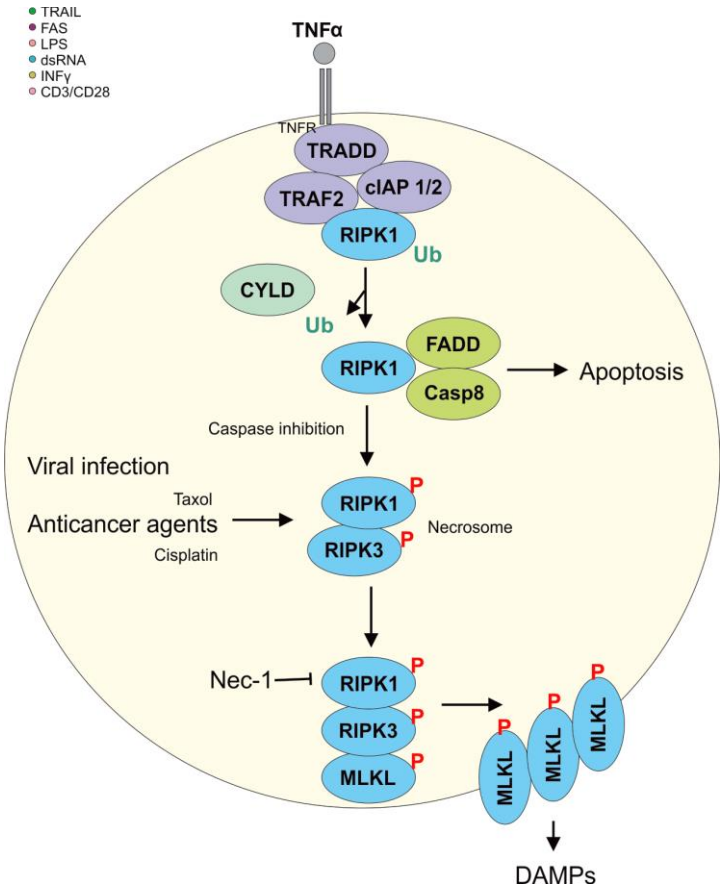

Figure 3. Mechanisms of necroptosis.
A) upon TNF α stimulation a complex with TRADD, TRAF2, cIAP1/2, and RIP1 is formed. RIP1 gets polyubiquitinated and degraded to induce a pro survival response and NF-kB activation. If RIPK1 is deubiquitinated by CYLD in the presence of CIAP inhibitors, RIP1 forms a complex with FADD and caspase 8 to induce apoptosis. If caspase 8 is blocked RIPK1 binds to RIPK3. RIPK3 gets autophosphorylated and recruits and phosphorylates MLKL. pMLKL oligomerises and locates to the plasma membrane and inserts and disrupts the plasma membrane to induce necroptosis [8].

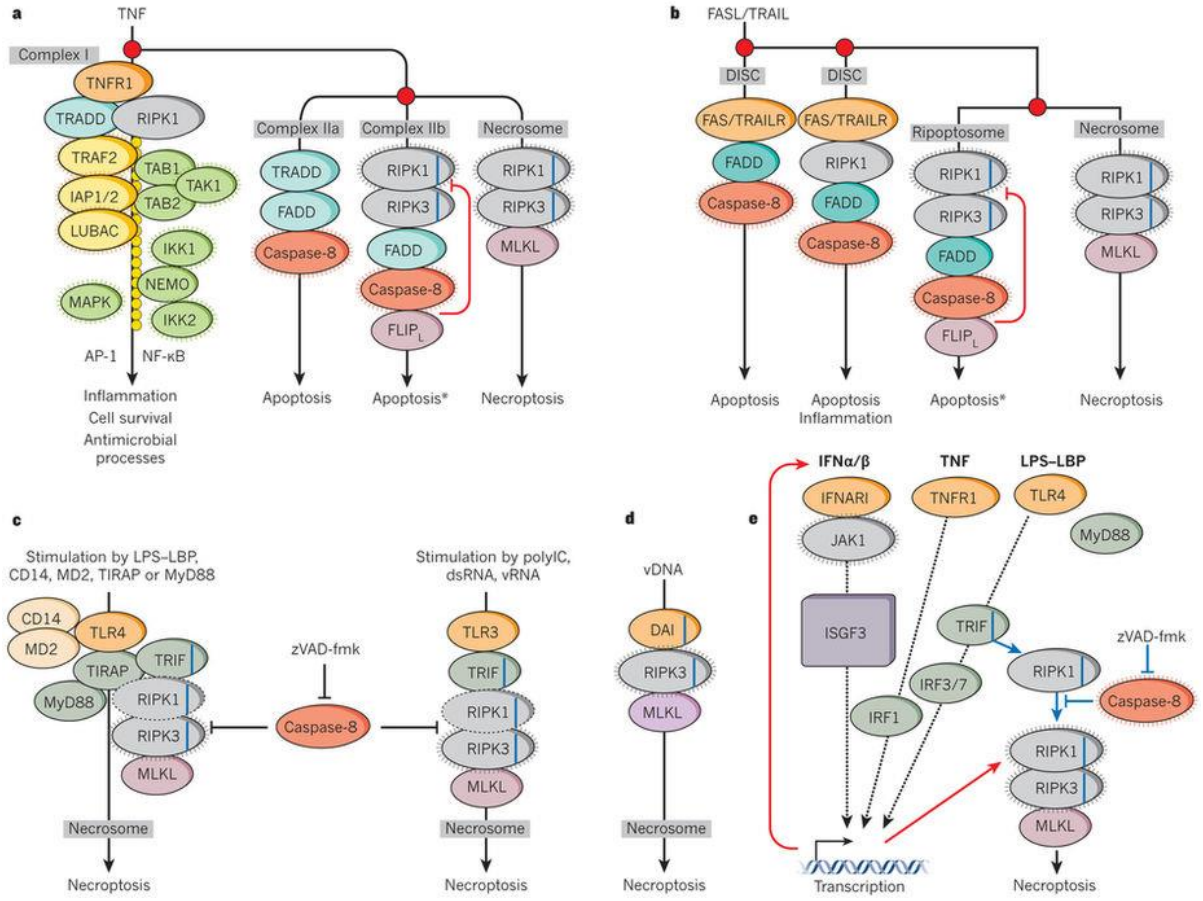

Figure 4. Different ways of complex formation to induce apoptosis or necroptosis.
A) TNF induction leads to complex I formation and MAPK activation and NF-κb activation though IKK2. B) upon FAS ligand stimulation DISC is formed that triggers caspase 8 dependent apoptosis. Ripotosome formation can also lead to caspase 8 dependent apoptosis. If caspase 8 is inhibited a necrosome is formed that leads to necroptosis. c) Upon stimulation with LPS, CD14, MD2, TIRAP or MyD88 TRL4 form a platform containing TRIF that bind to RIPK1 and RIPK3 to induce necroposis. D) viral DNA induce a protein named DAI that contains a RHIM domain and thereby binds to RIPK3 to trigger necroptosis. e) INF α and INF β induce Jak signaling and builds ISGF3, a transcription factor that can bind to the DNA to promote necrosome formation at the transcriptional level [36].

An important switching point is RIPK1: it determines if a cell survives or dies. In contrast, RIPK3 is always pro death but it can be suppressed by RIPK1. RIPK1 mediates cell death by apoptosis and necroptosis but it seems to be independent of NFκB activation. Mechanisms determining whether apoptosis or necroptosis occur are poorly understood. Some suggest that it depends on the catalytic activity of RIPK3 whether apoptosis or necroptosis occurs. If RIPK3 is catalytic active it triggers necroptosis. Indeed one of the most important factors in determining whether a cell dies by apoptosis or necroptosis is caspase 8. When caspase 8 is blocked the cell dies by necroptosis. Loss of cIAP may be supporting apoptosis [36].

Specific inhibitors of necroptosis are Necrostatin-1 (Nec-1), Necrosulfonamide (NSA), GSK843, and GSK872. Nec-1 inhibits RIPK1, NSA inhibits MLKL kinase and GSK843 and GSK872 inhibits RIPK3 [8].

Necroptosis in inflammation and cancer

Necroptosis is thought to be a potent inducer of immune response through their DAMP release. The necroptotic cell releases eat me signals - as Annexin A1, phosphatidylserine and C-type lectin (Clec9A) – which results in phagocyte recruitment. The dying cell gets engulfed by phagocytic cells like macrophages, monocytes, dendritic cells, and neutrophils which produce pro inflammatory cytokines and chemokines to trigger an adaptive immune response. Necroptosis triggers immune response through DAMP release. DAMPs as HMGB1, interleukin, and ATP can enhance immune response, but the role of how DAMPs get released by a necroptotic cell is not fully clarified. Through DAMP release a dying cell can induce an adaptive immune reaction by providing antigens and inflammatory stimuli for dendritic cells which then activate CD8+ cells through antigen cross priming. This results in expression of cytokines and chemokines to generate an anti-tumor response [37].

Necroptosis is linked to anti-tumor immunity. Different anti-cancer drugs such as DNA damaging agents induce necroptosis, as for example Cisplatin, which induce RIPK3 dependent necroptosis. Taxol an antimitotic chemotherapeutic drug activates RIPK1 and induces also necroptosis [8]. Upon Taxol treatment the two mitotic kinases Aurora A and Plk1 phosphorylate FADD resulting in a double phosphorylated FADD that activates RIPK1 and induces necroptosis [38]. Other agents like etoposide, 5- Fluorouracil and Sorafenib induce RIPK1 dependent necroptosis. Sorafenib is a multi-kinase inhibitor drug that induces autophagy and activates RIPK1. Together with Givinostat, Sorafenib induces RIPK1 dependent necroptosis through ROS production and Bim activation. Chalcone-24 acts on cIAP1 and cIAP 2 and degrades it and therefore promotes ripotosome activation. In cervical cancer cells polyinosine-polycytidylic acid (Poly (I:C)) cause RIPK3 dependent necroptosis and production of IL12 which induces an anti-tumor immune reaction [8].

RIPK1, RIPK3, MLKL, and CYLD are key players of necroptosis. Dysfunction or depletion of these proteins cause defective necroptosis. In some cancer cells alterations of these proteins prevent cells from necroptosis [8].

Heat shock proteins

Heat shock proteins are molecular chaperones and are needed for generation, function, and stability of proteins [39]. Heat shock proteins (Hsp), especially Hsp90, have an essential role in cancer treatment and tumor progression. Hsp90 bind to several kinases and pseudokinases and influences their functions. Loss of Hsp90 would result in ubiquitination and degradation of this kinases. One of the kinases in connection with necroptosis is RIPK1. Also RIPK3 was identified to be a target of Hsp90. Upon inhibition of Hsp90 and knockdown of its co-chaperone CDC37, phosphorylation of RIPK3 is blocked and necrosome formation inhibited. Also RIPK1 independent necroptosis is blocked by inhibition of Hsp90, indicating that Hsp90 act directly on RIPK3. Also the function of MLKL is modulated by Hsp90. Increased expression of Hsp90 results in increased MLKL oligomerization and membrane integration and therefore promotes MLKL dependent cell death. These findings were shown by overexpression of Hsp90 in RIPK3 deficient 293T cells which show enhanced MLKL induced necroptosis. Furthermore, inhibition of Hsp90 prevents oligomerization of MLKL and membrane integration. Treatment with Hsp90 inhibitors show decreased necroptosis induction. Therefore Hsp90 is an important regulator for necroptosis [40].

Transfer-RNA halves and fragments

Transfer RNA halves (tiRNAs) belong to a group of small non coding RNAs that are produced by angiogenin upon stress induction. Activated angiogenin cleaves mature transfer RNAs (tRNAs) in the anticodon loop to produce 5´and 3´ halves with 30-50 nucleotides [41]. 5´tiRNAs inhibit protein translation by replacing eukaryotic initiation factors [42].

TRNA fragments (tRFs) are independent of angiogenin cleavage. They are smaller than tiRNAs with about 12-30 nucleotides and results of cleavage at several cleavage sites. 5´tRF are produced by cleavage in the D-loop by Dicer. 3´tRF are produced by cleavage in the T loop by Dicer or angiogenin. tRNA fragments can also derive from pre-tRNA as 3´U tRFs that are cleaved by RNase Z and contain 3´trailer [41].

TRNA halves and fragments have several biological functions in biogenesis. They act on protein translation, stress granule assembly, RNA silencing, cell proliferation, apoptosis inhibition via cytochrome c, mRNA destabilization by sequestering YBX1 and tumor progression [7, 43]. 5´tiRNA can inhibit protein translation through replacement of eukaryotic initiation factors. Upon stress induction *e.g.* hypoxia, 5´tiRNA can induce formation of stress

granules and inhibition of protein synthesis [42]. Stress granules are formed from translational stalled mRNAs known as untranslating messenger ribonucleoproteins (mRNPs) [44]. Stress granules are involved translation by re-initiation or degradation, signaling pathways and antiviral response [44]. Interestingly, 5´tiRNA and not 3´tiRNA induce optimal translational inhibition and stress granule assembly [7]. In addition, tiRNAs and tRFs act on tumor progression. Upon cellular stress, stress granules are produced and translation is inhibited, but inhibited cell death can promote cancer growth. Furthermore, tRFs bind to YBX1 and therefore oncogenic mRNAs are destabilized which result in less metastasis formation [42].

Another important point is that tRNA halves interact with cytochrome c and therefore prevent cells from apoptosis. Cellular stress *e.g.* hyperosmotic stress leads to cytochrome c release from mitochondria and apoptosome formation and apoptosis. Under stress conditions released cytochrome c can also bind to a complex consisting of RNPs and tiRNAs, generated by angiogenin cleavage. This complex prevents cells from apoptosis and triggers cell survival [7].

There are many functions for tiRNAs and tRFs in signaling pathways and cellular response to stress expected. Furthermore, they are associated with human diseases like cancer and neurological disorders [42, 43].

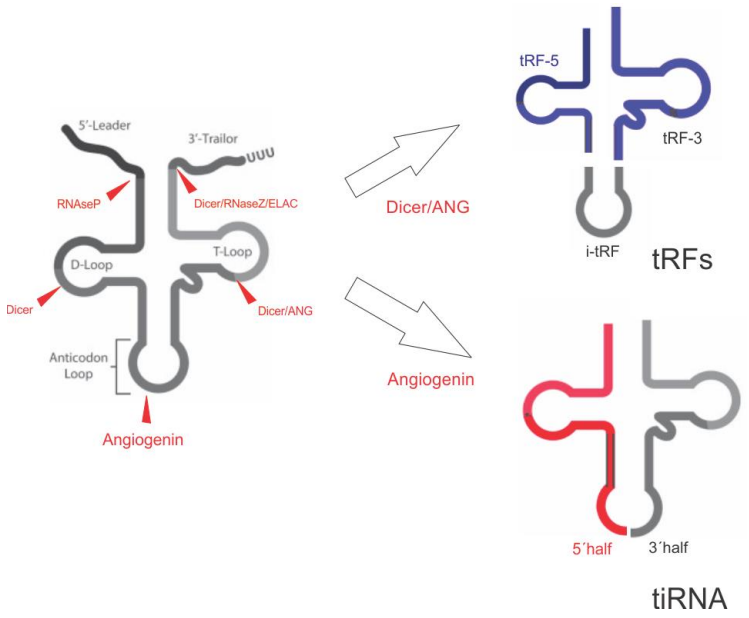

Figure 5. Generation of tRFs and tiRNA.
Pre-transfer RNA or mature tRNA is cleaved under stress conditions by angiogenin to produce 5´and 3´halfs. tRFs are produce by several cleavage sites. 3´tRF by Dicer or angiogenin cleavage in the T-loop and 5´tRF by Dicer cleavage in the D-loop. tRFs are shorter than tiRNAs with 12 to 30 nucleotides [41].

Hypothesis and outline of the project.

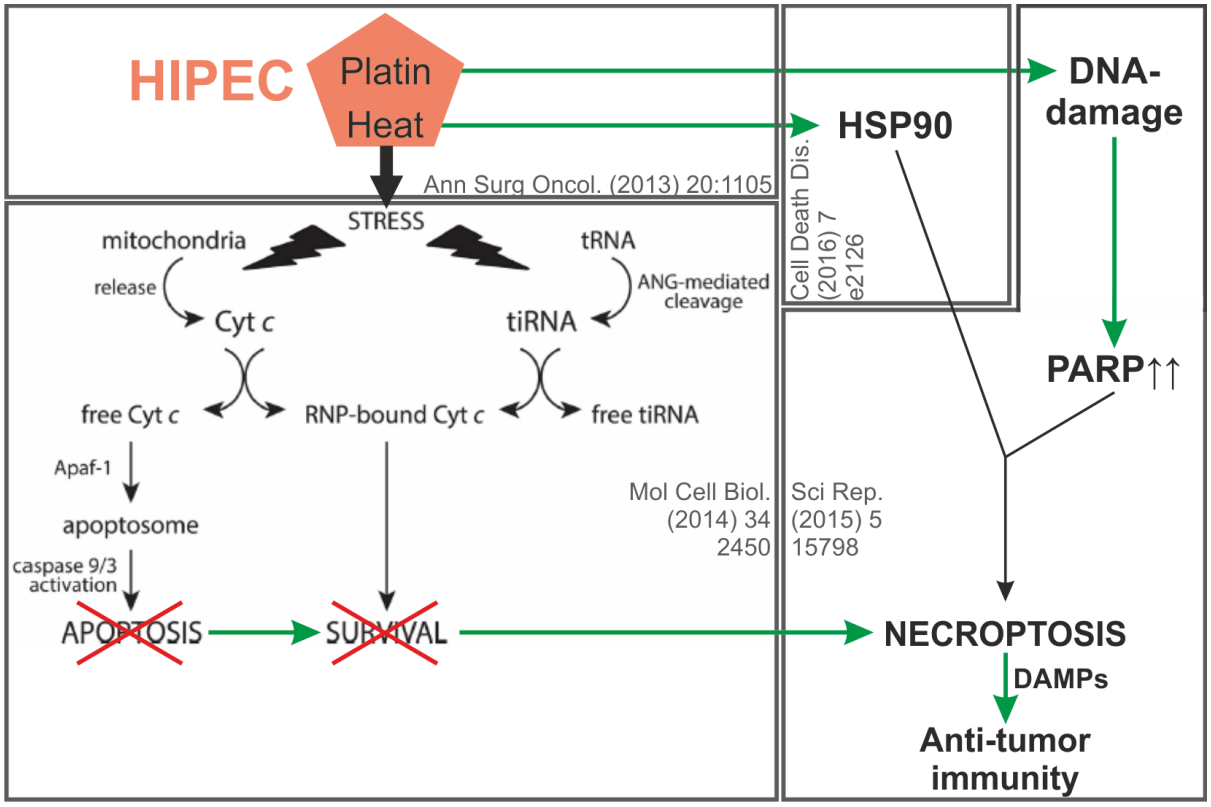

Figure 6. Schematic overview of the hypothesis for this work.
Platin and heat stress could cause tRNA cleavage by angiogenin resulting tiRNA. tiRNA can bind cytochrome c and prevent apoptosome formation and apoptosis. Heat shock could result in upregulation of Hsp90 which can promote necroptosis. Upon Carboplatin treatment DNA damage will be induced. If cell death by necroptosis occurs DAMPs are released that can cause an anti-tumor immunity. Image adapted from [7, 40, 45, 46].

Aim of this study was to elucidate the impact of HIPEC on tumor tissue and tumor cell line cells, *i.e.* whether they undergo apoptosis or necroptosis and the effect of tRNA halves (tiRNA) and tRNA fragments (tRFs) on these processes. A shift from apoptosis to necroptosis would be expected as favorable for patients because of the immunogenic nature of necroptosis. We used different high grade serious ovarian cancer tumor cell lines and immortalized non-malignant cell lines from the miliary or non-miliary spread type. Tumor cell lines from non-miliary spread type were ES-2 and Tyk-nu and from the miliary spread type, CAOV-3 and OVCAR-3. Fallopian tube cells, FT194 and FT33, and ovarian surface epithelial cells, IOSE364 and IOSE80, were used as precursor cell lines. Tumor cells from the miliary tumor spread type (CAOV-3 and OVCAR-3) were more epithelial-like and from putative tubal origin. Non miliary

tumor cells were regarded as more mesenchymal-like and putative from ovarian origin. FT cells were of tubal origin and IOSE of ovarian origin and used as reference cell lines [4-6].

The cells were treated with hyperthermic (42°C) compared to normothermic (37°C) chemotherapy. After treatment, cells were incubated in fresh cell culture medium for 30 minutes or 20 hours to estimate early and late effects, like necroptosis, tiRNA changes, or Hsp expression changes. Cells were fixed, embedded in agarose and then in paraffin to obtain FFPE cell blocks, and stained for apoptosis and necroptosis using typical markers. For apoptosis antibodies against cleaved PARP, M30, and caspase 3 and for necroptosis antibodies against pMLKL, RIPK3 and Hsp90 were used for staining. Stained cells were scanned with TissueFAX® and quantified with Cellprofiler. Additionally, co-localization was evaluated by confocal microscopy.

During hyperthermic chemotherapy treatment we expected a shift towards necroptosis. Hsp90 is a key player of necroptosis and could assist necrosome formation. Upon necroptosis anti-tumor immunity can be boosted through DAMP release of necroptotic cells which could be beneficial for patients' outcome. Furthermore we expected a change in tRNA fragment abundance. Upon HIPEC more tiRNA could be produced which can bind cytochrome c and therefore prevent apoptosome formation [7]. tRNA fragment abundance was determined after 30 minutes after chemotherapy treatment, as it is known that fragmentation of tRNAs is a fast stress response mechanisms. We wanted to find out if tiRNA is involved in triggering of necroptosis and therefore involved in better outcome for HGSC patients. Additionally, we looked for changes in DNA methylation after 20 hours after HIPEC treatment to search for fast epigenetic mechanisms.

Methods

Cell Culture

Different ovarian cancer cell lines of putative milary and non-milary spread type according to Auer *et al.* (2015 and 2017) classification were used for HIPEC treatment [4, 5]. Each two cell lines of milary spread type of putative tubal origin (OVCAR-3 and CAOV-3) and non-milary spread type of putative ovarian origin (ES-2 and Tyk-nu) and the corresponding precursor cell lines, fallopian tube cells (FT194 and FT33) of tubal origin and two IOSE (IOSE80 and IOSE364) of ovarian origin were cultivated to a high confluency of about 80% [4, 5]. Cells were cultured at 37°C with 5% CO2 in a humidified atmosphere with different media to create the best conditions for optimal cell growth as listed in Table 2 [5].

Cell lines	Tumor spread type	Cell culture medium
ES-2	non-miliary	RPMI with 10% FCS
Tyk-nu	non-miliary	α-MEM with 10% FCS
OVCAR-3	miliary	RPMI with 20% FCS
CAOV-3	miliary	DMEM with 10% FCS
IOSE80	Precursor cell line for non-miliary	Medium 199 (Sigma M5017) + Medium MCDB 105 (Sigma M6395) in a ratio of 1:1 with 5% FCS
IOSE364	Precursor cell line for non-miliary	Medium 199 (Sigma M5017)+ Medium MCDB 105 (Sigma M6395) in a ratio of 1:1 with 5% FCS
FT33	Precursor cell line for miliary	DMEM/HamsF12 (Gibco 32500-035) with 10% FCS
FT194	Precursor cell line for miliary	DMEM/HamsF12 (Gibco 32500-035) with 10% FCS

Table 2. Used cell lines with recommended and used cell culture media.

In vitro ”HIPEC“ treatment of tumor cell lines

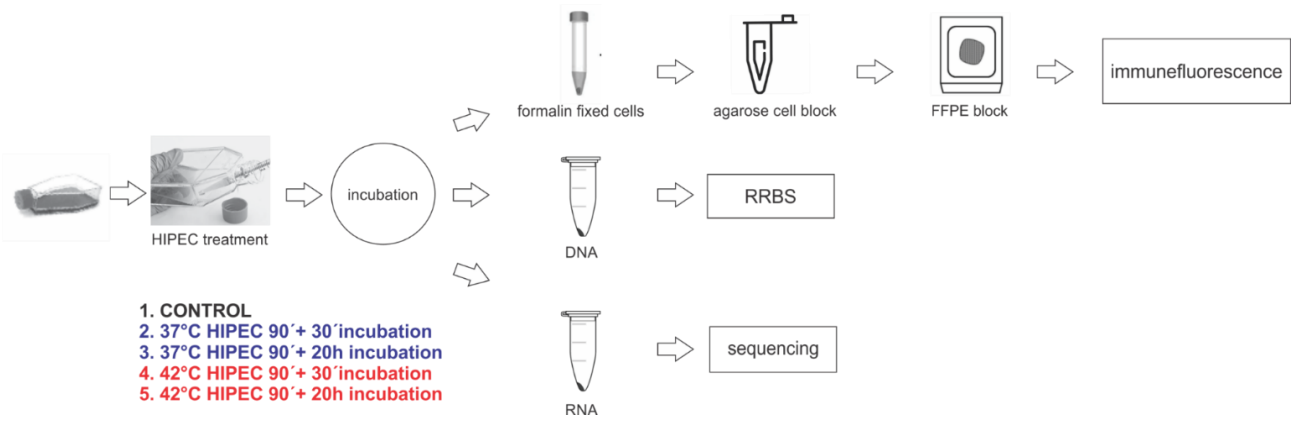

Figure 7. Scheme of the *in vitro* HIPEC treatment.
Cells were cultivated in T75 flasks and treated according HIPEC criteria for 90 minutes. We established 5 conditions – one control group, chemotherapy treatment at 37°C and 42°C with subsequent 30 minutes and 20 hours incubation in fresh cell culture medium after treatment to induce necroptosis. We took samples for RNA sequencing after 30 minutes and 20 hours to establish changes in tRNA fragment abundance. Additionally, we took samples for RRBS sequencing after 20 hours to analyze DNA methylation changes. The remaining cells were fixed and embedded in agarose and paraffin (FFPE cell blocks) and used for immunofluorescence staining.

Hyperthermic intraperitoneal chemotherapy (HIPEC) is experimentally used for treatment of patients suffering from high grade serous ovarian cancer. To simulate a HIPEC treatment *in vitro* we used four cancer cell lines and four precursor cell lines as described above. This cell lines were grown to a high confluency and treated according HIPEC conditions. Chemotherapy treatment was done for 90 minutes with subsequent different incubation times after chemotherapy treatment in fresh cell culture medium of 30 minutes for early events like Hsp90 or tRNA fragment increase or apoptosis and 20 hours for late events like necroptosis or DNA methylation changes.

Five conditions were used: 1) Control group cultivated at 37°C without chemotherapeutics 2) chemotherapy treatment at 37°C with 30 minutes post-incubation 3) chemotherapy treatment at 37°C with 20 hours post-incubation 4) chemotherapy at 42°C with 30 minutes post-incubation and 5) chemotherapy at 42°C with 20 hours post-incubation. Chemotherapy treatment was done with a solution of Paclitaxel (6 mg/ml) and Carboplatin (10 mg/ml), similar concentrations are planned also for usage in patients, in respective cell culture medium per cell line. Pre-warmed chemotherapeutic solution per condition were used to

incubate cells at 42°C or 37°C for 90 minutes. After 90 minutes, the solution was removed and cells were washed carefully with PBS. Fresh pre-heated medium was added and incubated for further 30 minutes or overnight for 20 h at 37°C with 5% CO2 to allow cells to develop early and late effects. After 30 minutes the first samples were taken. First, a small cell pellet was taken and lysed with QIAzol® Lysis Reagent (Qiagen) and stored at -80°C for RNA preparation to determine tRNA fragment abundance. Second, a cell pellet for DNA preparation was taken and stored at -20°C. The remaining cell solution was centrifuged at 1,300 rpm for 5 minutes and fixed with 4.5% formaldehyde with shaking for 30 minutes. Cells were re-suspended in PBS and centrifuged at 2,000 rpm at room temperature for five minutes. The cell pellet was resuspended in 1 ml PBS and transferred to a fresh 1.5 ml Eppendorf tube®. The suspension was centrifuged at 2,000 rpm for 5 minutes at room temperature. About 200-400 µl 1.5 % molten Agarose in PBS, depending on pellet size, were added and vortexed until cells were homogenous dispersed. Upon embedding of cells in agarose the solidified agarose blocks were removed from the tubes and incubated in 7.5% formaldehyde for further fixation and afterwards embedded into paraffin blocks. Later these FFPE cell blocks were sliced and used for immunofluorescence staining. For the samples after 20 hours incubation after HIPEC treatment the same procedures were performed.

Immunefluorescence (IF) staining of FFPE sections

Embedded agarose blocks of cell lines or ascites were cut in 4-5 µm sections and incubated for one hour at 58°C. For deparaffinization and rehydration, sections were incubated in xylene and a descending alcohol concentration row as follows: 2x xylene for 5 minutes, 2x 100% ethanol for 3 min, 1x 96% ethanol for 1 min, 1x 80% ethanol for 1 min and at least 1x 70% ethanol for 1 min. Slides were washed in distilled water for 5 minutes. Antigen retrieval was done in an autoclave with 1 mM EDTA at pH 8 for about 8 minutes until the autoclave reached 118°C. Afterwards the solution was cooled slowly until it reached room temperature. Non-specific binding sites were blocked by using Ultra V Blocking reagents (Thermo Fisher Scientific, USA) for exactly seven minutes. Slides were washed with PBS. Primary antibody solution in DAKO antibody diluent was added and incubated for one hour at room temperature in a humidified incubation tray.

One multicolor panel was used for staining with antibodies against pMLKL, RIPK3, and Hsp90 for necroptosis detection (Table 3). In addition, negative staining controls with missing primary antibodies were performed. After incubation slides were washed 3x with PBS with 0.1% Tween for 3 min. Secondary antibodies as described in Table 3 (1:1,000 dilution in 6% BSA) were incubated for 45 minutes at room temperature. Slides were washed 3x for 3 minutes each and nuclei were stained with DAPI for 5 minutes and mounted with Fluoromount-G® (Southern Biotech).

Primary antibody		Secondary antibody
Anti-MLKL (phosphor S358)	RabMab, ab287091; Abcam	anti-rabbit conjugated with Alexa Fluor® 488 (A11059, Invitrogen)
Anti-RIPK3	Mouse IgG2a, LS-C338650; LifeSpan BioSciences	anti-mouse IgG2a conjugated with Alexa Fluor® 647 (A21241, Invitrogen)
Anti- Hsp90 (mouse IgM)	Mouse IgM, ab13492; Abcam	anti-mouse IgM conjugated with Alexa Fluor® 555 (A21426, Invitrogen)

Table 3. Used antibody panel.

Data analysis – CellProfiler 2.2.0

The stained slides were scanned with TissueFAX® (TissueGnostics) and imaged via confocal microscopy (Zeiss, LSM700). CellProfiler™ software 2.2.0 was used for automated quantitative analysis [47]. Images from TissueFAX were loaded into the pipeline and metadata were extracted from corresponding file names. In the “Names and Types” step, fluorescent channels provided by file name suffixes from TissueFAX image files were assigned to the corresponing necroptosis markers (pMLKL, RIPK3, and Hsp90) to name the images in the program for further usage (*e.g.* Texa.tif corresponds to Hsp90). The first pre-analysis step is the “illumination correction” (using the *Fit Polynomial* function), correcting for uneven illumination in the pictures. With this step illumination artifacts can be corrected by the program to improve further quantitative fluorescence readouts.

Next the primary objects which are the nuclei were identified from corrected DAPI stained images, using allowed diameters of 6 to 140 pixel per units, the global threshold strategy and the Otsu method (Fig. 8). Afterwards clumped objects were identified by the “measure object neighbours” step and thereby objects were separated. On the basis of the primary object identification (*i.e.* the cell nuclei), the cytoplasm of each cell was defined by the

"ExpandOrShrink" function (*i.e.* 15 pixels). Then the upper quantile fluorescence intensity of the cytoplasm region (without the nucleic region) was determined for each marker and two of them plotted in scatter plots (X- and Y-axes) and the third coded as color of the points, from blue (low) to red (high) [47].

The confocal images were analyzed via software Imaris x64 7.4.2 (Bitplane AG, Zurich, Switzerland).

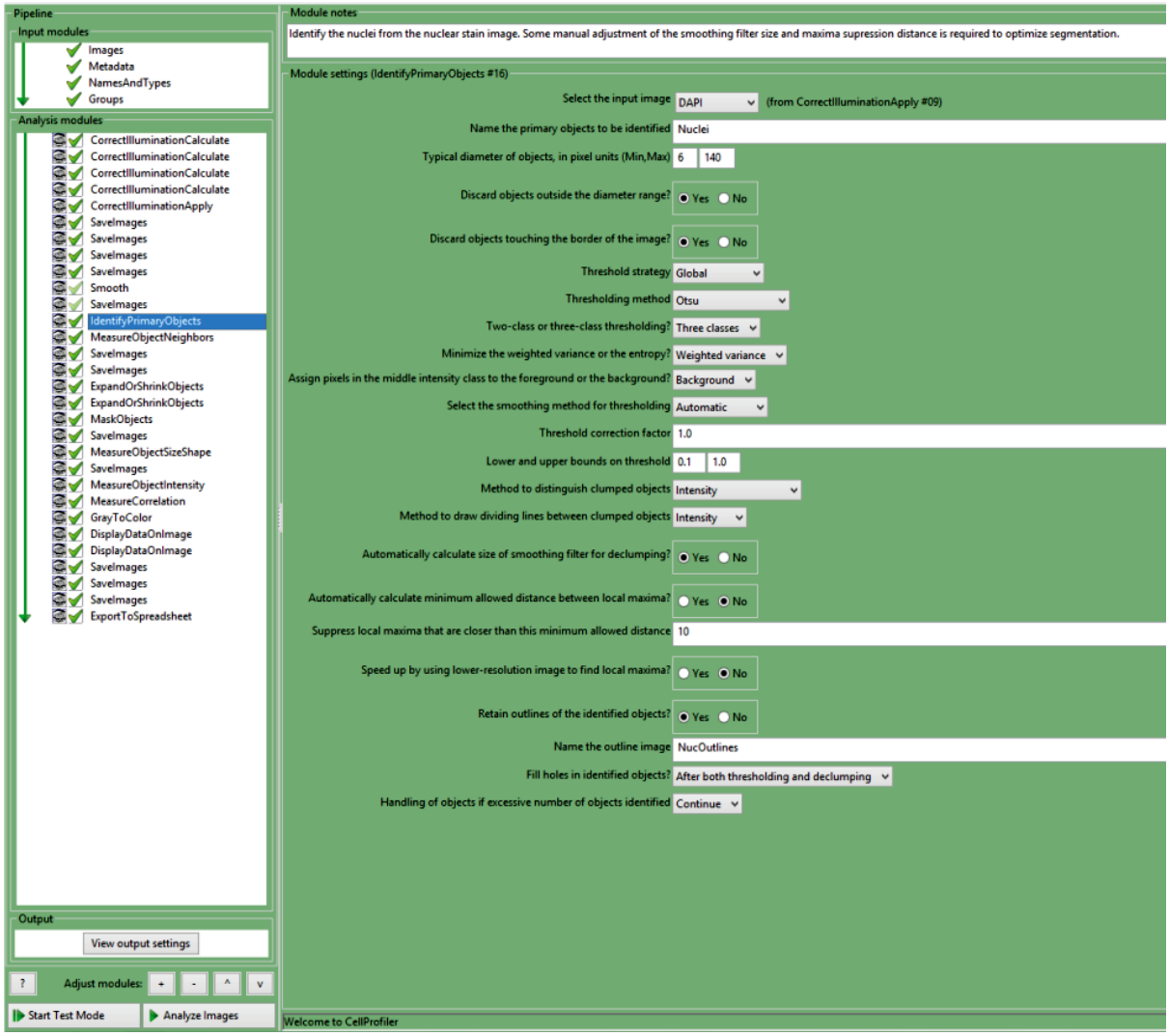

Figure 8. Used CellProfiler Pipeline.

Overview of input and analyses modules of the CellProfiler pipeline used for quantification of the fluorescence intensities. First, images were corrected to reduce unwanted illumination artifacts and to normalize fluorescence intesitites. Second, nuclei were determined from corrected DAPI.tif images (recorded via TissueFAX) with diameter constraints from 6 to 140 pixel per unit. The Otsu method and a global thresholding strategy were used with intensities between 0.1 and 1.0 as thresholds to distiguish between objects and background. Output images of this module were named nuclei outlines which represent the nuclei. Third, clumped objects were seperated and cytoplasm was defined from primary objects (nuclei). The upper quartile fluorescence intensity of the cytoplasm (without the nucleic region) was calculated to determine the staining intensity of each marker and each cell, used for further analyses. [47].

RNA Preparation

RNA samples collected in Qiazol® from different cells lines (as described above) were isolated according Qiagen® miRNeasy® Mini Kit. Cells were used at counts of about 10^5 cells per 700 µl Qiazol®. The homogenate was incubated for 5 min at room temperature and 4 µl of a mixture of small (ExiSeq Spike-in (Exiqon)) and large (ERCC RNA Spike-In Mix, Thermo Fisher Scientific) RNAs was added as spike-in controls for further integrative analyses. Afterwards 140 µl Chloroform were added according to Qiagen® protocol, incubated and centrifuged. Upper aqueous phase was taken for large and small RNA isolation in Qiacube® with miRNeasy® mini kit aqueous phase A and B protocols. After RNA preparation, concentrations of small RNA and large RNA were determined with UV-spectroscopy on a Nanodrop and QuantiFluor® RNA System (Promega) on a Varioscan. In addition, quality control was performed via RNA and small RNA chips on an Agilent 2100 Bioanalyzer to determine the RNA integrity number (RIN) of large RNAs and the miRNA quality of small RNAs for RNA sequencing.

RNA libraries and sequencing

Small RNAs were prepared according NEBNext® Multiplex small RNA library Prep Kit for Illumina®(New England Biolabs). Isolated small RNAs were used in a concentration of 70 ng total RNA. Libraries were prepared according Protocol. Quality was checked on an Agilent 2100 Bioanalyzer high-sensitivity DNA chip. Afterwards molarity of the miRNApeak compared to the adaptor-dimer peak was estimated by the Agilent 2100 Bioanalyzer software and the effective amount for pooling was estimated. After pooling a size selection clean-up was done by using Zymo Select a Size DNA Clean and Concentrator™ (Zymo Research). The cutoff was made adjusted to 125 bp with 85% Ethanol. Quality of the final library pool was again checked with Agilent 2100 Bioanalyzer. The RNA pools were sequenced with 50 bp single end with Illumina HiSeq 3000. Sequencing was done by Christoph Bock at the Biomedical Sequencing Facility (CeMM/MUW).

DNA Preparation and Sequencing

DNA was collected from cell lines for each condition, three conditions as described above: control, 37°C and 42°C chemotherapy after 20 hours. DNA was isolated according QIAamp® DNA FFPE isolation protocol. After DNA preparation, concentrations of DNA was determined with QuantiFluor® dsDNA Sample Kit (Promega) on a Varioscan. Reduced representation bisulfite sequencing (RRBS) was done by Christoph Bock at the CeMM using RRBS protocol as described in [24].

Coverslip experiments

Two cell lines ES-2 and OVCAR-3 were used for further necroptosis experiments. Both cells were cultivated in respective cell culture medium on coverslips.

Sterile Coverslips with a diameter of 13 mm were coated with 0.2% gelatin solution (2% gelatin solution from Sigma in PBS) and incubated for 30 minutes in 37°C 5% CO2 incubator. After 30 minutes the gelatin solution was removed and 100 µl of cell suspension with 10^5 cells for ES-2 and $2x10^5$ cells for OVCAR-3 were pipetted on each gelatin coated coverslip. Cells were incubated for two hours. Afterwards 2 ml medium were added and cultivated overnight. Next day cells were treated according HIPEC criteria. We used 14 conditions for ES-2 and OVCAR-3 treatment as described in Table 4. We used two different temperatures at 37°C and 42°C with and without chemotherapy treatment with two different time points after 20 hours and 48 hours and all in duplicates. Furthermore, we inhibited necroptosis with Necrostatin-1 (Sigma) at a concentration of 50 µM at 37°C and 42°C with and without chemotherapy. Necrostatin-1 was added during chemotherapy treatment and after chemotherapy treatment into fresh cell culture medium. Additionally we had two control groups at two different time points (20 hours and 48 hours) for primary antibody control staining.

Chemotherapy treatment was done for 90 minutes with Carboplatin (10 mg/ml) and Paclitaxel (6 mg/ml). After 90 minutes cells were washed with PBS and incubated with fresh cell culture medium for 20 hours and 48 hours. After incubation cells were stained immunofluorescently.

Temperature	Treatment	Incubation	Panel	Primary Antibody
37°C	without Chemotherapy	20h	P1	pMLKL, RIPK3, Hsp90
37°C	without Chemotherapy	20h	P2	Caspase3, M30, cleaved PARP
37°C	with Chemotherapy	20h	P1	pMLKL, RIPK3, Hsp90
37°C	with Chemotherapy	20h	P2	Caspase3, M30, cleaved PARP
37°C	with Chemotherapy	48h	P1	pMLKL, RIPK3, Hsp90
42°C	without Chemotherapy	20h	P1	pMLKL, RIPK3, Hsp90
42°C	without Chemotherapy	20h	P2	Caspase 3, M30, cleaved PARP
42°C	with Chemotherapy	20h	P1	pMLKL, RIPK3, Hsp90
42°C	with Chemotherapy	20h	P2	Caspase3, M30, cleaved PARP
42°C	with Chemotherapy	48h	P1	pMLKL, RIPK3, Hsp90
37°C	with Chemotherapy and Nec-1	48h	P1	pMLKL, RIPK3, Hsp90
42°C	with Chemotherapy and Nec-1	48h	P1	pMLKL, RIPK3, Hsp90
42°C	without Chemotherapy	20h	AB CTRL	Antibody Diluent
42°C	without Chemotherapy	48h	AB CTRL	Antibody Diluent

Table 4. Conditions for ES-2 and OVCAR-3 coverslip experiments.
Chemotherapy treatment was done at 37°C or 42°C with Carboplatin and Paclitaxel for 90 minutes with an incubation period of 20 hours or 48 hours after treatment. P1 or P2 are used multicolour immunefluorescence staining panels with necroptosis or apoptosis markers (Table 5). (AB CTRL= primary antibody control, done with Antibody diluent; Nec-1= Necrostatin-1)

ICC Staining

Cells on coverslips were fixed with 4% paraformaldehyde at room temperature for 15 minutes. Cells were washed with PBS and permeabilized with 0.2% Triton X for 5 minutes. After another washing steps, cells were blocked with UltraV Protein Block (Thermo Scientific) for 7 minutes and washed once. We established two antibody panels to stain for necroptosis and apoptosis markers. Primary staining solution containing pMLKL, RIPK3 and Hsp90 for the first panel (necroptosis) and M30, cleaved PARP and caspase 3 for the second panel (apoptosis) was added and incubated for one hour at room temperature in the dark (Table 5). Antibodies were prepared and used in DAKO antibody diluent. Additionally, a negative control for primary antibodies was performed. The secondary staining solution for panel 1 was prepared as follows: anti-rabbit IgG conjugated with Alexa Fluor® 488, anti-mouse IgG2a conjugated with Alexa Fluor® 647 and anti-mouse IgM conjugated with Alexa Fluor®555 diluted 1:1000 in 6% BSA. The secondary staining solution for panel 2 contained anti-rabbit IgG conjugated with Alexa Fluor® 488, anti-mouse IgG2b conjugated with Alexa Fluor® 555 and anti-mouse IgG1 conjugated with Alexa Fluor®647 (Table 5). The secondary antibody staining solution was incubated for 1 hour at room temperature in the dark. Afterwards the

coverslips were washed with PBS-T (PBS containing 0.1% Tween®). Cells were counterstained with DAPI for 5 minutes. After three washing steps in PBS, cells were mounted with Fluoromount-G® (SouthernBiotech) and incubated overnight. Coverslips were analyzed via confocal microscopy (Zeiss, LSM 500) and analyzed via Imaris x64 7.4.2.

Panel	Primary antibody		Secondary antibody
1	Anti-MLKL (phosphor S358)	RabMab, ab287091; Abcam	anti-rabbit conjugated with Alexa Fluor® 488 (A11059, Invitrogen)
	Anti-RIPK3	Mouse IgG2a, LS-C338650; LifeSpan BioSciences	anti-mouse IgG2a conjugated with Alexa Fluor® 647 (A21241, Invitrogen)
	Anti- Hsp90 (mouse IgM)	Mouse IgM, ab13492; Abcam	anti-mouse IgM conjugated with Alexa Fluor® 555 (A21426, Invitrogen)
2	Anti- M30	Mouse IgG2b, 12140349001, Roche	anti-mouse IgG2b conjugated with Alexa Fluor® 555 (A21147, Life Technologies)
	Anti- cleaved PARP	Mouse IgG1, ab110315; Abcam	anti-mouse IgG1 conjugated with Alexa Fluor® 647 (A21240, Invitrogen)
	Anti-active caspase 3 fragment	Rabbit IgG, 559565; BD Pharmingen	anti-rabbit conjugated with Alexa Fluor® 488 (A11059, Invitrogen)

Table 5. Used antibody panels.

Immunogenicity of necroptosis

Treatment of ES-2 and OVCAR-3 cells

Two cell lines, one of of miliary (OVCAR-3) and one of non-miliary (ES-2) spread type were chosen. Both were cultivated in 6 well plates at high confluency and treated according HIPEC criteria. Following conditions were employed: 1) 37°C without chemotherapy (CTRL), 2) 37°C with chemotherapy, 3) 37°C with Necrostatin-1, 4) 37°C with chemotherapy and Necrostatin-1, 5) 42°C without chemotherapy (only heat shock), 6) 42°C with chemotherapy (HIPEC) 7) 42°C with Nec-1, and 8) 42°C with chemotherapy and Nec-1. Both cell lines (ES-2 and OVCAR-3) were treated in duplicates according all eight conditions. For chemotherapy treatment Paclitaxel and Carboplatin were used. Necrostatin-1 was used at a concentration of 50 µM. After 90 minutes treatment, cells were washed carefully with PBS and fresh cell culture medium was added for 20 hours. For Nec-1 conditions, 50 µM Nec-1 was also added to fresh cell culture medium to inhibit necroptosis during incubation. After 20 hours supernatant was collected and centrifuged at 400 g for 10 minutes, aliquoted for further experiments and

stored at -80°C. Cell were harvested using a cell scraper in PBS. Afterwards they were harvested (2,000 rpm, 10 min, RT) and lysed with 350 ml Qiazol® detergent.

Isolation of peripheral blood mononuclear cells (PBMC) with Ficoll

Blood samples were taken from four voluntary female donors and collected in three EDTA tubes. Isolation of peripheral blood mononuclear cells (PBMC) was done with Ficoll. Ficoll was pipetted in leukoSep tubes and centrifuged. Then whole blood was added. Tubes were centrifuged without brakes at 10°C with 1,600 rpm for 20 minutes. Afterwards red blood cells cells were removed. The layer between ficoll and serum should be clear. Tubes were refilled to 50 ml with PBS and centrifuged without brakes at 10 °C with 1,200 rpm for 7 minutes. The supernatant was removed. The cell pellet was vortexed and PBS was added to gain a volume of 50 ml. Afterwards they were centrifuged without brakes at 10 °C with 1,200 rpm for 7 minutes. Supernatant was removed and pellet was resuspended in 50 ml MACS Puffer. The suspension was again centrifuged without brakes at 10 °C with 1,200 rpm for 7 minutes. Cells were counted using Sysmex cell counter.

Isolation of $CD14^+$ cells

Isolation of $CD14^+$ cell was done with pan monocyte isolaton kit (Miltenyi Biotec). For 10^7 cells 80 µl MACS Puffer and 15 µl CD14 microbeads were used. Calculated MACS Puffer and CD14-microbead solution was added to the cell pellet and incubated for 8 minutes on ice. Afterwards they were mixed and incubated for 8 minutes again. 50 ml MACS Puffer were added and solution was centrifuged without brakes at 10 °C with 1,200 rpm for 7 minutes. Pellet was vortexed and about 3 ml MACS Puffer was added. Cell suspension was loaded on a MACS column which was fixed on a magnet. Flow through was collected (T-, B-cells) and column was washed with MACS Puffer. Afterwards $CD14^+$ cells were eluted from microbeads by using MACS buffer with the column removed from the magnet. T-, B-cells and monocytes were counted by Sysmex.

Blood monocyte activation through DAMPS

Immunogenic necroptotic cell death would result in DAMP release. Therefore we used supernatant of two cells lines (OVCAR-3 and ES-2) which were treated with eight different conditions - 42°C or 37°C with or without chemotherapy treatment and 42°C or 37°C with or without chemotherapy treatment and Nec-1 as described above. ES-2 cells at HIPEC conditions underwent necroptosis, therefore they should release DAMPS which active immune cells. Besides this eight conditions we performed a negative control with used cell culture media (RPMI with 10% FCS for ES-2 cells and RPMI with 20% FCS for OVCAR-3 cells) and a positive control with Lipopolysaccharide (LPS). LPS is known to activate blood monocytes. The cell supernatants were incubated with blood monocytes for 20 hours. Afterwards IL6 was measured with Siemens BNII Nephelometer. This experiment was done in duplicates with two independent IL6 measurements.

Results

Evidence for Necroptosis

Quantified analysis of necroptosis upon in vitro HIPEC treatment

To proof whether HIPEC treatment can cause a shift from apoptotic cell death towards necroptotic cell death and therefore induce anti-tumor immunity, we performed an in vitro HIPEC treatment with ovarian cancer and immortalized progenitor cell lines. We used tumor cell lines of putative miliary spread type, CAOV-3 and OVCAR-3, and putative non-miliary spread type, ES-2 and Tyk-nu, and precursor cell lines of putative tubal FT194 and FT33, and putative ovarian origin IOSE80 and IOSE364 for in vitro HIPEC treatment [4-6]. We compared three conditions: 37°C chemotherapy (normothermic), 42°C chemotherapy (hyperthermic) and mock (without chemotherapy) treated cells. The cell lines were treated according usual in vivo HIPEC conditions, *i.e.* 90 minutes, with Paclitaxel (6 mg/ml) and Carboplatin (10 mg/ml). Afterwards cells were incubated for 30 minutes and 20 hours in fresh cell culture medium to assess the impact of HIPEC directly after treatment and after 20 hours to analyze short and late post-HIPEC effects. Cells were trypsinized, formalin-fixed, embedded in agarose and paraffin to get FFPE cell blocks, sectioned, and stained immunofluorescently for necroptosis using putative necroptosis marker pMLKL, RIPK3, and Hsp90. Stained slides were scanned on a TissueFAX® microscope and analyzed via CellProfiler™ to quantify the upper quartile fluorescent intensity in cytoplasm of pMLKL, RIPK3 and Hsp90 of each cell (Fig.9).

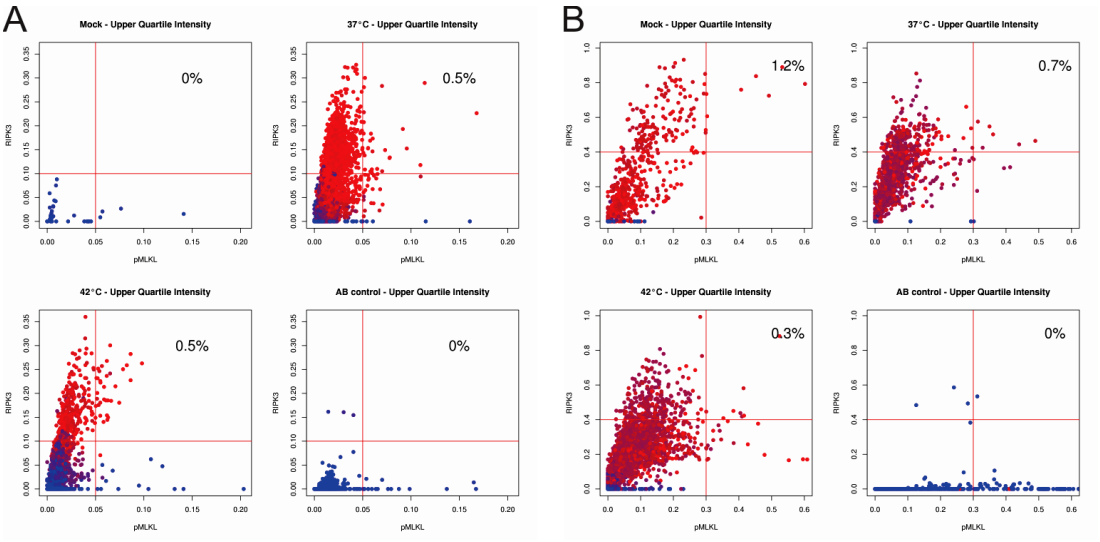

OVCAR 3 miliary serous ovarian cancer cell line

CAOV3 miliary serous ovarian cancer cell line

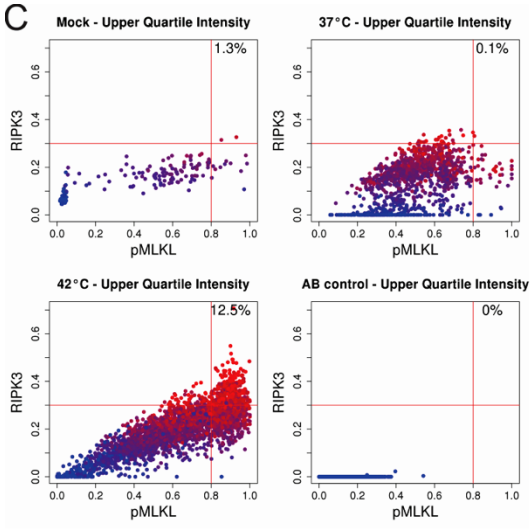

ES2 non miliary serous ovarian cancer cell line

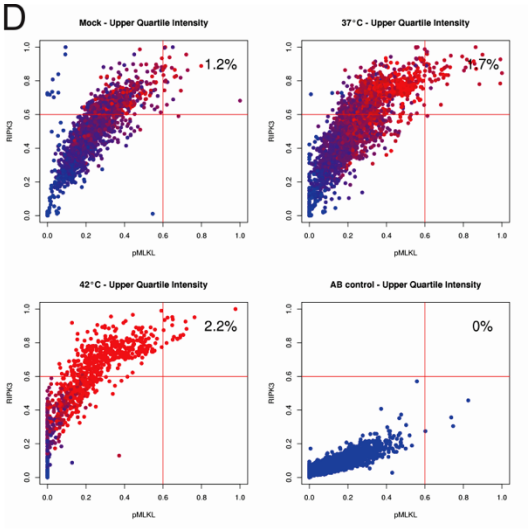

Tyk-nu non milary serous ovarian cancer cell line

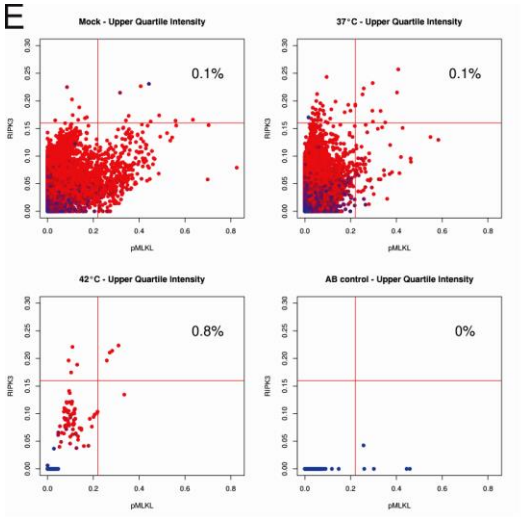

IOSE80 Immortalized ovarian surface epithelial cell line

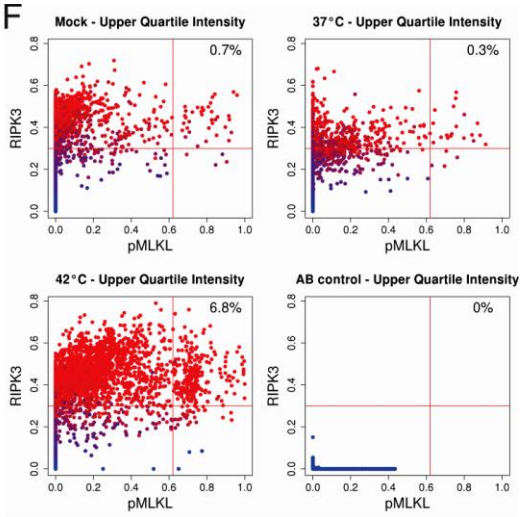

IOSE 364 Immortalized ovarian surface epithelial cell line

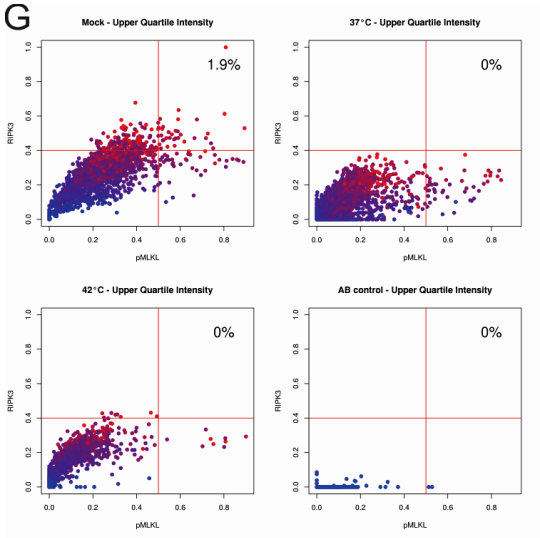

FT194 fallopian tube epithelial cell line

Figure 9. Scatter plot of pMLKL, RIPK3, and Hsp90 staining in tumor cells of both spread types after 20 h post-HIPEC cultivation

Miliary cell lines **A)** OVCAR-3, **B)** CAOV-3 and non-miliary cell lines **C)** ES-2 and **D)** Tyk-nu. **E)** IOSE80 and **F)** IOSE364 represent precursor cell lines of putative ovarian origin and **G)** FT194 of putative tubal origin. Every point represents the upper quartile fluorescent staining intensity in the cytoplasm. The X-axis shows the upper quartile fluorescent intensity of pMLKL and the Y-axis the upper quartile fluorescent intensity of RIPK3. Hsp90 is coded in the color of the points from blue to red with red as highest intensity. Cells were treated with chemotherapy at 37°C and 42°C for 90 minutes and 20 hours incubation in fresh cell culture medium for necroptotis induction and without chemotherapy as control group (Mock). AB control means antibody control with missing primary antibody.

Cells of putative miliary spread type, CAOV-3 and OVCAR-3, showed after HIPEC conditions no increase of putative necroptotic cells (*i.e.* pMLKL and RIPK3 positivity) compared to the 37°C chemotherapy condition or the mock treated cells. Interestingly, in OVCAR-3 cells were no differences between 37°C and 42°C chemotherapy treatment. In CAOV-3 cells were even little higher levels of RIPK3 and pMLKL double stained cells with 0.7% at the 37°C chemotherapy condition in comparison to 0.3% at 42°C. In general, there were only a few necroptotic cells in CAOV-3 and OVCAR-3 as shown by low percentages of high upper quartile fluorescent staining intensities for necroptosis markers and no significant difference in comparison to untreated cells (Fig. 9A,B).

Contrary to these results, ES-2 and Tyk-nu, cells of putative non-miliary spread type, showed increased pMLKL and RIPK3 fluorescent staining intensities at 42°C chemotherapy treatment. ES-2 cells showed the highest increase of cell lines upon *in vitro* HIPEC treatment with 12.5% of cells with high upper quartile fluorescent staining intensities of both markers. Whereas, Tyk-nu cells showed little increase of pMLKL and RIPK3 with 2.2% at HIPEC conditions. At 37°C chemotherapy and mock treatment both cell lines, ES-2 and Tyk-nu, showed only few cells with high fluorescent staining intensities of necroptosis markers, *i.e.* significantly less than at the 42°C chemotherapy treatment condition. ES-2 and Tyk-nu are both tumor cell lines of putative non-miliary spread type. Consistent to this finding, IOSE80 and IOSE364, both immortalized epithelial cells of putative ovarian origin and therefore assumed as precursor cell lines for tumors of non-miliary spread type [3-5], also showed increased percentages of cells with high fluorescent staining intensities of necroptosis markers at HIPEC conditions. IOSE364 showed the largest increase with 6.8% cells with high upper quartile fluorescent staining intensities of necroptosis markers at 42°C in comparison to 0.3% of cells at 37°C and 0.7% of cells in untreated cells. We also performed in vitro HIPEC treatment on FT194 cells, which are of putative tubal origin and used as reference cell line for tumors of miliary tumor spread type [3-5]. Consistent with results shown above for CAOV-3 and OVCAR-3 cells of miliary tumor spread type, they showed no increase (Fig.9).

To summarize these findings, cells lines of putative non-miliary ovarian cancer and their putative non-malignant ovarian precursor cell lines reacted with increased necroptosis upon chemotherapy treatment at hyperthermic conditions compared to normothermic conditions.

The largest difference was seen in ES-2 cells. Cell lines of putative miliary ovarian cancer and putative non-malignant precursor cells of tubal origin show no signs of necroptosis (Fig.10).

This is the first evidence of necroptosis in ovarian cancer cells of the non-miliary tumor spread type upon HIPEC treatment. Ovarian cancer cells of miliary tumor spread type seem not to react with necroptosis after HIPEC treatment.

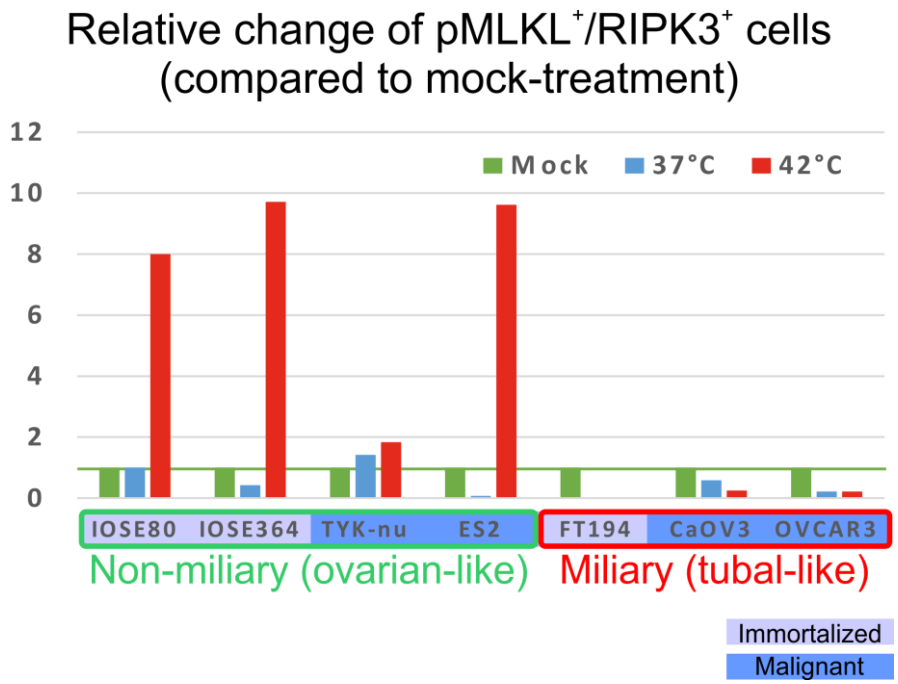

Figure 10. Comparison of the relative change of pMLKL⁺/RIPK3⁺ cells compared to untreated cells in both tumor spread types of non-miliary and miliary and their putative non-malignant precursor cells.
Non-miliary tumor cells, which are presumed to be more ovarian like [3-5], and immortalized ovarian surface epithelial cells showed higher percentages of cells with pMLKL and RIPK3 positivity at 42°C chemotherapy treatment compared to 37°C and untreated (mock) cells. Tumor cells of miliary spread type, which are presumed to be more tubal like [3-5], and immortalized fallopian tube cells showed no increase of pMLKL and RIPK3 positive cells and therefore no signs of induced necroptosis. Tumor cells of non miliary spread type and immortalized ovarian surface epithelial cells (IOSE) show increased signs of necroptosis at HIPEC conditions. All comparisons were normalized to the mock treated condition (green line at 1) and therefore the Y-axis shows percentage increases at 37°C and 42°C chemotherapy conditions compared to the mock condition.

Co-localization of pMLKL, RIPK3, and Hsp90 upon HIPEC treatment

Upon first evidence of necroptosis indicated by higher cytoplasmic pMLKL and RIPK3 concentrations after in vitro HIPEC treatment in non-miliary ovarian cancer cells we also examined for co-localization of pMLKL and RIPK3 with confocal microscopy. RIPK3 and activated plasma membrane pore forming protein pMLKL are the core proteins for necrosomes [8]. Therefore we looked for co-localization of pMLKL and RIPK3 in each cell line via confocal microscope (LSM70). HGSC tumor cell lines were treated according in vitro HIPEC conditions as described above (mock, 42° (HIPEC-like) or 37° normothermic chemotherapy treatment with subsequent 20 hours incubation in cell culture medium), fixed and agarose and paraffin embedded, sliced and stained immunofluorescently for necroptosis markers pMLKL, RIPK3, and Hsp90.

In cells of putative non-miliary spread type ES-2, IOSE80, and IOSE364 treated with chemotherapy at 42°C both, pMLKL and RIPK3, as expected and interestingly, Hsp90 are co-localized at the cell boarders. A literature research revealed that Hsp90 seems to be also an essential key player for necroptosis [40], which strengthens further our interpretation of the staining patterns as necroptosis. In cell lines of miliary spread type OVCAR-3, CAOV-3, and FT 194 no co-localization of pMLKL, RIPK3, and Hsp90 was found. There is only increased staining for Hsp90 at 42°C, as expected for a heat shock protein.

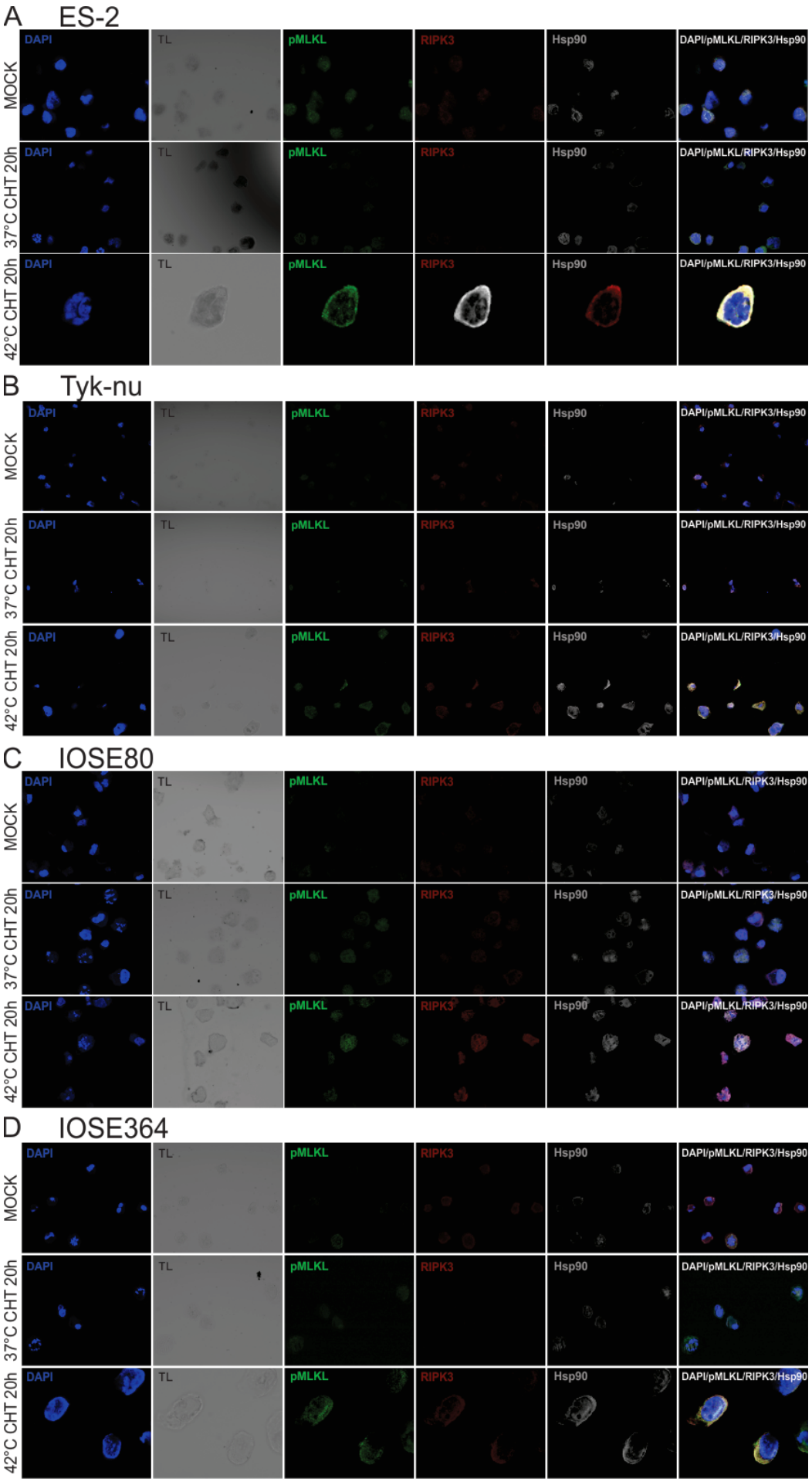
A ES-2
B Tyk-nu
C IOSE80
D IOSE364
MOCK
37°C CHT 20h
42°C CHT 20h
DAPI
TL
pMLKL
RIPK3
Hsp90
DAPI/pMLKL/RIPK3/Hsp90

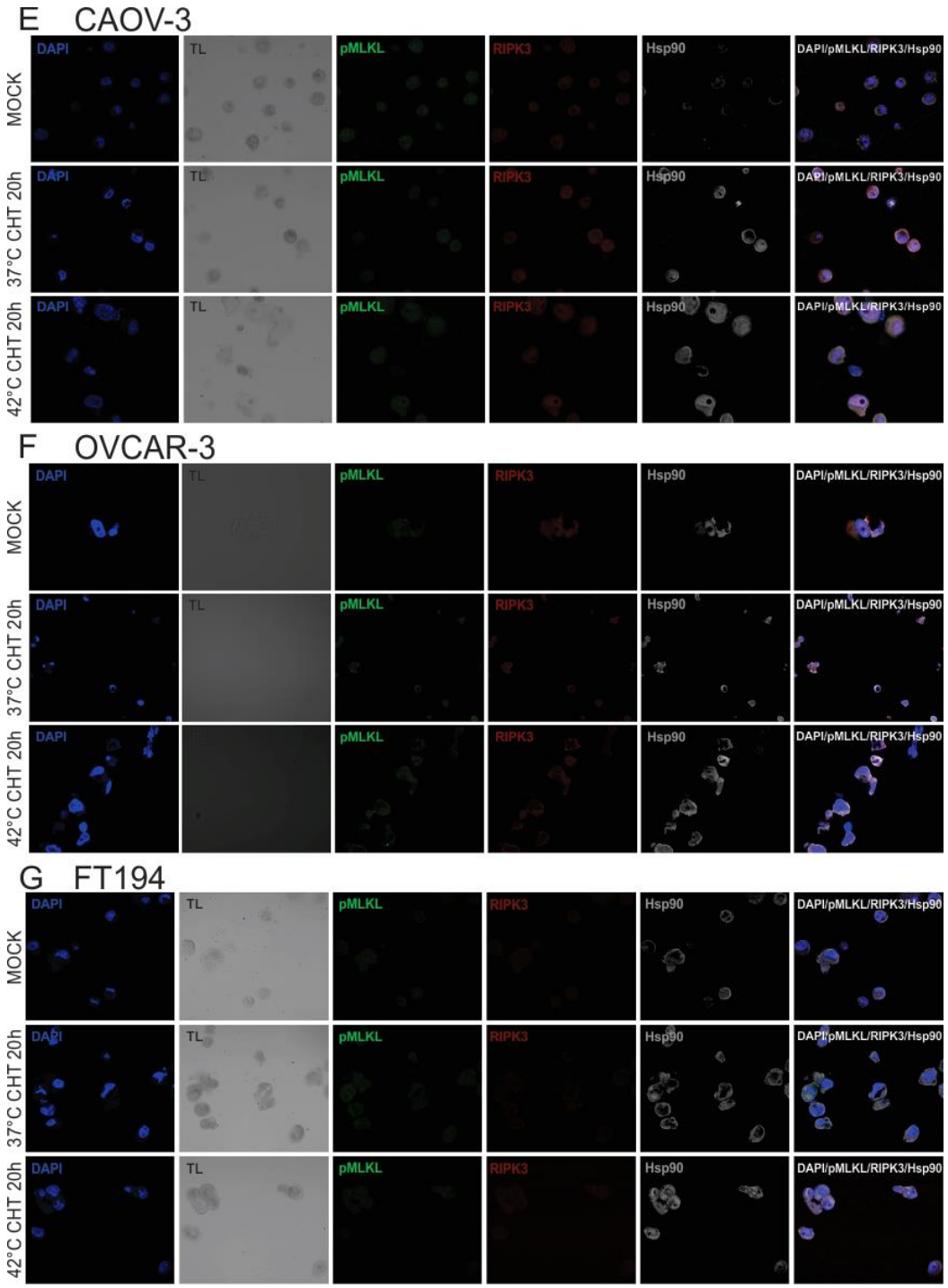

Figure 11. Confocal microscopy images of miliary (tubal) and non-miliary (ovarian) cell lines treated with HIPEC or normothermic chemotherapy conditions and controls.

Cells were treated without chemotherapy (mock) or at 37°C or 42° with chemotherapy and incubated for 20 hours in fresh cell culture medium. Used cell lines were of miliary (OVCAR-3, CAOV-3) or non-miliary (ES-2, Tyk-nu) spread type. FT194 was used as reference cell line for miliary tumor cells and IOSE cell lines were used as reference cell line for non-miliary spread type [3-5]. Cells were stained immunofluorescently for necroptosis with anti-pMLKL, RIPK3, and Hsp90 antibodies. Co-localized triple staining was only found in cell lines of non-miliary spread type (A-D). Cells of miliary spread type show no co-localization of these markers at cell boarders. Only Hsp90 was upregulated in miliary cells after chemotherapy treatment (E-G).

Further evidence for necroptosis

To investigate further our previous findings, we performed coverslip experiments with cells of non-miliary tumor spread type (ES-2) and miliary tumor spread type (OVCAR-3) to analyze the impact of hyperthermia (42°C without chemotherapy) alone on co-localization of pMLKL, RIPK3, and Hsp90. Furthermore we added an elongated incubation time of 42 hours to the 30 min and 20 hour post-treatment condition. According to Chen *et al.,* expression levels of RIPK3 and MLKL increased up to 36 - 48 hours upon physical compression of cell with 1.0 MPa as necroptosis induction [48]. Therefore we decided to add a 42 hours period of incubation after HIPEC treatment to account for the optimal time for necroptosis induction as decribed by Chen *et al*. To prove further our interpretation of the pMLKL-RIPK3 double stainings as signs for necroptosis we used 50 µM Necrostatin-1 (Nec-1), a specific inhibitor of necroptosis, together with HIPEC conditions and looked for the impact on staining intensities and frequencies. Necrostatin-1 inhibits necrosome formation by inhibiting RIPK1 [8, 48]. To estimate the optimal concentrations we used 20 µM and 50 µM, according to Chen *et al.* whereas we got the best inhibition at 50 µM [48]. We cultivated cells of non-miliary tumor spread type (ES-2) and miliary tumor spread type (OVCAR-3) on gelatin coated coverslips. Cells were treated with and without chemotherapy for 90 minutes at 37°C or 42°C with 20 hours and 42 hours incubation. An additional condition was Nec-1 inhibition at 42°C and 37°C with chemotherapy during HIPEC treatment and during incubation in fresh cell culture medium for 20 hours and 42 hours. Afterwards cells were fixed and stained immuno-fluorescently for necroptosis with antibodies against pMLKL, RIPK3, and Hsp90 and for apoptosis with antibodies against caspase 3, cleaved PARP and M30 and imaged via confocal microscopy.

Necroptosis is inhibited by Necrostatin-1

By using bright-field microscopy we found that cell death in ES-2 cells treated with chemotherapy at 42°C was inhibited by Necrostatin-1 indicating cell death by necroptosis (Fig. 12. Consistent with recent findings, OVCAR-3 did not undergo necroptosis and were not inhibited by Necrostatin-1.

The brightfield images in ES-2 cells at 42°C show increased cell death at chemotherapy (CHT) treated cells compared to untreated cells (CTRL). If we compare untreated cells (CTRL) with chemotherapy and Nec-1 (CHT+ Nec-1) condition at 42°C we see no differences. Therefore

cell death is inhibited upon Nec-1 treatment indicating cell death by necroptosis. At 37°C is less cell death and less inhibition of Nec-1. As we found necroptosis at 42°C chemotherapy treatment in ES-2 cells in previous stainings these findings underline our statement. In OVCAR-3 cells there is no difference between the conditions (Fig. 12).

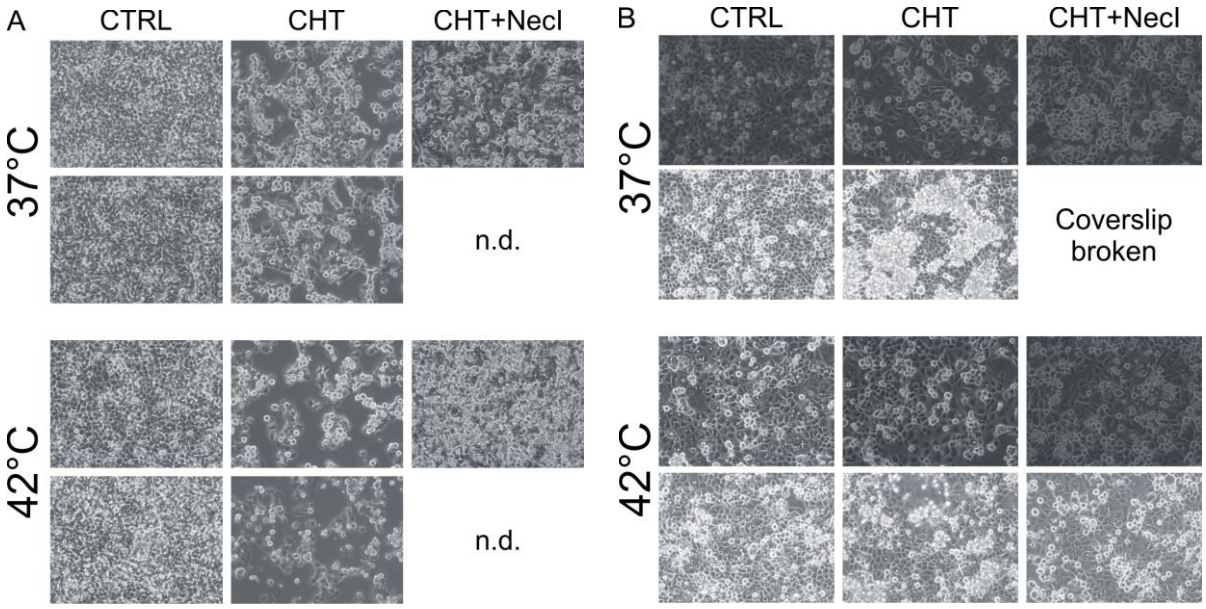

Figure 12. ES-2 (left) and OVCAR-3 (right) cells treated with or without chemotherapy (CHT) and Necrostatin-1 (Nec-1) at 37°C and 42°C.
A) ES-2 cell treated with and without chemotherapy at 37°C and 42°C and 50 µM Necrostatin-1. At HIPEC conditions (42°C and chemotherapy treatment) cells died and detached from coverslips, which is inhibited by Necrostatin-1. B) In OVCAR-3 cells there is no cell death. Cells are similar confluent in all conditions.

Co-localization of pMLKL, RIPK3 and Hsp90

In ES-2 cells treated at HIPEC conditions (42°C and chemotherapy) pMLKL, RIPK3, and Hsp90 are localized at cell boarders. At 37°C with and without chemotherapy and 42°C without chemotherapy no co-localization of the three marker was seen. Additionally, in Necrostatin-1 inhibited cells no triple staining of pMLKL, RIPK3, and Hsp90 was seen (Fig. 13-15).

In OVCAR-3 cells there is a low frequency of pMLKL positivity in all conditions, but no increase of RIPK3 and no co-localization of all three markers. Hsp90 is increased only at hyperthermic conditions (42°C). In Necrostatin-1 inhibited cells there is also little staining of pMLKL. Because of the missing co-localization and previous findings this striking result was interpreted as negative sign for necroptosis (Fig.16-18).

Extended time point 42h

As described above, we decided to add an additional time period of 42 hours post-HIPEC treatment to check for later necroptosis events, as inferred from Chen *at al.* [48]. Contrary to the results from Chen *et al*. there seems to be already a stagnation in new necroptosis with reduced signs of necroptosis after 42 hours incubation after HIPEC treatment in ES-2 cells. In ES-2 cells treated with chemotherapy at 37°C with increased incubation time, there are no signs of necroptosis.

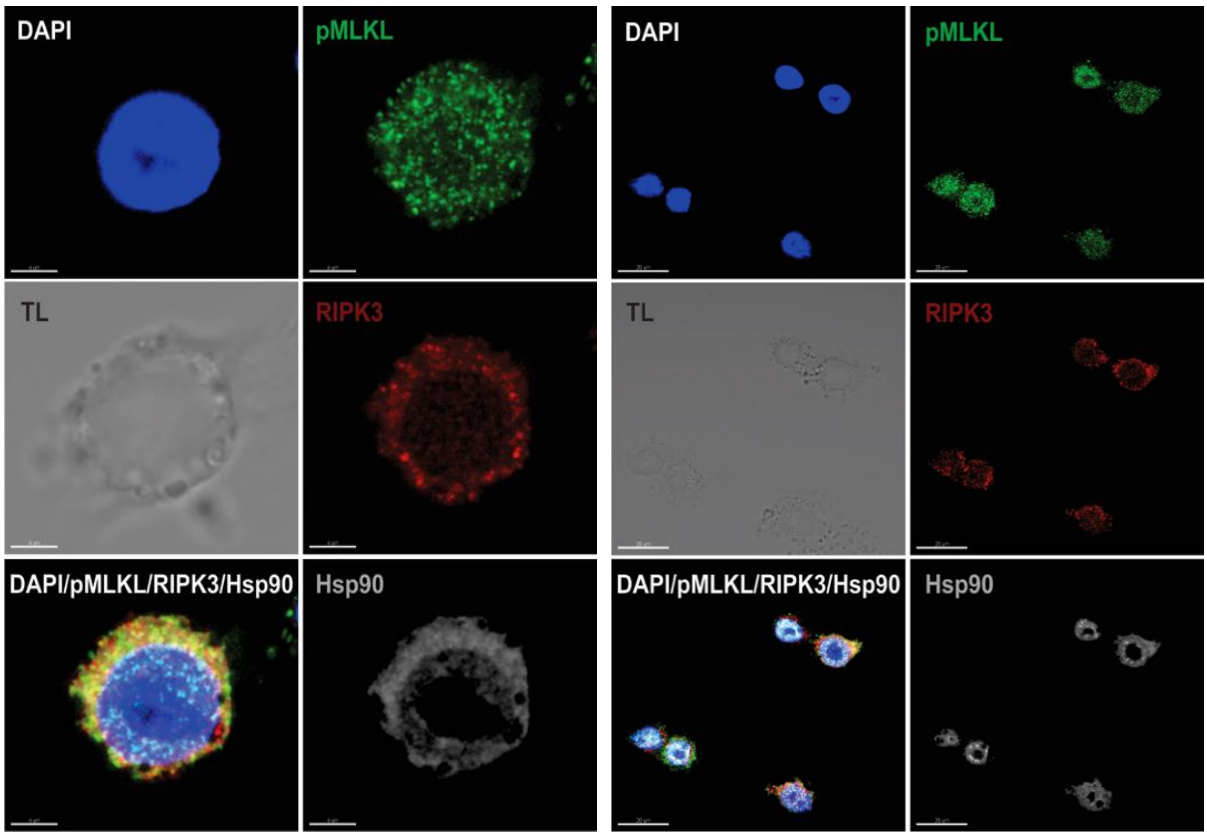

Figure 13. pMLKL,RIPK3, and Hsp90 staining of ES-2 cells after HIPEC treatment.
pMLKL, RIPK3, and Hsp90 staining of ES-2 cell treated with 42°C chemotherapy and incubated for 20 hours with fresh cell culture medium. pMLKL, RIPK3, and Hsp90 are localized at cell boarders indicating necroptosis.

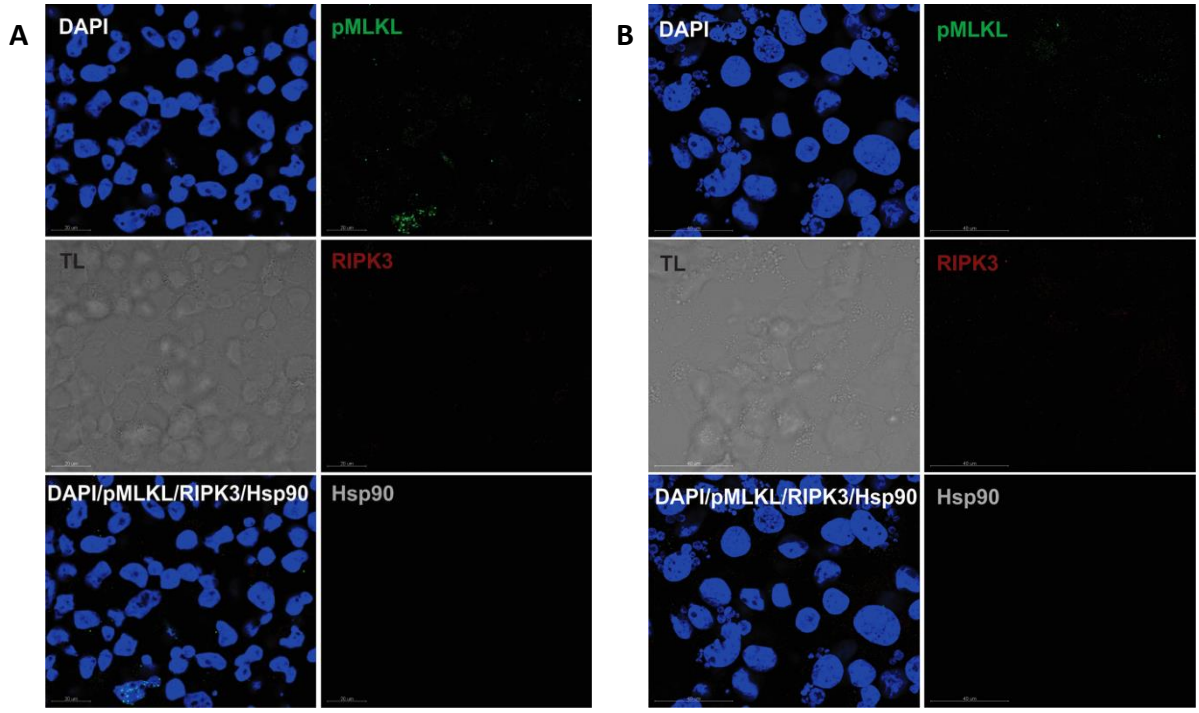

Figure 14. pMLKL, RIPK3, and Hsp90 staining of ES-2 cells after 42°C treatment and after Nec-1 inhibiton and HIPEC treatment.

A) Untreated (without chemotherapy) ES-2 cells at 42°C and 20h incubation show no signs of necroptosis. B) ES-2 cells treated with chemotherapy and Necrostatin-1 at 42°C and 20h incubation

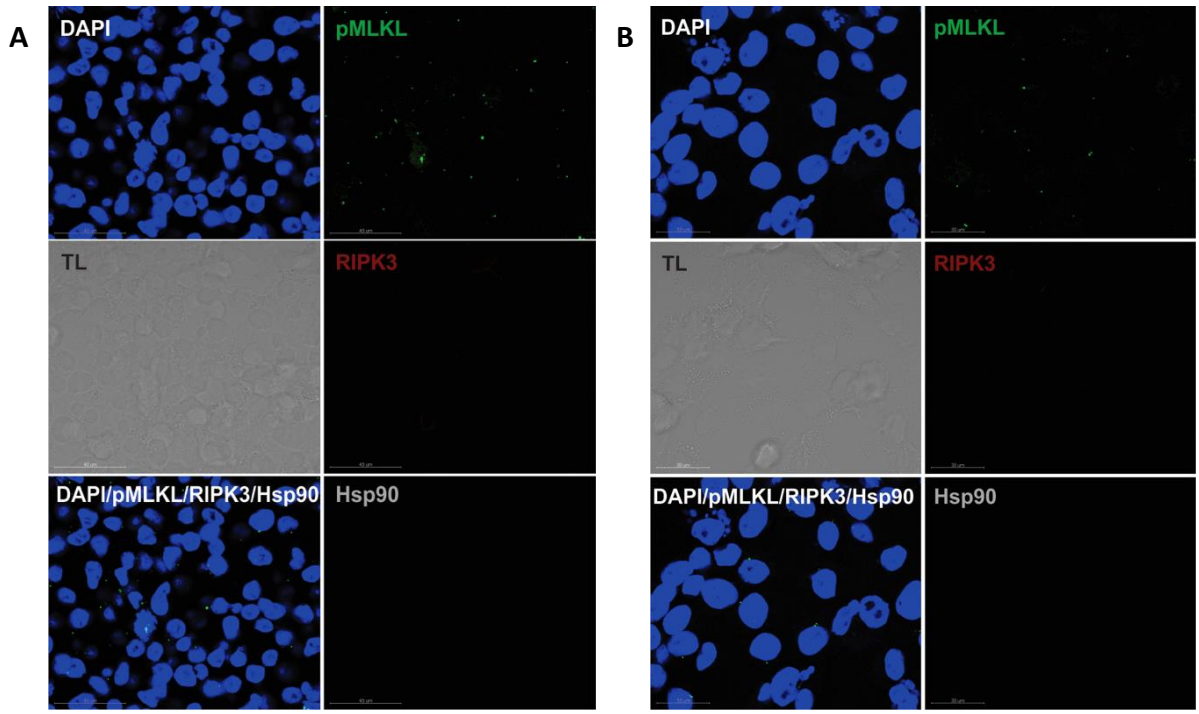

Figure 15. pMLKL, RIPK3, and Hsp90 staining of ES-2 cells at 37°C.

A) ES-2 cells untreated at 37°C B) ES-2 cells treated with chemotherapy at 37°C.

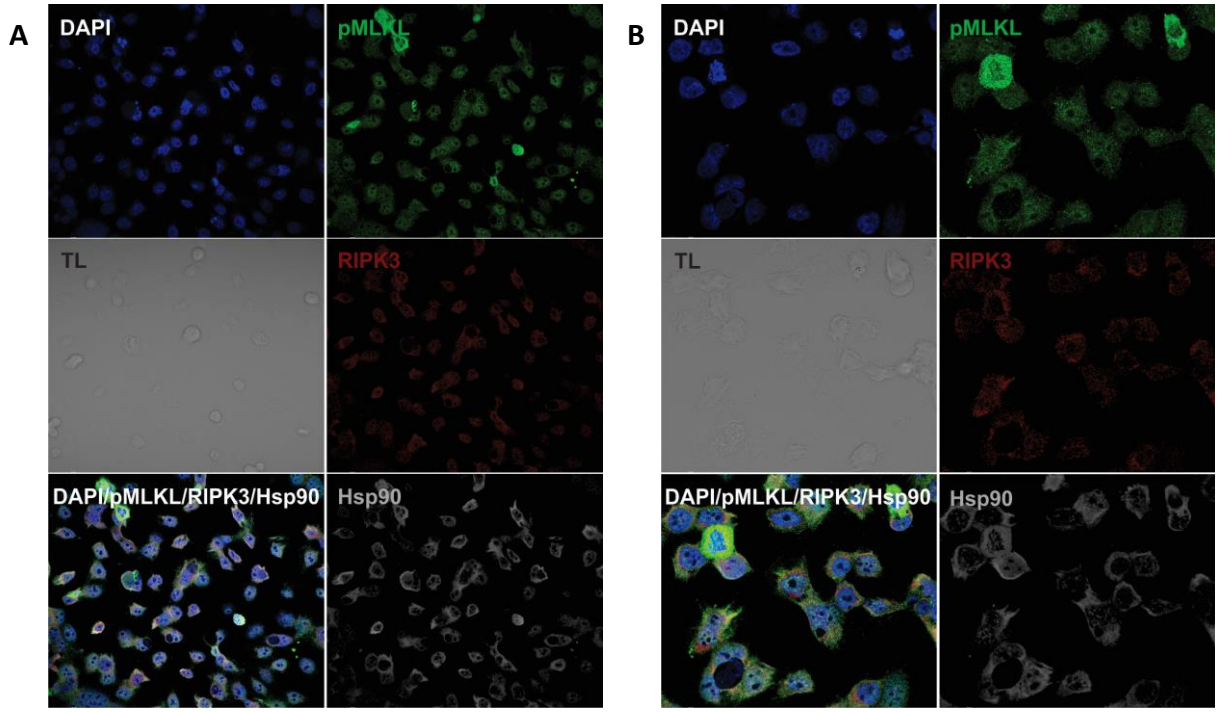

Figure 16. OVCAR-3 cells stained for pMLKL, RIPK3, and Hsp90.
A) pMLKL, RIPK3, and Hsp90 staining of OVCAR-3 cells treated with chemotherapy and incubated for 20 hours with fresh cell culture medium. B) OVCAR-3 after 20 hours without chemotherapy treatment at 42°C.

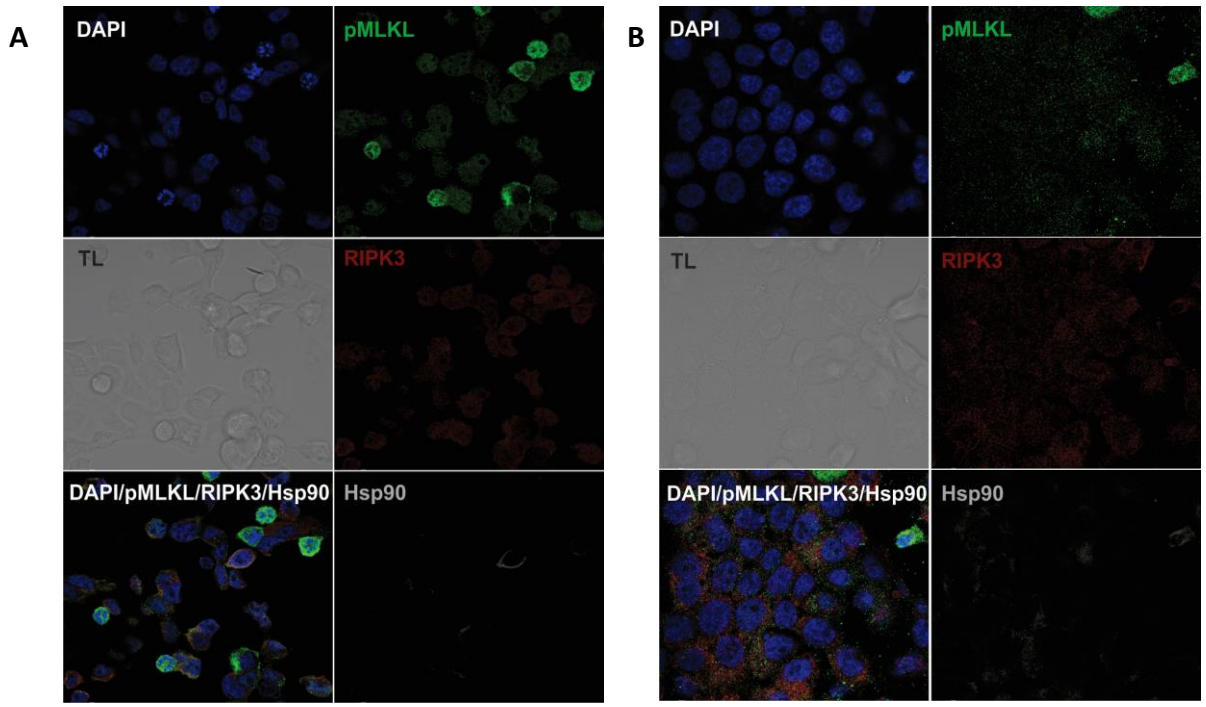

Figure 17. OVCAR-3 cells stained for pMLKL, RIPK3, and Hsp90.
A) OVCAR-3 after 20h treated with chemotherapy at 37°C. B) OVCAR-3 after 20h treated without chemotherapy at 37°C.

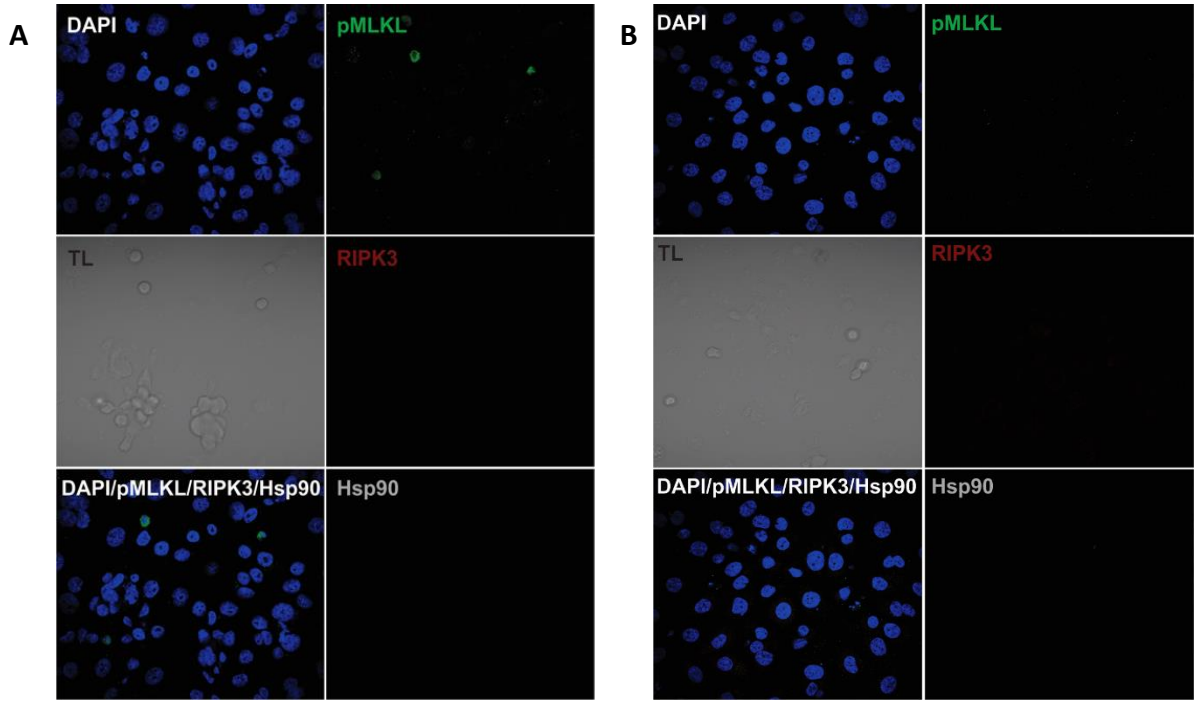

Figure 18. pMLKL/RIPK3/Hsp90 staining of OVCAR-3

A) OVCAR-3 after 42 hours with chemotherapy at 42°C and inhibited with Nec-1. B) OVCAR-3 treated after 42 hours and chemotherapy at 42°C without Nec-1

Cell death by apoptosis

To exclude other forms of cell death we stained for apoptosis with caspase 3, M30 and cleaved PARP. In both cell lines ES-2 and OVCAR-3 basic apoptosis with only a few apoptotic cells were found in all conditions. Therefore, there is no indication for increased cell death at HIPEC conditions by apoptosis after 20 h post-HIPEC growth (Fig. 19).

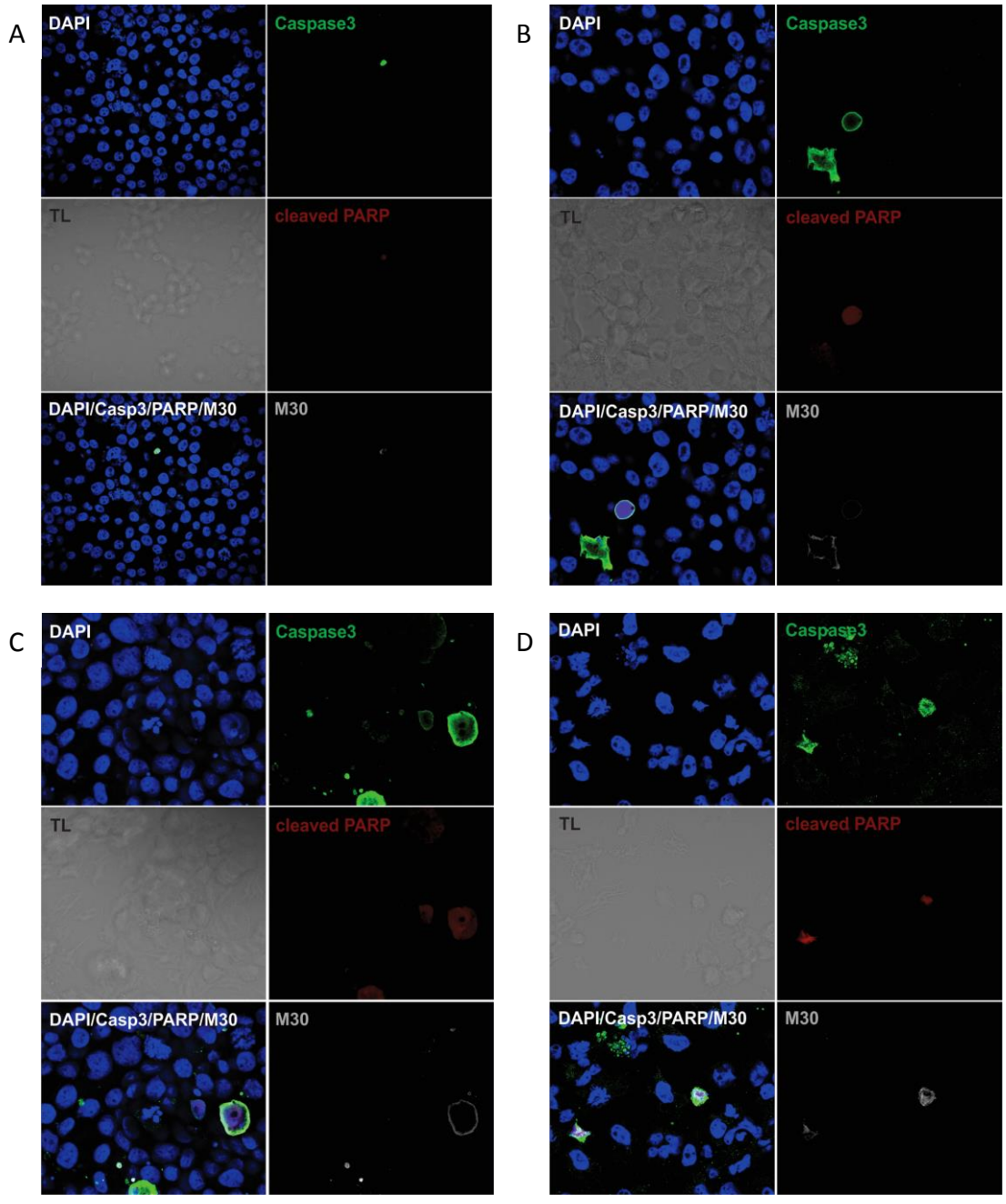

Figure 19. Confocal microscopy images of apoptosis in ES-2 and OVCAR-3 cells.
A) ES-2 cells treated according HIPEC conditions and stained for apoptosis (Caspase3, M30 and cleaved PARP) B) ES-2 cells after 20 hours and at 42°C without chemotherapy and stained for apoptosis. C) OVCAR-3 cells at 37°C treated with chemotherapy and incubated for 20 hours. D) OVCAR-3 cells after 20 hours at 42°C without chemotherapy.

Cell line expression of RIPK1, RIPK3 and caspase 8

RIPK1 and RIPK3 are key regulators in necroptosis [8]. Therefore we checked if RIPK1 and RIPK3 are expressed at all in our cell lines to ensure that this cell lines are even capable to undergo necroptosis.

Upon necroptosis initiation by *e.g.* TNFR, TRIF, TLR3, TLR4, or ZBP1 RIPK1 activates RIPK3 which leads to MLKL phosphorylation and oligomerization [49]. This mechanism requires inhibition of caspase 8 which is an essential branching point whether the cells undergo apoptosis or necroptosis. Activity of caspase 8 could lead to apoptosis [8, 36, 49]. Therefore we further checked if our cells also express caspase 8 and are potentially able to undergo apoptosis. From public RNA Sequencing data we found expression of RIPK1, RIPK3, and caspase 8 (Fig 20B) with slightly higher RIPK3 expression in putatively miliary cell lines, CAOV-3 and OVCAR-3. In addition, RNA sequencing data from isolated ovarian cancer tumor cells of miliary and non miliary spread type obtained from tumor tissues of HGSC patients and from non-malignant progenitor cell lines showed expression of RIPK3 (Fig. 20A). These data were obtained from rRNA-depleted RNA Sequencing data by Auer *et al.* [4].Here the situation is ambiguous. In solid tumors (primary (P) and metastases (M)) miliary spreading tumors seem to have higher RIPK3 expression whereas in ascitic tumor cells (single floating (A) or tumor cell aggregates, spheroids (S)) of miliary tumors there seem to be slightly lower expression of RIPK3.

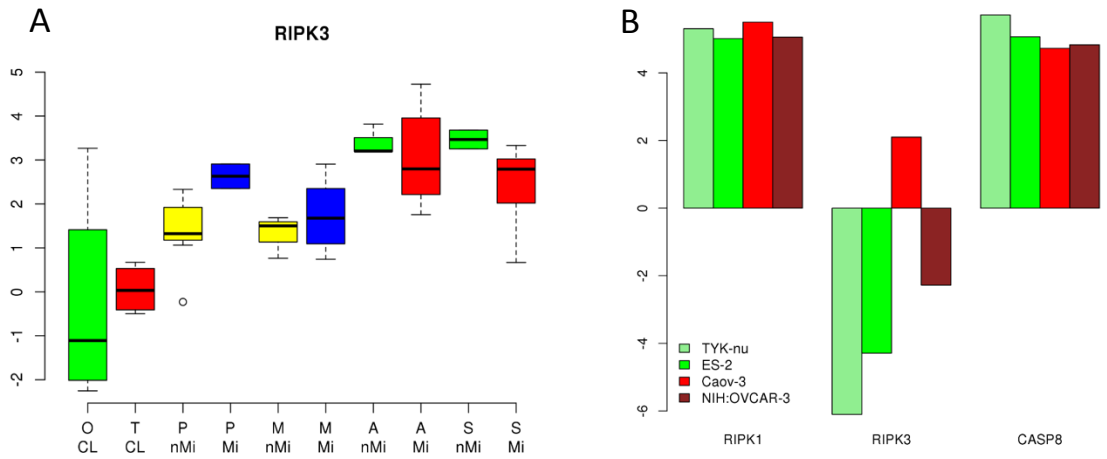

Figure 20. RIPK3, RIPK1, and caspase 8 expression data.

A) RIPK3 expression profile extracted from RNA sequencing data from isolated tumor cells of HGSC patients. Data were obtained from immortalized cell lines (CL) of ovarian (O) or tubal origin (T), Primary ovarian tumors (P), Metastasic tumors (M), single ascites tumor cells (A), or isolated spheroidal tumor

cells (S) of HGSC patients of both tumor spread types, miliary (Mi) and non-miliary (nMi). B) RIPK1, RIPK3, and caspase 8 expression extracted from public RNA Sequencing data for Tyk-nu, ES-2, CAOV-3, and OVCAR-3 cell lines.

Immunogenic cell death through DAMP release

To figure out whether HIPEC treatment can induce immunogenic cell death, we incubated supernatants of HIPEC, control, and 42°C treated cells and HIPEC treated cells inhibited with necrostatin-1 with naïve monocytes isolated from healthy women. Necroptosis is thought to be an immunogenic form of cell death which mediates by DAMP release an immune reaction [8, 36].

We treated ES-2 and OVCAR-3 cells with and without chemotherapy at 37°C and 42°C with 20 hours post-treatment incubation in fresh cell culture medium and collected the supernatants. As negative control, necrostatin-1 was added to all conditions. As positive control lipopolysaccharide (LPS) was used. We incubated these supernatants of treated cells with isolated blood monocytes from four human donors for 20 hours. Afterwards IL6 levels were measured.

We found increased levels of IL6 in ES-2 cells treated with hyperthemic chemotherapy and also little increased levels after normothermic chemotherapy, which was inhibitable by necrostatin-1 (Fig. 21). OVCAR-3 cells showed no significant differences between the conditions in IL6 levels (data not shown). Blood monocytes reacted on necroptosis with increased IL6 production in ES-2 cells, indicating an immunogenic cell death.

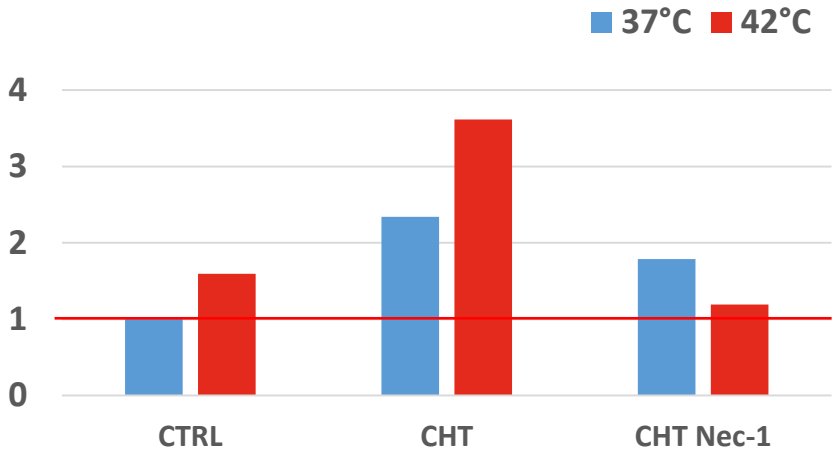

Figure 21. relative IL6 measurements in ES-2 cells.
CHT means chemotherapy treatment at 37°C (blue) or 42°C (red) and in the control (CTRL) are without chemotherapy at normothermic (37°C) or heat shock (42°C) treated cells. CHT+ Nec-1 means chemotherapy treatment and inhibition with Nec-1 during chemotherapy treatment and during incubation period.

Hsp90 is an essential key player promoting necroptosis

Several publications implicate a role of Hsp90 in necroptosis. According to Zhao *et al.* Hsp90 promotes MLKL stability and necroptosis [50]. Hsp90 is also essential for RIPK1 and RIPK3 caused necrosome formation [40].

Indeed, our findings also indicate a substantial role of Hsp90 in necroptosis as shown by co-localization of Hsp90 with RIPK3 and pMLKL (confocal microscopy) in all cases of putative necroptosis. To further investigate this finding we looked at shotgun proteomics data from cell free ascites. These data were obtained from ascites collected from HGSC patients of both tumor spread types by our collaboration partner from the Department of Analytical Chemistry from the University of Vienna (Ch. Gerner). Ascites was centrifuged at high speed to get a cell free supernatant which was analyzed via shotgun mass spectrometry. Proteins were identified and quantified. We found higher levels of both types of Hsp90 proteins, Hsp90-alpha and Hsp90-beta, coded by genes HSP90AA1 and HSP90AB1, respectively)) in cell free ascites of non-miliary tumor spread type. Type beta is constitutively expressed and type alpha is stress-inducible. Levels of soluble proteins of both types of Hsp90 are significantly lower in ascites of the miliary spread type ($p<0.05$).

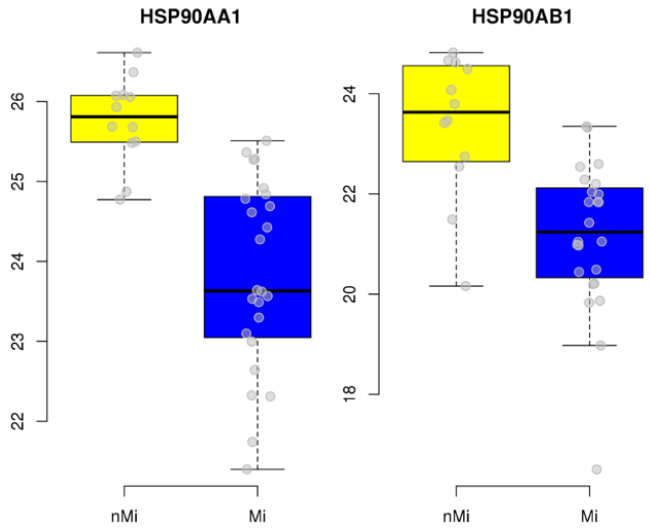

Figure 22. Levels of Hsp90-alpha and Hsp90-beta in cell free ascites of both tumor spread types.
Left. Levels of Hsp90 type alpha (HSP90AA1) which is stress-inducible. Right. Levels of Hsp90 type beta (HSP90AB1) which is constitutively expressed. (nMi, non-miliary; Mi, miliary; Hsp90, heat shock protein 90)

Levels of tiRNA are lower in tumor cells of non miliary spread type.

tRNA halves, especially 5' halves, are presumed to inhibit apoptosis by binding to cytochrome c and therefore prevent from apoptosome formation and apoptosis [7]. According to our hypothesis and the results described above (*i.e.* necroptosis only in non-miliary tumor cell lines after HIPEC-like treatment) we expected higher levels of tRNA fragments in cells of non-miliary spread type and a higher increase upon hyperthermic treatment which could promote a shift towards necroptosis.

We treated ovarian cancer tumor cells of different tumor spread types (ES-2, Tyk-nu, CAOV-3, and OVCAR-3), and immortalized ovarian surface epithelial cells (IOSE364 and IOSE80) and fallopian tube epithelial cells (FT194) with chemotherapy at 42°C and 37°C with 30 minutes and 20 hours incubation as described in the Methods section "in vitro HIPEC treatment". Additionally we performed a control with untreated cells. RNA was isolated and prepared for small RNA sequencing. We used the small RNA fraction from the RNA isolation with RNAs less than 200 nucleotides. Libraries were pooled and sequenced 50 bp single end on a Illumina HiSeq3000. After bioinformatical data analysis, we found higher levels of 5´tiRNA in cell of miliary spread type in comparison to non-miliary cells, contrary to our initial expectation

5´ halves after 37°C chemotherapy treatment after two hours (90 min of incubation and 30 min post-treatment growth in culture medium) were higher in cell lines of miliary spread type (FT194, CAOV-3, and OVCAR-3) as shown in Figure 23. 5´tiRNA expression in IOSE80 and IOSE364 cells increased after 2 hours and decreased after 20 hours at 37°C and 42°C (Fig. 24). IOSE cells are of ovarian origin and used as reference cell line for non-miliary tumor cells [3-5]. In the non-miliary cancer cells lines ES-2 and Tyk-nu, 5´halves decreased after chemotherapy treatment (Fig. 25). In immortalized tubal cells (FT194) and miliary tumor cell lines (CAOV-3 and OVCAR-3) 5´halves increased after 20 hours after chemotherapy treatment with higher levels at 42°C (Fig. 26) compared to 37°C. In general tiRNA levels are higher at 42°C chemotherapy treatment conditions in all cell lines, which may be beneficial for necroptosis induction, but are general higher in all conditions in miliary or tubal cell lines compared to non-miliary or ovarian cell lines.

As shown in Figure 26 there were higher levels of 5´halves at 42°C after 2 hours and 20 hours compared to 37°C in both malignant cell lines but not in the immortalized precursor cell line FT194. In non-miliary tumor cells there was a decrease of 5´tiRNA after 2 hours and 20 hours

compared to the control condition, regardless of the treatment condition (Fig. 25). Whereas IOSE cells showed an increase after 2 hours which normalized after 20 hours to the initial control 5'tiRNA concentration (Fig. 24).

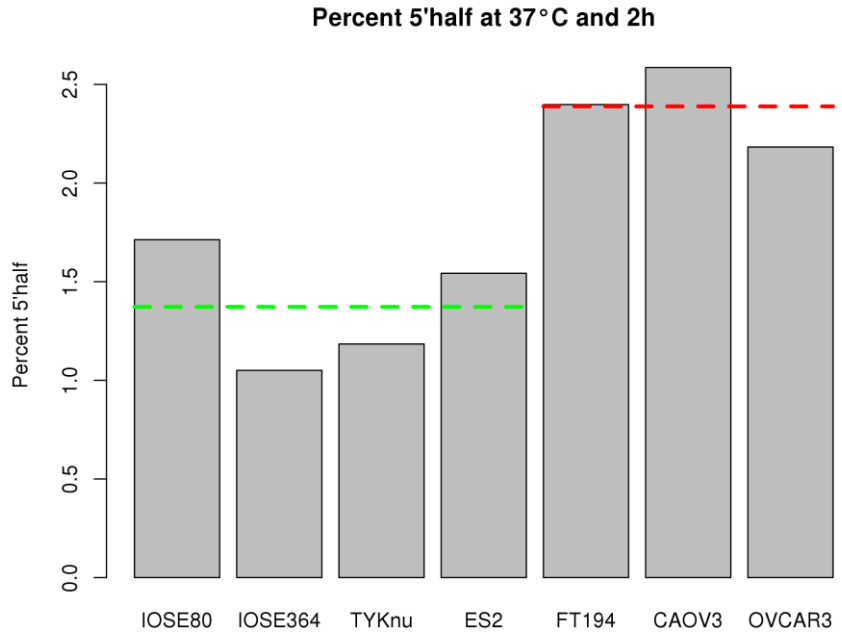

Figure 23. Levels of 5´halves at 37°C and 2 hours in miliary and non-miliary cells.
Levels of 5´tiRNA halves after chemotherapy treatment at 37°C after 2 hours (90 minutes chemotherapy treatment and 30 minutes incubation in fresh cell culture medium) of miliary (CAOV-3 and OVCAR-3), non-miliary (Tyk-nu and ES-2) tumor cell lines and immortalized tubal (FT194) and ovarian surface epithelial cells (IOSE). Green and red lines are the median levels of both groups, non-miliary and IOSE and miliary and FTE, respectively.

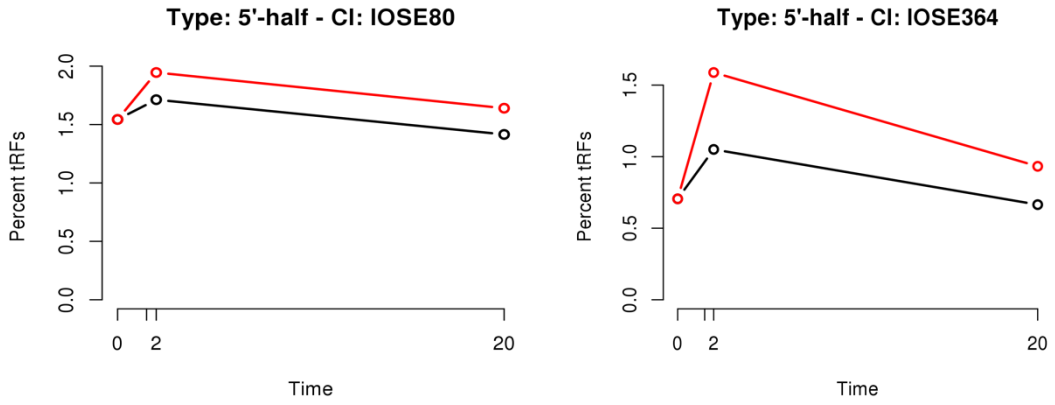

Figure 24. Abundance of 5´tiRNA in IOSE80 (left) and IOSE364 (right) at 37°C treated with chemotherapy (black line) and 42°C treated with chemotherapy (red line) after 2 hours and 20 hours.

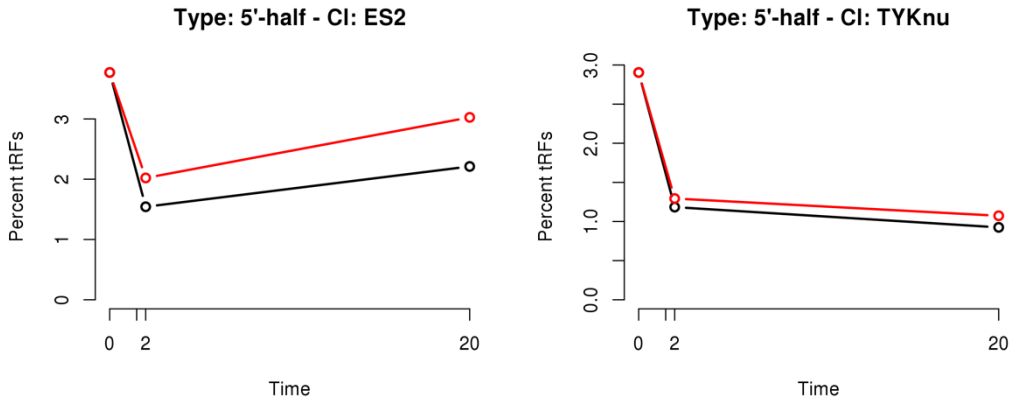

Figure 25. Abundance of 5´tiRNA in ES-2 (left) and Tyk-nu (right) at 37°C treated with chemotherapy (black line) and 42°C treated with chemotherapy (red line) after 2 hours and 20 hours.

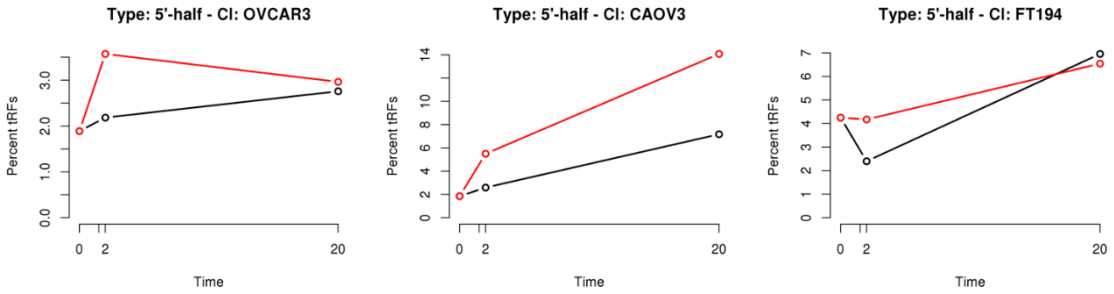

Figure 26. Abundance of 5´tiRNA in FT194 (left), CAOV-3 (middle) and OVCAR-3 (right) at 37°C treated with chemotherapy (black line) and 42°C treated with chemotherapy (red line) after 2 hours and 20 hours.

We further compared the relative percent change from 37°C to 42°C chemotherapy treatment after 2 hours and 20 hours of cell lines of both tumor spread type as shown in Figure 27. Here we also saw a higher increase of 5´halves from the 37°C to the 42°C condition in cells of the miliary spread type after 2 hours compared to the non-miliary spread type, which after 20 hours persisted in the non-miliary spreading cell lines but abolished in the miliary spreading cell lines. Taken together, initial concentrations of 5´halves are higher in tumor cells of miliary spread type and the increase from 37°C to 42°C is also higher in this type, but less stable after 20 h incubation (Fig. 27).

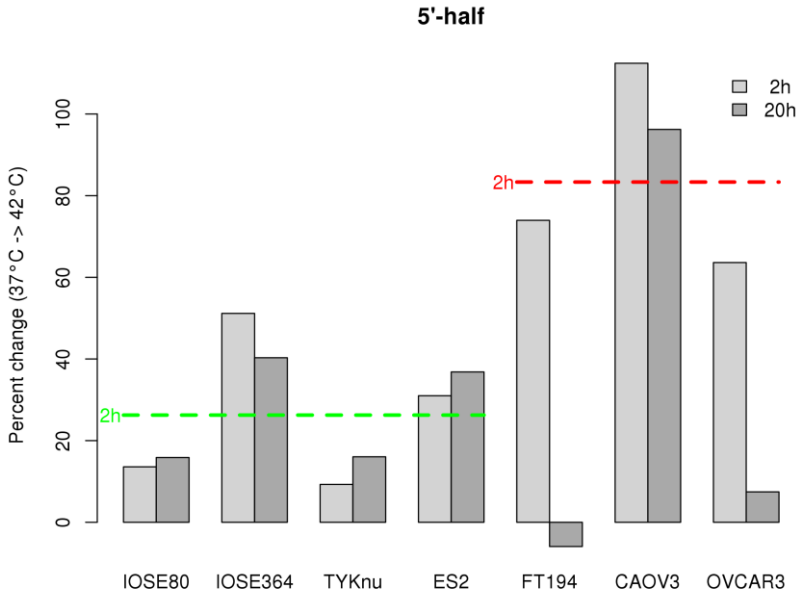

Figure 27. Percent change from 37°C to 42°C of 5´halves after 2 hours and 20 hours after chemotherapy treatment. Green and red lines are the median increases in both groups after 2 hours, non-miliary and OSE-like and miliary or FTE-like, respectively.

Comparison of 5'tiRNA fragments abundance and angiogenin and angiogenin inhibitor expression in miliary and non-miliary tumors of HGSC patients

To analyze tRNA fragments in tissues of HGSC patients we used small and rRNA depleted RNA-sequencing data from our group [3, 4]. Floating tumor cell aggregates (spheroids) were collected from ascites of HGSC patients. Additionally, single tumor cells (ascites) and solid tumors (primary and metastatic tumors) were also collected from HGSC patients, tumor tissues enzymatically digested and EpCAM-positive cells isolated by a magnetic bead approach (EpCAM is a marker for epithelial cells and cancer cells) Small RNAs and large RNAs were isolated from these enriched tumor cells and sequenced [3, 4].

We found higher levels of tRNA fragments in miliary tumor cells compared to non-miliary tumor cells, except in the primary ovarian tumor tissues. tRF levels were significantly higher in miliary ascites derived cells, either spheroids or single tumor cells, but significantly lower in primary solid tumor tissues, compared to non-miliary cells. Metastatic solid tissues were not different between miliary and non-miliary (Fig.28A). Compared to our results obtained

from the malignant and immortalized precursor cell lines, the results obtained from floating tumor cell lines fits to these results: higher concentrations in miliary compared to non-miliary. 5´and 3´halves are produced by angiogenin cleavage as described in the Introduction [41]. Therefore, we also determined the expression of angiogenin in tumor cells and tumor tissue. Surprisingly, we found lower angiogenin levels in miliary tumor cells in ascites (Fig. 28B), mirroring exactly the situation of tRF levels. This is unexpected, as a direct correlation would be expected if angiogenin is the enzyme producing tRFs. Therefore, we further analyzed the expression levels of the inhibitor of angiogenin, ribonuclease/angiogenin inhibitor 1 (RNH1). Interestingly, the expression of RNH1 mirrored again the expression of angiogenin and looked therefore like the abundance of the tRFs, indicating the inhibitor as the driving factor of the tRFs abundance differences between miliary and non-miliary. (Fig. 28C). We summarized these findings in a scheme (Fig. 30). In miliary tumor cells in ascites are higher levels of tRNA fragments but contrary to this lower levels of angiogenin, which produces tRFs. But there are also lower levels of angiogenin inhibitor RNH1, resulting in decreased inhibition of angiogenen and therefore finally higher levels of tRNA fragments. Shotgun proteomics of cell free ascites (done by Christopher Gerner) also found lower levels of the angiogenin inhibitor RNH1 in patients with miliary tumor spreading, fitting to the expression values of RNH1 in ascitic tumor cells.

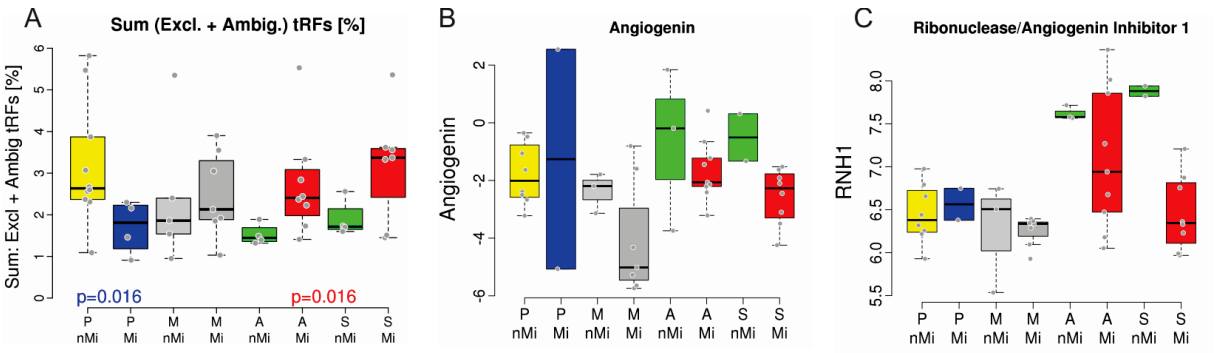

Figure 28. A) Abundance of tRNA fragments in tumor cells and tumor tissue of HGSC patients B) Expression of angiogenin in tumor cells and tissues C) Expression of angiogenin inhibitor RNH1 in tumor cells and tissue. Data were obtained from small RNA and rRNA depleted RNA sequencing of tumor cells and tissue collected from HGSC patients [3, 4]. (P, solid primary ovarian tumor; M, solid metastatic tumor; A, single ascites tumor cells; S, spheroids; Mi, miliary; nMi: non-miliary)

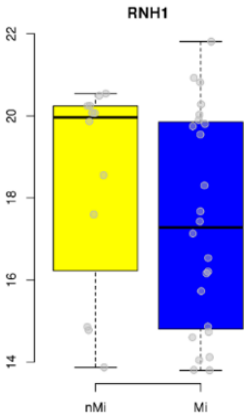

Figure 29. Shotgun proteomics of cell free ascites of patients with miliary (Mi) and non-miliary (nMi) tumor spread.

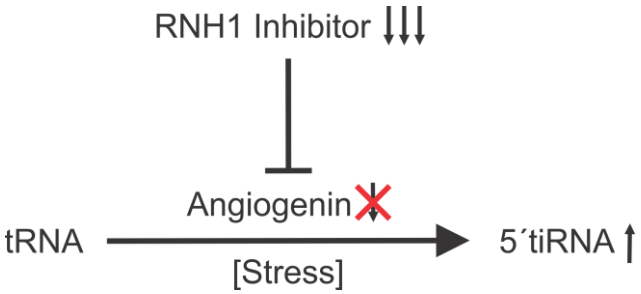

Figure 30. Scheme of angiogenin mediated tRNA cleavage in miliary ascites tumor cells.

In summary, in cell lines of putative miliary tumor spread and their corresponding immortalized precursor cells are initially higher levels of 5'tiRNAs and higher relative increases of 5'tiRNAs after HIPEC-like treatments but no signs of necroptosis. In non-miliary tumor cells are lower initial levels and lower relative increases of 5'tiRNAs after HIPEC-like treatments but increased signs of necroptosis. This is contrary to our hypothesis that 5'tiRNAs could promote a shift from apoptotic to necroptotic cell death.

Additionally, in ES-2 cells we found an indication for immunogenic necroptotic cell death shown by increased activation of naïve blood monocytes by the supernatants of these cells, indicated by increased IL6 release.

Early epigenetic changes after chemotherapy treatment

To analyze early epigenetic events after HIPEC-like treatment on cell culture cells reduced representation bisulfite sequencing (RRBS) was performed before and after treatment in four cell lines, two of putative miliary (OVCAR-3 and FT194) and two of putative non-miliary (ES-2 and IOSE80) spread type or their precursor cells. DNA was collected from seven cell lines of miliary and non-miliary spread type without treatment (IOSE364, IOSE80, Tyk-nu, ES-2, FT 194, CAOV-3, and OVCAR-3) and four cell lines (IOSE80, ES-2, OVCAR-3, and FT194) after 37°C (normothermic) and 42°C (hyperthermic)chemotherapy treatment and subsequent 20 hours incubation in fresh cell culture medium. DNA was isolated, bisulfite treated, libraries generated and sequenced for 50 bp single end with Illumina HiSEQ3000 using the reduced representation bisulfite sequencing (RRBS) protocol (this was done in collaboration with the Biomedical Sequencing Facility (BSF; Christoph Bock) [24]. After RRBS sequencing, mapping and CpG calling median 4.4 million Beta-values (estimate of the methylation level using the ratio between methylated and unmethylated alleles) of CpGs for each sample were obtained. Bioinformatic analysis revealed methylation differences already after 20 hours affected by chemotherapy treatment. *Long interspersed nuclear element 1* (*LINE1*), which is a transposable element in the human genome, was hypomethylated upon stress induction with chemotherapeutics regardless of temperature, 42°C or 37°C, after 20 hours as shown in Figure 31A. Following these early methylation changes we looked also for expression differences of *LINE1* from our RNA sequencing data. *LINE1* expression was determined from small RNA sequencing data from cell lines bevor and after chemotherapy treatment of 132 LINE-1 sequences (Fig. 31B). LINE1 expression was slightly increased only in ES-2 cells after chemotherapy treatments, fitting to the results obtained by RRBS sequencing, where ES-2 showed the by far highest hypomethylation of LINE1.

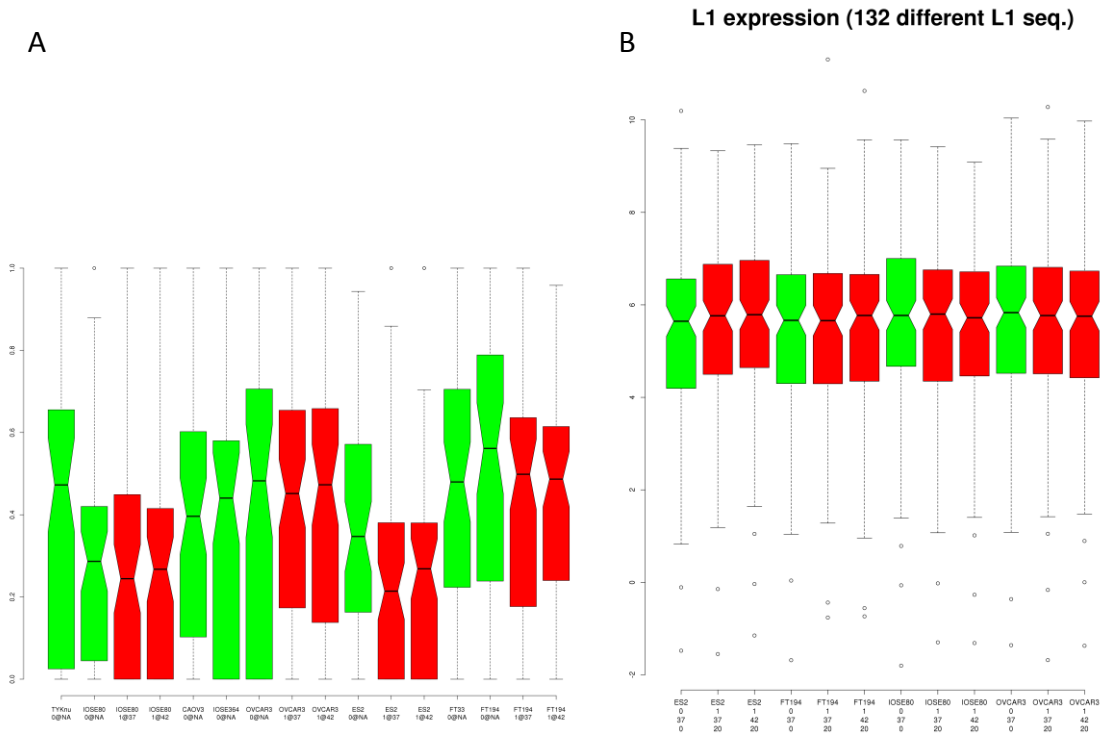

Figure 31. Methylation changes in *LINE1* and expression of *LINE1.*
A) *LINE1* methylation. Hypomethylation of *LINE1* after chemotherapeutic treatment at 37°C and 42°C (red bars) compared to untreated cells (green bars). Y-axis, boxplot of Beta values of all CpGs mapped to LINE1 sequences. B) Expression differences in 132 LINE1 sequences. (0, control, without chemotherapy; 1, with chemotherapy treatment at 37°C or 42°C; two time points: zero (0) and after 20 hours).

Using a fast and sensitive calling algorithm for detecting of differentially methylated regions from bisulfite sequencing data, METILENE v0.2-7 [51], we compared controls with chemotherapy treated samples and found 195 significant (false discovery rate, FDR<5%) regions differentially methylated between controls and chemotherapy treated conditions. (Table. 6)

								Mean Beta-value	
Chromosome	Start	End	Q-value	Mean difference	CpGs	Raw p-value	Adj. p-value	CTRL	CHT
chr21	8406699	8407913	0.0012	0.146316	47	1.10E-11	8.40E-09	0.64453	0.49821
chr21	8450886	8452065	0.0057	0.142582	49	1.50E-11	4.00E-08	0.63683	0.49425
chr2	**106466097**	**106466169**	**0.035**	**0.207438**	**10**	**8.10E-09**	**2.50E-07**	**0.69829**	**0.49085**
chr7	63762044	63762686	0.11	0.26	15	5.60E-08	7.60E-07	0.66513	0.40513
chr17	26962987	26963033	0.15	0.358875	10	1.00E-10	1.00E-06	0.67876	0.31989
chr1	228623552	228623910	0.34	0.134369	20	6.10E-08	2.30E-06	0.64318	0.50881

chrY	11314141	11315368	0.35	0.136975	40	2.50E-08	2.50E-06	0.47693	0.33996
chr7	56370522	56370968	0.44	0.14983	14	7.60E-05	3.10E-06	0.59141	0.44158
chr21	8225468	8226057	1	0.145588	27	6.10E-07	1.80E-05	0.66008	0.51449
chr1	228634780	228635125	1	0.126118	17	5.80E-07	3.00E-05	0.62386	0.49774

Table 6. Output of METILENE finding regions differentially methylated between control and chemotherapy treated cells (Only the first 10 of 195 significant regions are shown).

Interestingly, the third significant region (bold in Table 6) is inside a CpG-island (Chr2: 106,465,873-106,468,480) for the gene called *RANBP2-like and GRIP domain containing 3* (*RGPD3*) (Fig. 33). RGPD3 is located on chromosome 2 and is putatively a member of the nucleoporin family. It has high sequence similarity to proteins involved in RNA transport [52, 53]. Ran proteins are GTP binding proteins involved in nuclear transport [54].

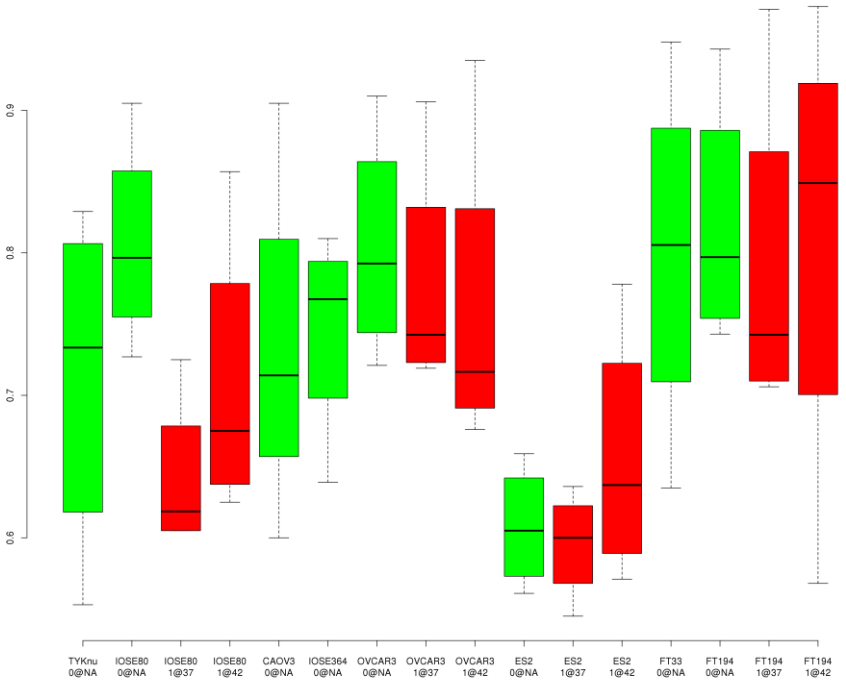

Figure 32. Hypomethylation of RGPD3 after chemotherapy treatment.
Chemotherapy treatment at 37°C or 42°C in red bars and controls in green bars. RGPD3 is significantly hypomethylated upon chemotherapy treatment at 37°C and 42°C in all cell lines except ES-2. (0, without chemotherapy; 1, with chemotherapy treatment @ 37°C or 42°C). Y-axis, boxplot of the beta values of all called CpGs mapped to the CpG-island of the gene RGPD3.

Using publicly available RNA-sequening data from 303 HGSC patients (The Cancer Genome Atlas, TCGA) a co-association network was built with 20,501 nodes and 4.3 mio edges (Tool for Inferring Network of Genes, TINGe, [55]). This hairball network was planar filtered and yielded finally a small world and scale-free network of 20,501 nodes and 47,581 edges (Multiscale Embedded Gene Co-expression Network Analysis, MEGENA, [56]), which was further sub-clustered into 653 hierarchically nested clusters with hub genes. Using the beta values of all untreated cell lines and comparing between miliary spreading of tubal origin (OVCAR-3, CAOV-3, and FT194) on one side and non-miliary of ovarian origin (ES-2, Tyk-nu, IOSE80, and IOSE364) on the other side revealed ten significantly differentially methylated networks (Table 7).

NetworkID	Nodes	Raw p-value	FDR
c1_2	2111	1.58E-29	1.02E-26
c1_5	851	6.32E-07	0.000203
c1_87	652	9.52E-07	0.000204
c1_7	671	3.16E-06	0.000507
c1_11	671	2.53E-05	0.002707
c1_13	424	2.46E-05	0.002707
c1_305	583	3.03E-05	0.002784
c1_154	**24**	**0.000119**	**0.009586**
c1_89	344	0.000335	0.023935
c1_75	27	0.000564	0.036237

Table 7. Differentially methylated networks between miliary cell lines of tubal origin and non-miliary cell lines of ovarian origin (FDR, false discovery rate).

Interestingly, the smallest of all significant networks was c1_154 – with nearly all genes hypomethylated in miliary – with the hub genes PAX8, TGFR2, NCAM1, and EMX2. PAX8 is known as fallopian tube specific gene, and therefore used as marker for ovarian cancer (fallopian tubes secretory cells are thought to be the origin of most HGSC cases, see Introduction). We confirmed the different expression of PAX8 in these cell lines and in miliary (high) and non-miliary (low) HGSC tissues already in our publication from Auer *et al.* [5]. Our data indicate that an epigenetically regulated network around the hub genes PAX8, TGFR2, NCAM1, and EMX2 could initially arise from the epigenetic differences between fallopian tube and ovarian epithelial cells (PAX8) but could also be involved in the different spreading

characteristics (NCAM1, a cell adhesion protein which is a member of the immunoglobulin superfamily and involved in cell-to-cell interactions).

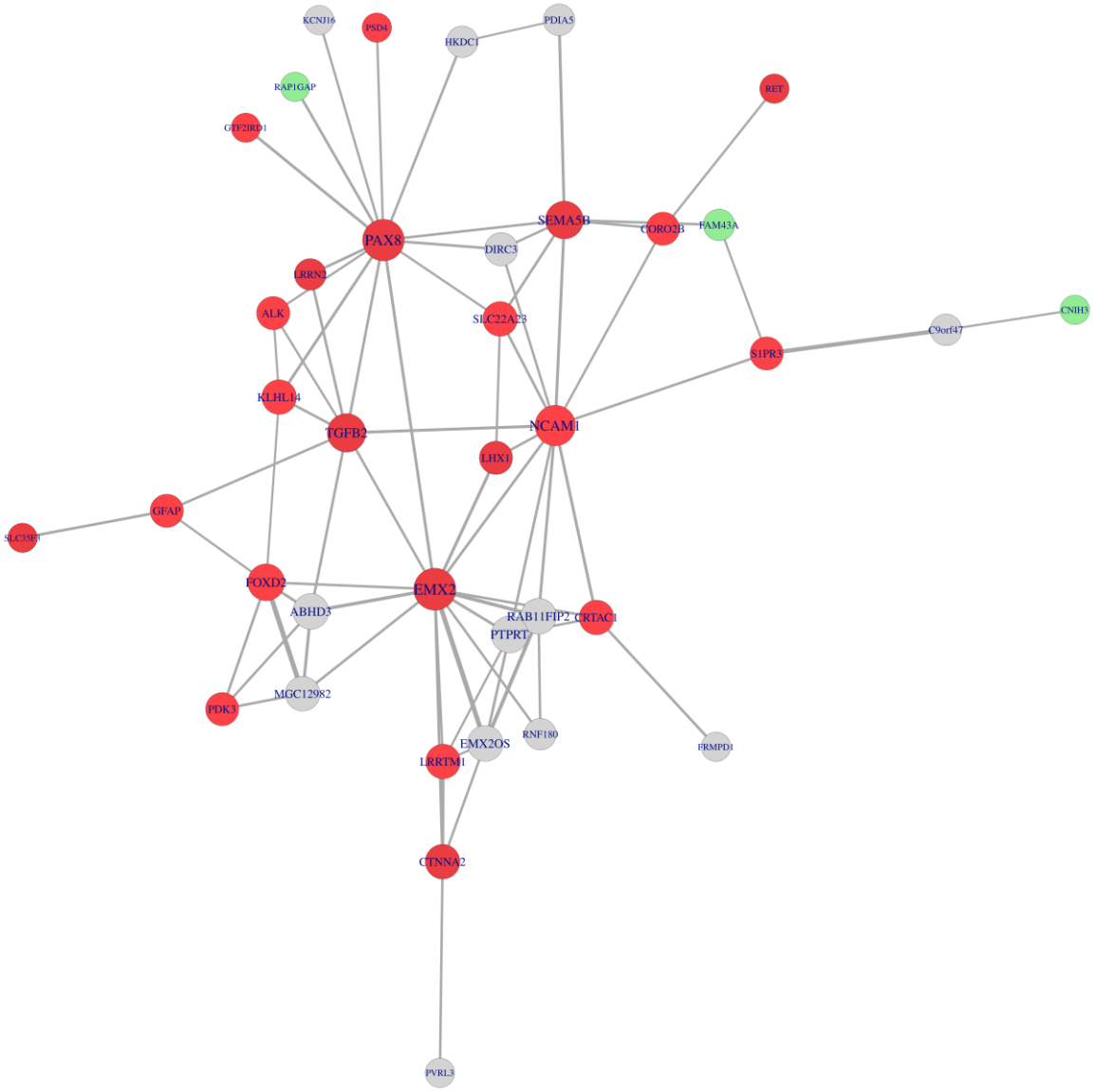

Figure 33. Differentially methylated cluster c1_154 between miliary and non-miliary cell lines.
Co-associated sub-network consisting of 38 genes four of them hub genes, *PAX8, EMX1, NCAM1* and *TGFB2.* Red means hypomethylated in miliary/tubal; green, hypermethylated in miliary/tubal, and grey, no methylation data available for these genes. Large circles indicate hub genes.

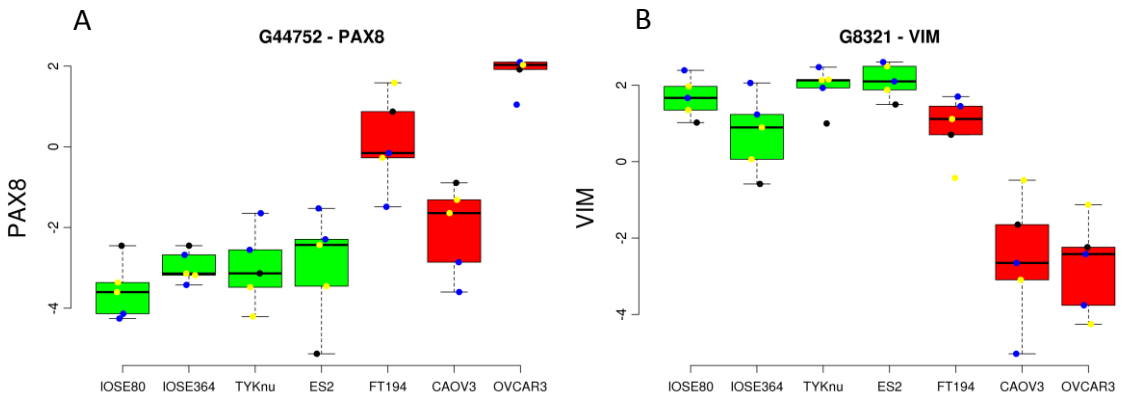

Figure 34. Expression differences in miliary and non-miliary cell lines (estimated from RNA-sequencing). A) Box blots represent expressions of *PAX8* (A) and vimentin (B) in indicated cell lines. All conditions are shown (blue, control and chemotherapy at 37°C and 42°C after 2 h post treatment start, and yellow, after 20 h post-treatment start). (Cell lines of milary spread type are CAOV-3, OVCAR-3, and FT194 as precursor cell line and cell lines of non-miliary spread type are ES-2 and Tyk-nu with IOSEs as precursor cell lines [4, 5]).

To compare global methylation beta values of all called CpGs we generated boxplots of all analyzed cell lines and conditions (Fig. 36). Interestingly, one non-miliary (ES-2) and all ovarian derived cell lines (IOSE80 and IOSE364) showed lower median methylation beta values, with the exception Tyk-nu, compared to all miliary or tubal derived cell lines (CAOV-3, OVCAR-3, FT33, and FT194).

Further research is required to validate these methylation differences in solid tumor tissues (primary and metastasis), single ascites tumor cells and spheroids of HGSC patients.

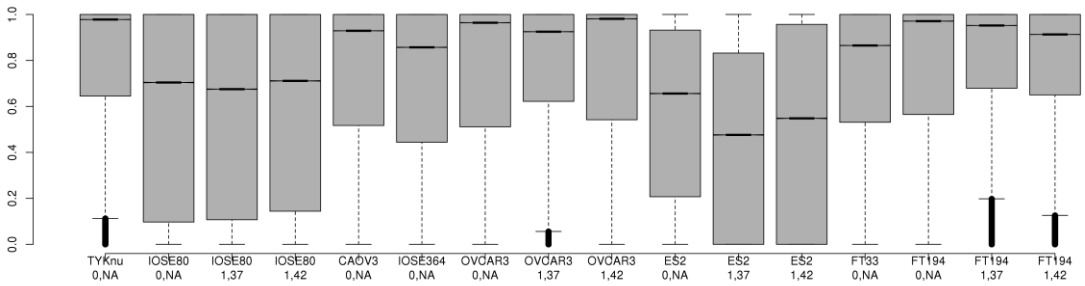

Figure 35. Boxplots of beta values of all called CpGs in all cell lines and all examined conditions. (0 and NA, control, without chemotherapy treatment; 1, chemotherapy treatment at 37°C or 42°C).

Discussion

Ovarian cancer has the highest mortality of all gynecologic malignancies. Patients are diagnosed at advanced stage and often develop peritoneal carcinomatosis which is the most challenging issue. We described two types of peritoneal carcinomatosis which we called miliary and non-miliary [3-5, 57]. We also showed that patients with miliary tumor spread had a significant worse outcome compared to patients with non-miliary tumor spread [3, 4]. To improve the outcome of patients, especially of patients with miliary tumor spread, new therapeutic strategies are needed and one of them could be the hyperthermic intraperitoneal chemotherapy (HIPEC). The positive effects of HIPEC were recently reported by Van Driel *et al.* (2018) where they showed that median overall survival was increased by nearly one year with only few side effects, but the molecular mechanisms of HIPEC remains largely unknown [58].

Here, we report first evidences for an immunogenic necroptotic cell death after hyperthermic intraperitoneal chemotherapy of non-miliary ovarian cancer cells. Cell lines of non-miliary spread (ES-2, Tyk-nu, IOSE80 and IOSE364) showed increased necroptosis at hyperthermic chemotherapy conditions (42°C), with the highest increase of 12.5% in ES-2, compared to normothermic chemotherapy (37°C) and control conditions (Fig. 9C-F). Cell lines of miliary spread showed no increased necroptosis at any conditions (Fig. 9A-B, 9G). As direct proofs for necroptotic cell death are difficult, necroptosis was defined in this work by co-localization of pMLKL and RIPK3 at cell boarders and the inhibitability of this co-localization by a specific inhibitor of necroptosis, *i.e.* necrostatin-1. Co-localization of RIPK3, pMLKL, and Hsp90 was found in non-miliary cells at hyperthermic chemotherapy conditions (42°C) (Figs. 11 and 13). MLKL and RIPK3 are besides RIPK1 essential proteins in necroptosis and phosphorylation of MLKL, leading to pMLKL, is one of the key-events in necroptosis initiation. Several stimuli including some chemotherapeutics result in activation and phosphorylation of RIPK1 which subsequentially result in phosphorylation of RIPK3 and thereby forming the so called necrosome. This leads to autophosphorylation of MLKL which then oligomerizes and translocates into the plasma membrane and disrupts the cytoplasmic membrane. Disruption of the membrane leads to cell leakage which results in the release of so called damage associated molecular patterns (DAMPs) [8]. Therefore necroptosis is considered as an immunogenic form of cell death, compared to apoptosis, which is considered as immunogenic

silent. Both chemotherapeutic classes used in this work, platin based and taxanes, can stimulate necroptosis in some *in vitro* experiments, *e.g.* Cisplatin activates RIPK3 directly and Taxol activates RIPK1 [8].

We found that only non-miliary serous ovarian cancer lines showed increased necroptosis events (as defined above) after chemotherapy treatment only at hyperthermic conditions. HIPEC was reported to have several beneficial effects, including increased penetration of the chemotherapeutics into the tissue through hyperthermia and therefore increased cytotoxicity of chemotherapeutic agents [10]. Additionally, chemotherapeutic agents can be tolerated at higher concentrations through their local administration, compared to the usual systemic administration of chemotherapy [9, 10]. To rule out that already hyperthermia alone, *i.e.* without chemotherapy, increases necroptosis, we performed hyperthermic treatment at 42°C alone and compared to the effects at normothermic chemotherapy and HIPEC conditions. At hyperthermic conditions, we didn´t find increased frequencies of necroptosis. Only with addition of chemotherapeutics at hyperthermic conditions we saw increased co-localization of necroptosis markers at the cell boarder (Figs. 13 and 14). Interestingly, we also found Hsp90 localized at cell boarders together with pMLKL and RIPK3 (Fig. 11). Hsp90 is reported to promote necrosome assembly and pMLKL oligomerization and translocation [40]. Zhao *et al.* reported an essential role of Hsp90 in pMLKL and RIPK3 stability, activation of both, and therefore necrosome formation [50]. This report strengthens the interpretation of our results as necroptosis further. We found that both types of Hsp90, the inducible (alpha) and constitutively expressed (beta) types are higher expressed in serous ovarian cancer cells of the non-miliary spread type (Fig. 22).

To strengthen our interpretation of increased cell death by necroptosis in non-miliary cell lines, we also wanted to exclude the other major form of cell death, apoptosis. We found only a few positive cells with caspase 3, M30 or cleaved PARP staining, regardless of the condition, interpreted as basic apoptosis usually seen in every cell culture cells (Fig. 19). Therefore, we could exclude apoptosis as main reason for cell death events at 20 h after HIPEC treatment *in vitro*. Confirming our evidence of increased necroptosis in non-miliary tumor cell lines at HIPEC conditions, necroptosis was inhibited by necrostatin-1 in stainings of treated cells (Fig. 14B)

One major aim of chemotherapy treatment in cancer, besides the direct destroying of tumor cells, is to promote a tumor directed immune reaction. Necroptosis is presumed to be an

immunogenic form of cell death promoted by DAMP release. DAMPs are molecules like "*non-histone chromatin-binding protein high mobility group box 1"* (HMGB1), ATP, Hsp90, and Hsp70 which can induce an immune response [10].

In our research, we found activation of naïve blood monocytes isolated from healthy women if they were incubated 20 h with cell free supernatants of cells treated with HIPEC conditions compared to cells treated with normothermic chemotherapy, hypothermia alone, or mock. Activation of monocytes was measured by IL6 increase, an early immune response cytokine. Activation of IL6 was completely inhibited by necrostatin-1 at the HIPEC condition. Heat shock proteins are reported to promote alone an immune response through exposure on cell surface or as DAMP release which is recognized by antigen presenting cells (APC), like dendritic cells, which then mediate antigen cross presentation and activation of T-cells [10, 59]. Therefore, it was of further interest whether hyperthermic treatment alone can also induce immunogenicity. At hyperthermic conditions we found no increased levels of IL6. Taken together, HIPEC conditions led to an immunogenic cell death whereas hyperthermic or chemotherapy treatments alone did not, which was inhibitable by necrostatin-1 (Fig. 21).

According to our working hypothesis, we proposed that tiRNA production upon heat stress during hyperthermic treatment conditions could shift cell death from apoptosis to necroptosis. Upon stress induction with chemotherapy and heat we suggested that tRNAs are cleaved by angiogenin and tRNA fragments (tiRNA), especially 5'tiRNAs, are produced. 5'tiRNAs are known to bind to free cytochrome *c* in the cytoplasm, released from mitochondria after apoptosis initiating signaling, and forms a ribonucleoprotein complexes (RNP) which prevents cytochrome *c* to induce apoptosis. Cytochrome *c* is necessary in apoptosome formation by binding to Apaf-1. This process is inhibited by 5'tiRNAs which are bound to cytochrome *c* [7]. Upon apoptosis inhibition by 5'tiRNA fragments we proposed a shift towards necroptosis. In previous studies it has been reported that 5´tiRNA can lead to translational inhibition and stress granule assembly but not 3´tiRNA [7]. Therefore we focused on 5´halves (5'tiRNAs). In contrast to our hypothesis, we found higher levels of 5´tiRNAs upon 37°C chemotherapy treatment and even higher increases upon HIPEC treatment compared to the 37°C condition after 2 hours in cells of the miliary spread type in comparison to cells of non-miliary spread type (Figs. 23 and 27). To remind, miliary tumor cells showed no signs of increased necroptosis after HIPEC treatment conditions. Our results imply that changes in

5’tiRNAs abundance seem not to be the key process for increased necroptosis, at least in miliary tumor cells.

In non-miliary tumor cell lines (ES-2 and Tyk-nu) and their precursor cell lines (IOSE80 and IOSE364) the following picture of 5’tiRNA changes was seen: Increase of 5’tiRNAs was always seen in HIPEC conditions compared to normothermic chemotherapy conditions, but only in immortalized precursor cell lines an overall increase was seen compared to the mock treated controls (Figs. 24 and 25). In miliary cell lines, malignant like CAOV-3 and OVCAR-3 or immortalized precursors like FT194, the situation was more complex (Fig. 36).

To sum up, we saw changes in 5’tiRNA abundance after HIPEC treatment which is similar in cell lines of different tumor spread types. The concentrations of 5´tiRNA after 2 hours after normothermic chemotherapy treatment were higher in miliary tumor cells and were even higher induced after hyperthermic chemotherapy conditions (Fig. 27). In miliary cancer cells 5’tiRNA increased (CAOV-3 and OVCAR-3) and in non-miliary cancer cells 5´tiRNA decreased (ES-2 and Tyk-nu) after any chemotherapy treatment (Figs. 25 and 26). In both tumor subtypes 5’tiRNAs levels were higher at a temperature of 42°C in comparison to 37°C, which was expected from its functions as early stress response molecules. In the relative changes from 37°C to 42°C we saw an increase of 5´tiRNAs which was higher in miliary tumor cell lines in comparison to non-miliary tumor cell lines and their corresponding precursor cell lines (Fig. 27).

According to literature 5´halves are reported to sequester YBX1 which resulted in mRNA destabilization and degradation [60]. Goodarzi *et al*. (2015) reported that specific tRNA fragments in breast cancer sequester YBX1 and therefore prevent from stabilization of oncogenic transcripts which resulted in degradation of oncogenic transcripts. This process would suppress cancer progression [60]. Additionally, they found decreased concentrations of tRNA fragments in metastatic tumors and malignant tissues in comparison to normal tissues [60]. Furthermore, they stated that tRFs are upregulated under hypoxic stress conditions.

We also found an upregulation of tRNA fragments upon stress induction with chemotherapy and heat, but more pronounced in miliary cells. Contrary, in non-miliary cells tRNA fragments were downregulated after stress induction. Miliary cells are more epithelial and tumor spread was reported as “*directly metastasis”* where floating tumor cells adhere directly onto the

peritoneal wall. Non-miliary tumor cells are more mesothelial and could show more of a "normal metastatic spread" via circulatory systems [5].

In general, tiRNA levels of both subtypes differ and react on HIPEC treatment (Fig. 36, 37). How this process influence clinical outcome is under further investigation. As known, high grade serous ovarian cancer patients with non-miliary tumor spread type have a better clinical outcome compared to patients with miliary tumor spread type [4, 5]. Initial tiRNA levels were higher in non-miliary cancer cells compared to normal cells (Fig. 25). As reported by Goodzari *et al.* higher tiRNA levels are found in normal and non-metastatic tissue, therefore tRNA fragments could repress metastatic spread [60]. This could be a possible explanation that the high tiRNA levels in non-miliary could be co-responsible for the better clinical outcome.

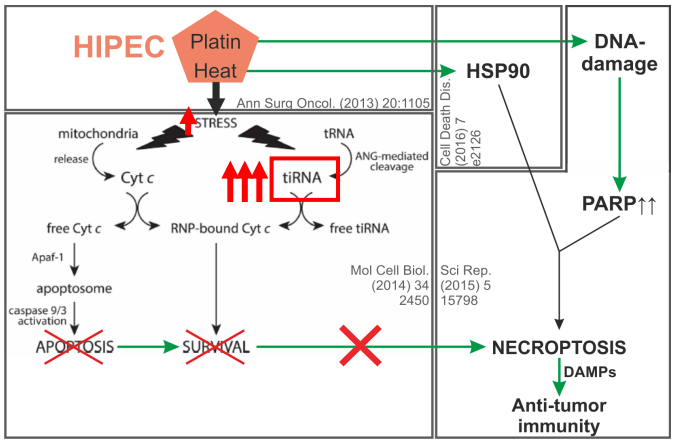

Figure 36. 5´tiRNA levels in cells of miliary tumor spread type.
Higher levels after 2 hours and higher increases from 37°C to 42°C of 5´tiRNA in cells of miliary spread type.

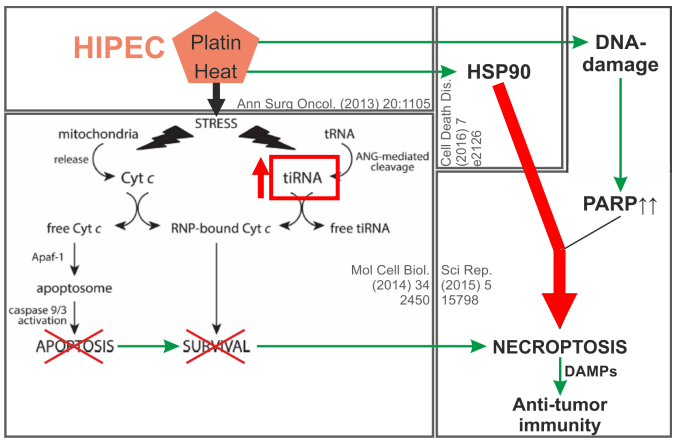

Figure 37. 5´tiRNA levels in cells of non-miliary tumor spread type.
Lower levels and lower increases from 37°C to 42°C of 5´tiRNA fragments in cells of non-miliary spread type, but increased signs of necroptosis. Hsp90 is a key regulator in necrosome formation.

In tumor tissues of HGSC patients we also found higher levels of tRNA fragments in spheroids and single tumor cells from ascites and in metastatic tumor tissues of the miliary tumor spread type. However, in primary ovarian tumor tissues it was the other way round (Fig.28A), there was a higher concentration of tRNA fragments in non-miliary tumor cells. Surprisingly, angiogenin levels in spheroids of miliary tumor cells were lower (Fig. 28B). This result is contrary to the fact that angiogenin is reported to cleave tRNA fragments (Fig. 30). Levels of angiogenin inhibitor (RNH1) were much lower in cell of milary spread type (Fig. 28C), suggesting less inhibition of angiogenin and therefore allowing a higher activity, fitting to the higher levels of tRNA fragments in miliary tumor cells. RNH1 levels were much higher in non-miliary tumor cells leading to more inhibition of angiogenin and therefore less cleavage of tRNAs.

We also searched for differences in global DNA-methylation status after HIPEC treatment. Interestingly we found already differences in DNA-methylation after 20 hours after chemotherapy treatment in all cell lines. Significant differences were found in the repetitive sequences *LINE1* and the CpG-island of the gene *RGPD3* (among others). *RanBP2-like and GRIP domain-containing protein 3* (*RGPD3*) is presumed to act in intracellular trans nucleus transport and is highly expressed in ovarian cancer [52, 53]. Nuclear transporter are also known to be involved in chemotherapy resistance, possibly by transporting chemotherapeutic drugs out of the nucleus. The CpG-island of *RGPD3* showed hypomethylation after chemotherapy treatment after 20 hours in IOSE, FTE, ES-2, and OVCAR-3 cells (Fig. 32), possibly indicating a first epigenetic mechanism for resistance development. *Long interspersed nuclear element 1* (*LINE-1*) showed hypomethylation upon stress induction with chemotherapeutics at 37°C and 42°C after 20 hours (Fig. 31). Taken together, we saw the first epigenetic reaction on chemotherapy already after 20 hours.

We reported necroptosis in serous ovarian cancer cell lines of the non-miliary spread type. However in cells of miliary spread type we found no increased signs of necroptosis. Expression data showed RIPK1, RIPK3 and Caspase 8 expression in all cell lines, therefore all cell line should be able to undergo necroptosis (Fig. 20).

Auer *et al.* (2015) reported reduced expression of genes defining a tumor spread factor (TSF) which correlated with a better overall survival of HGSC patients with putative non-miliary

tumor spread. This tumor subtype appears with bulky tumor nodules and showed a reduced epithelial cell characteristic. Immunologically, non-miliary tumor cells have a more inflamed status elevated by higher IL7, IL8, RIPK2 and NF-κB levels and a more adaptive immune response [4-6]. By contrast miliary tumor cells have more innate immune response and a worse overall survival. Because of the worse overall survival of the miliary tumor spread type, it would be necessary to find improved treatment for this kind of ovarian cancer patients. But according to our results, HIPEC would work better to patients of the non-miliary spread type, therefore treatment for miliary HGSC patients still needs to be improved.

Immunogenic cell death was found after hyperthermic chemotherapy only in non-miliary ovarian cancer cells which are of mesenchymal origin [4]. Epithelial to mesenchymal transition is a crucial event in promoting cancer metastasis, at least in other cancer entities [61]. The mesenchymal characteristic allows a cancer cell to leave the tumor tissue and to increase their survivability during circulation in circulatory systems (blood or lymphatic) due to stem cell like properties which can correlate with a more aggressive metastatic potential [62]. Our findings indicate a potential benefit of chemotherapy in combination with hyperthermia in non-miliary tumor cells, which are more mesenchymal in HGSC. Therefore, hyperthermia in combination with systemic chemotherapy could be used in other tumor entities with high metastatic potential, defined by a mesenchymal phenotype. Hyperthermia in combination with other therapeutic strategies as radiotherapy or chemotherapy could improve response to the treatment, as we showed probably by induction of an immunogenic necroptotic cell death. Additionally in relapsed patients hyperthermia could also improve outcome [63]. Summarized, as we reported an immunogenic necroptosis in mesenchymal non-miliary tumor cells after HIPEC-like treatment, whole-body hyperthermia in combination with chemotherapy could improve outcome in other tumor entities with high metastatic potential.

References

1. Ichim, G. and S.W. Tait, *A fate worse than death: apoptosis as an oncogenic process.* Nat Rev Cancer, 2016. **16**(8): p. 539-48.
2. Karst, A.M. and R. Drapkin, *Ovarian cancer pathogenesis: a model in evolution.* J Oncol, 2010. **2010**: p. 932371.
3. Bachmayr-Heyda, A., et al., *Small RNAs and the competing endogenous RNA network in high grade serous ovarian cancer tumor spread.* Oncotarget, 2016. **7**: p. 39640-39653.
4. Auer, K., et al., *Peritoneal tumor spread in serous ovarian cancer-epithelial mesenchymal status and outcome.* Oncotarget, 2015. **6**(19): p. 17261-17275.
5. Auer, K., et al., *Comparative transcriptome analysis links distinct peritoneal tumor spread types, miliary and non-miliary, with putative origin, tubes and ovaries, in high grade serous ovarian cancer.* Cancer Lett, 2016.
6. Auer, K., et al., *Role of the immune system in the peritoneal tumor spread of high grade serous ovarian cancer.* Oncotarget, 2016. **7**(38): p. 61336-61354.
7. Saikia, M., et al., *Angiogenin-cleaved tRNA halves interact with cytochrome c, protecting cells from apoptosis during osmotic stress.* Mol Cell Biol, 2014. **34**(13): p. 2450-63.
8. Chen, D., J. Yu, and L. Zhang, *Necroptosis: an alternative cell death program defending against cancer.* Biochim Biophys Acta, 2016. **1865**(2): p. 228-36.
9. van Driel, W.J., et al., *The role of hyperthermic intraperitoneal intraoperative chemotherapy in ovarian cancer.* Curr Treat Options Oncol, 2015. **16**(4): p. 14.
10. Zunino, B., et al., *Hyperthermic intraperitoneal chemotherapy leads to an anticancer immune response via exposure of cell surface heat shock protein 90.* Oncogene, 2016. **35**(2): p. 261-8.
11. Aust, S., et al., *Absence of PD-L1 on tumor cells is associated with reduced MHC I expression and PD-L1 expression increases in recurrent serous ovarian cancer.* Sci Rep, 2017. **7**: p. 42929.
12. Landen, C.N., Jr., M.J. Birrer, and A.K. Sood, *Early events in the pathogenesis of epithelial ovarian cancer.* J Clin Oncol, 2008. **26**(6): p. 995-1005.
13. Meinhold-Heerlein, I., et al., *The new WHO classification of ovarian, fallopian tube, and primary peritoneal cancer and its clinical implications.* Arch Gynecol Obstet, 2016. **293**(4): p. 695-700.
14. Zeppernick, F. and I. Meinhold-Heerlein, *The new FIGO staging system for ovarian, fallopian tube, and primary peritoneal cancer.* Arch Gynecol Obstet, 2014. **290**(5): p. 839-42.
15. Prat, J. and F.C.o.G. Oncology, *FIGO's staging classification for cancer of the ovary, fallopian tube, and peritoneum: abridged republication.* J Gynecol Oncol, 2015. **26**(2): p. 87-9.
16. Eckert, M.A., et al., *Genomics of Ovarian Cancer Progression Reveals Diverse Metastatic Trajectories Including Intraepithelial Metastasis to the Fallopian Tube.* Cancer Discov, 2016. **6**(12): p. 1342-1351.
17. Lengyel, E., *Ovarian cancer development and metastasis.* Am J Pathol, 2010. **177**(3): p. 1053-64.
18. Kazazi-Hyseni, F., J.H. Beijnen, and J.H. Schellens, *Bevacizumab.* Oncologist, 2010. **15**(8): p. 819-25.
19. Chen, A., *PARP inhibitors: its role in treatment of cancer.* Chin J Cancer, 2011. **30**(7): p. 463-71.
20. Bakrin, N., et al., *Hyperthermic intraperitoneal chemotherapy (HIPEC) in ovarian cancer.* J Visc Surg, 2014. **151**(5): p. 347-53.
21. Tentes, A.A., et al., *Cytoreductive surgery combined with hyperthermic intraperitoneal intraoperative chemotherapy in the treatment of advanced epithelial ovarian cancer.* J Oncol, 2012. **2012**: p. 358341.
22. Xu, H., et al., *The role of CD44 in epithelial-mesenchymal transition and cancer development.* Onco Targets Ther, 2015. **8**: p. 3783-92.
23. Gialeli, C., A.D. Theocharis, and N.K. Karamanos, *Roles of matrix metalloproteinases in cancer progression and their pharmacological targeting.* FEBS J, 2011. **278**(1): p. 16-27.
24. Klughammer, J., et al., *Differential DNA Methylation Analysis without a Reference Genome.* Cell Rep, 2015. **13**(11): p. 2621-33.
25. Koukoura, O., et al., *DNA methylation profiles in ovarian cancer: implication in diagnosis and therapy (Review).* Mol Med Rep, 2014. **10**(1): p. 3-9.
26. Knudson, A.G., *Two genetic hits (more or less) to cancer.* Nat Rev Cancer, 2001. **1**(2): p. 157-62.
27. Jones, P.A. and S.B. Baylin, *The fundamental role of epigenetic events in cancer.* Nat Rev Genet, 2002. **3**(6): p. 415-28.
28. Herman, J.G. and S.B. Baylin, *Gene silencing in cancer in association with promoter hypermethylation.* N Engl J Med, 2003. **349**(21): p. 2042-54.
29. Baylin, S.B., *DNA methylation and gene silencing in cancer.* Nat Clin Pract Oncol, 2005. **2 Suppl 1**: p. S4-11.
30. Bird, A., *DNA methylation patterns and epigenetic memory.* Genes Dev, 2002. **16**(1): p. 6-21.

31. Kim, H.J. and S.C. Bae, *Histone deacetylase inhibitors: molecular mechanisms of action and clinical trials as anti-cancer drugs.* Am J Transl Res, 2011. **3**(2): p. 166-79.
32. Suzuki, H., et al., *A genomic screen for genes upregulated by demethylation and histone deacetylase inhibition in human colorectal cancer.* Nat Genet, 2002. **31**(2): p. 141-9.
33. Earp, M.A. and J.M. Cunningham, *DNA methylation changes in epithelial ovarian cancer histotypes.* Genomics, 2015. **106**(6): p. 311-21.
34. Zeller, C., et al., *Candidate DNA methylation drivers of acquired cisplatin resistance in ovarian cancer identified by methylome and expression profiling.* Oncogene, 2012. **31**(42): p. 4567-76.
35. Elmore, S., *Apoptosis: a review of programmed cell death.* Toxicol Pathol, 2007. **35**(4): p. 495-516.
36. Pasparakis, M. and P. Vandenabeele, *Necroptosis and its role in inflammation.* Nature, 2015. **517**(7534): p. 311-20.
37. Meng, M.B., et al., *Necroptosis in tumorigenesis, activation of anti-tumor immunity, and cancer therapy.* Oncotarget, 2016. **7**(35): p. 57391-57413.
38. Jang, M.S., et al., *Cooperative phosphorylation of FADD by Aur-A and Plk1 in response to taxol triggers both apoptotic and necrotic cell death.* Cancer Res, 2011. **71**(23): p. 7207-15.
39. Neckers, L. and S.P. Ivy, *Heat shock protein 90.* Curr Opin Oncol, 2003. **15**(6): p. 419-24.
40. Yang, C.K. and S.D. He, *Heat shock protein 90 regulates necroptosis by modulating multiple signaling effectors.* Cell Death Dis, 2016. **7**: p. e2126.
41. Anderson, P. and P. Ivanov, *tRNA fragments in human health and disease.* FEBS Lett, 2014. **588**(23): p. 4297-304.
42. Green, D., W.D. Fraser, and T. Dalmay, *Transfer RNA-derived small RNAs in the cancer transcriptome.* Pflugers Arch, 2016. **468**(6): p. 1041-7.
43. Fu, Y., et al., *Small Non-coding Transfer RNA-Derived RNA Fragments (tRFs): Their Biogenesis, Function and Implication in Human Diseases.* Genomics Inform, 2015. **13**(4): p. 94-101.
44. Protter, D.S. and R. Parker, *Principles and Properties of Stress Granules.* Trends Cell Biol, 2016. **26**(9): p. 668-79.
45. Pelz, J.O., et al., *Hyperthermic intraperitoneal chemotherapy in patients with peritoneal carcinomatosis: role of heat shock proteins and dissecting effects of hyperthermia.* Ann Surg Oncol, 2013. **20**(4): p. 1105-13.
46. Shin, H.J., et al., *Doxorubicin-induced necrosis is mediated by poly-(ADP-ribose) polymerase 1 (PARP1) but is independent of p53.* Sci Rep, 2015. **5**: p. 15798.
47. Carpenter, A.E., et al., *CellProfiler: image analysis software for identifying and quantifying cell phenotypes.* Genome Biol, 2006. **7**(10): p. R100.
48. Chen, S., et al., *RIPK1/RIPK3/MLKL-mediated necroptosis contributes to compression-induced rat nucleus pulposus cells death.* Apoptosis, 2017. **22**(5): p. 626-638.
49. Galluzzi, L., et al., *Molecular mechanisms of cell death: recommendations of the Nomenclature Committee on Cell Death 2018.* Cell Death Differ, 2018. **25**(3): p. 486-541.
50. Zhao, X.M., et al., *Hsp90 modulates the stability of MLKL and is required for TNF-induced necroptosis.* Cell Death Dis, 2016. **7**: p. e2089.
51. Juhling, F., et al., *metilene: fast and sensitive calling of differentially methylated regions from bisulfite sequencing data.* Genome Res, 2016. **26**(2): p. 256-62.
52. Rappaport, N., et al., *Rational confederation of genes and diseases: NGS interpretation via GeneCards, MalaCards and VarElect.* Biomed Eng Online, 2017. **16**(Suppl 1): p. 72.
53. Rebhan, M., et al., *GeneCards: integrating information about genes, proteins and diseases.* Trends Genet, 1997. **13**(4): p. 163.
54. Avis, J.M. and P.R. Clarke, *Ran, a GTPase involved in nuclear processes: its regulators and effectors.* J Cell Sci, 1996. **109 (Pt 10)**: p. 2423-7.
55. Aluru, M., et al., *Reverse engineering and analysis of large genome-scale gene networks.* Nucleic Acids Res, 2013. **41**(1): p. e24.
56. Song, W.M. and B. Zhang, *Multiscale Embedded Gene Co-expression Network Analysis.* PLoS Comput Biol, 2015. **11**(11): p. e1004574.
57. Auer, K., et al., *Role of the immune system in the peritoneal tumor spread of high grade serous ovarian cancer.* Oncotarget, 2016. **7**: p. 61336-61354.
58. van Driel, W.J., et al., *Hyperthermic Intraperitoneal Chemotherapy in Ovarian Cancer.* N Engl J Med, 2018. **378**(3): p. 230-240.
59. Murshid, A., J. Gong, and S.K. Calderwood, *The role of heat shock proteins in antigen cross presentation.* Front Immunol, 2012. **3**: p. 63.
60. Goodarzi, H., et al., *Endogenous tRNA-Derived Fragments Suppress Breast Cancer Progression via YBX1 Displacement.* Cell, 2015. **161**(4): p. 790-802.

61. Tsai, J.H. and J. Yang, *Epithelial-mesenchymal plasticity in carcinoma metastasis.* Genes Dev, 2013. **27**(20): p. 2192-206.
62. Chang, A.I., et al., *Involvement of mesenchymal stem cells in cancer progression and metastases.* Curr Cancer Drug Targets, 2015. **15**(2): p. 88-98.
63. Peeken, J.C., P. Vaupel, and S.E. Combs, *Integrating Hyperthermia into Modern Radiation Oncology: What Evidence Is Necessary?* Front Oncol, 2017. **7**: p. 132.